Design, characterisation and in vitro evaluation of a multicompartment carrier in the submicron range

York-Durán, María José

Publication date:
2018

Document Version
Publisher's PDF, also known as Version of record

Technical University of Denmark

DEPARTMENT OF MICRO- AND NANOTECHNOLOGY

PhD Thesis

Design, characterisation and *in vitro* evaluation of a multicompartment carrier in the submicron range

Supervisor:

Assoc. Prof. Leticia Hosta-Rigau, PhD

Co-Supervisor:

Prof. Thomas Lars Andresen, PhD

PhD Candidate:

María José York-Durán, MSc

30/11/2018

Acknowledgements

First of all I would like to thank my supervisor, Associate Professor Leticia Hosta-Rigau for giving me the opportunity to do science for more than three years and for her valuable guidance during this journey. I would also like to thank my co-supervisor Professor Thomas Lars Andresen for giving me unlimited access to his laboratories.

Next, I would like to thank Associate Professor Esben Thormann and Dr. Xiaoyan Liu from DTU chemistry for their valuable contribution on the QCM-D measurements and analysis.

A PhD thesis could not be written without valuable help. A deep thank goes to the lab technicians (Ole, Jannik, Lotte and Lene), for making everyone´s life easier in the 423 building. Big thanks to the CBIO group for welcoming me and being there to answer numerous questions. In particular to Sara (for helping me setting up the argon line and for showing me what being in love with science actually looks like), to Martin Kræmer (for helping me with NMR spectrums, translating my abstract into Danish and for singing Adele songs out loud in the 115 lab with me), to Viktoria (for proof-reading the Danish abstract and being a good friend), to Mette, Ditte and Anthie (for answering my infinite amount of questions during my PhD) and to Gael (for helping me with liposome formulations and for convincing me that I could survive my PhD).

A special thank goes to the members of the 3Bs group (Adriana, Cédric, Maria, Pramod, Michelle, Xiaoli and Jing). A good PhD thesis requires good office mates. I would personally like to thank Maria for being there from the beginning of this journey not only professionally but also personally, to Pramod for the wonderful work optimizing the synthesis of the microgels and for the long conversations in front of the fume hood, to Michelle for making my PhD a happier place (I will always remember you every time I eat a peach☺), to Xiaoli for an excellent job proof reading my thesis and to Jing for always cheering me up.

Doing a PhD is already a difficult task, but doing it away from your family and friends is even harder. However, few people managed to give me a home away from home. Milena, Viktoria, Michelle, Ana, Ditte, Mette and Anthie I will never forget you ♥.

Por último a los más importantes, a mi familia por su inmenso apoyo incondicional. A mis padres, Leida y José, por sus valores, por siempre tener fe en mí y por permitirme llegar a dónde he llegado. A mis hermanos, Sheila, María y José por siempre hacerme reír, por acordarse de mi cada día y por interesarse por mi ciencia. A mis sobrinos, Isabella y Lucas, por hacer mi vida infinitamente más feliz. A mi segunda familia, Luisa, Antonio, María y Coral, por escuchar mis desahogos, por animarme a seguir y por preocuparse por mí. A mis amigas, Alba y Laura, por no olvidarme y por ser mi gran apoyo ♥. Para acabar, gracias infinitas a la persona que se aseguró de que me alimentase, de que siguiera cuerda y de que nunca perdiese la sonrisa, a mi esposo Daniel.

Abstract

Inspired by the compartmentalized structure of eukaryotic cells (which isolate crucial functions on separate compartments), carriers containing multiple compartments have attracted a great deal of attention due to its potential in a wide range of fields (*i.e.*, biomedicine, drug delivery or biomimicry). The two main applications of multicompartment carriers to date are as traditional drug delivery vehicles or microreactors to degrade waste/harmful products or to support the synthesis of biomolecules. As drug delivery carriers, thanks to their compartmentalized structure they offer the ability to encapsulate multiple (incompatible) therapeutic molecules within the same carrier in distinct separated compartments while ensuring the co-localization of such therapeutic molecules at the target site. As microreactors, the multicompartment platforms allow the encapsulation and protection of enzymes in independent sub-compartments offering the opportunity to perform cascade and/or parallel enzymatic reactions at the intracellular or extracellular level.

Despite the great efforts invested in the development of these carriers, most of them are in the micron range which limits their therapeutic potential. Aiming to move the field forward, a new multicompartment carrier in the submicron range with potential as dual-cargo drug delivery vehicle and extracellular microreactor is presented in this PhD thesis. For this, two different building blocks, namely microgels (MGs) and liposomes where chosen with the aim to achieve two different cargo release profiles (a promising approach for tandem release). While the cargo encapsulated within the MGs will experience a fast release due to the MGs large pores, the cargo encapsulated within the liposomes is expected to be released in a slower rate. In particular, poly(N-isopropylacrylamide-*co*-acrylic acid) MGs were chosen as a core and were subsequently decorated with liposomes attached by electrostatic interactions. Since liposomes suffer from low structural stability in physiological environments, the assembly was coated with a polydopamine (PDA) layer. Next, the assembly was terminated by functionalising the PDA layer with poly(*L*-

lysine)-grafted-poly(ethylene glycol) (PLL-*g*-PEG) to endorse the multicompartment carrier with low-fouling properties.

First, the assembly was thoroughly optimised by evaluating two different sizes of MGs (*i.e.*, MG_{700} and MG_{350}) as the optimal core for the multicompartment carrier in terms of colloidal stability, facile production and PEGylation effect upon incubation with relevant cell lines (*i.e.*, RAW 264.7, macrophages, HUVEC, endothelial cells and HeLa cancer cells as an example of therapeutic target). Based on the findings, the MG_{700} was selected as the core for subsequent experiments. Next, the potential of the multicompartment carrier as dual-cargo vehicle was investigated by loading model molecules (*i.e.*, methylene blue and calcein) in the MG and liposome cores. The results showed a slower release profile from the liposomes than MGs indicating a promising system for tandem release. Importantly, the cell/carrier interaction was thoroughly investigated taking into consideration the dynamics of the human physiology in terms of shear stress (produced by blood flow and interstitial fluid in tumours). The findings regarding the impact of shear stress on cell uptake/association, cellular uptake pathway and PEGylation effect highlight the importance of including shear stress when developing a new carrier. Finally, the potential of the multicompartment carrier as extracellular microreactor was evaluated in test tubes. For this, catalase (CAT) was encapsulated within the liposome core in order to perform the cascade reaction of reactive oxygen species detoxification as proof-of-concept. The results showed a successful detoxification of superoxide radical due to the antioxidant activity of PDA yielding H_2O_2 and a mix of products. This H_2O_2 was also successfully scavenged by the CAT loaded within the liposomes used to assemble the microreactor, yielding H_2O and O_2. What is more, the microreactor was reused for at least five enzymatic cycles demonstrating its potential to perform cascade reactions in a continuous manner which is highly important in therapeutic applications.

Dansk resumé

Carriers indeholdende adskillige opdelte rum har tiltrækt en del opmærksomhed (f.eks inden for biomedicin, *drug delivery*, *biomimicry*). Disse er inspireret af eukaryote celler, som isolerer nødvendige funktioner i separate rum.

De to hovedsagelige applikationer af de rumopdelte *carriers* er til dato som traditionelle *drug delivery* værktøjer eller som mikroreaktorer til degradering af affald/skadelige produkter eller som support til syntesen af biomolekyler. Som *drug delivery* værktøj er disse, takket være deres rumopdelte strukturer, i stand til at indkapsle adskillige (inkompatible) terapeutiske molekyler i samme *carrier* i distinkte opdelte rum, og samtidigt sikre co-lokalisationen af disse terapeutiske molekyle til samme mål.

Som mikroreaktorer kan de rumopdelte *carriers* tillade indkapsling og beskyttelse af enzymer i underopdelte rum, hvilket giver mulighed for at udføre kaskade- og/eller parallelle enzymatiske reaktioner på intra- eller ekstracellulært niveau.

På trods af den store indsats investeret i udviklingen af disse *carriers* er de fleste af dem i micrometer størrelse, hvilket begrænser deres terapeutiske potentiale. Med målsætningen om at rykke dette forskningsfelt fremad, er der i denne PhD afhandling præsenteret nye multi-opdelte *carriers* i størrelser mindre end en micrometer. To forskellige byggeblokke er udvalgt for at kunne opnå dette. Disse er henholdsvis mikrogeler (MGs) og liposomer, som blev udvalgt for at kunne opnå to forskellige profiler for frigivelsen af indholdet (en lovende tilgang til at kunne opnå tandem-release). Indholdet ladet i MGs vil opleve en hurtigere frigivelse, grundet de store porer i MGs, mens inholdet i liposomer forventes at blive frigivet over længere tid. Nærmere bestemt blev poly(N-isopropylacrylamide-*co*-acrylic acid) MGs udvalgt som kerne, for efterfølgende at dekorere kernen med liposomer, som er sammenholdt af elektrostatiske interaktioner. Eftersom liposomer har lav strukturel stabilitet i fysiologisk miljø blev sammensætningen coated med et polydopamine (PDA) lag yderst. Derefter blev sammensætningen termineret ved

funktionalisering af PDA laget med poly(*L*-lysine)-grafted-poly(ethylene glycol) (PLL-*g*-PEG) for at ydstyre den multiopdelte carrier med low-fouling egenskaber.

Først, blev monteringen af denne konstruktion optimeret ved evaluering af to forskellige størrelser af MGs, henholdsvis MG_{700} og MG_{350}, for at få den mest optimale kerne for en mutli-opdelt *carrier*, med henblik på colloidial stabilitet, let produktion, og PEGylerings effekt ved inkubering med relevante cellelinjer (RAW 264.7, makrofager, HUVEC, endotel celler og HeLa cancer celler, som et eksempel på et terapeutisk mål). MG_{700} blev udvalgt baseret på disse eksperimenter som kerne for efterfølgende forsøg. Derefter blev potentialet af den multiopdelte carrier som et dual-cargo værktøj undersøgt ved at loade model molekylerne methylene blue og calcein i MGs og liposom kernerne. Resultaterne herfra viste en langsommere frigivelse fra liposomerne end for MGs, hvilket tydede på et lovende system for tandem-release.

Vigtigt var, at celle/*carrier* interaktionerne blev grundigt undersøgt med henblik på dynamikken af den menneskelige fysiologi i forhold til mekanisk tryk (skabt af blodtrykket og ekstracellulærvæske i tumorer). Resultaterne med hensyn til indflydelsen fra det mekaniske tryk på cellulært optag/association, cellulære optagelsesvej, og PEGylerings effekt belyser vigtigheden af at inkludere det mekaniske tryk i udviklingen af en ny *carrier*. Til slut, blev potentialet af den multiopdelte carrier som extracellulær mikroreaktor evalueret i reagensglas. Til dette blev katalase (CAT) indkapsuleret i liposomernes kerne for at kunne udføre kaskade reaktioner til detoksificering af reaktive oxygen arter, som *proof-of-concept*. Resultaterne heraf viste succesfuld detoksificering af superoxid radikaler grundet den antioxidante aktivitet af PDA, hvilket resulterer i H_2O_2 og en blanding af produkter. Det producerede H_2O_2 blev med succes opfanget af det liposomalt indkapslede CAT fra sammensætningen af mikroreaktoren, som resulterede i dannelse af H_2O og O_2. Derudover blev mikroreaktoren genbrugt til mindst fem enzymatiske cyklusser, som demonstrerer dennes potentiale til at udføre kaskade reaktioner i en kontinuer facon, hvilket er vigtigt til terapeutiske applikationer.

Table of Contents

Abbreviations

$^{\cdot}OH$	Hydroxyl radical
A:	Absorbance
A_0:	Absorbance at time zero
A_∞:	Absorbance at maximum incubation time.
AAc:	Acrylic acid
ANOVA:	Analysis of variance
APS:	Ammonium persulfate
A_t:	Absorbance at different time points
BA:	*N,N*'-methylenebiscarylamide
BSA:	Bovine serum albumin
BSA-FITC:	Fluorescein isothiocyanate -labelled bovine serum albumin
Cal:	Calcein
CAT:	Catalase
CAT-FITC:	Fluorescein isothiocyanate -labelled CAT
CLSM:	Confocal laser scanning microscope
CME:	clathrin-mediated endocytosis
CMFI:	Cell mean fluorescence intensity
cRGDY:	Cyclic arginine-glycine-aspartic acid
CUE:	Cellular uptake efficiency
CvME:	caveolae-mediated endocytosis
DA:	Dopamine
DIC:	Differential interference contrast
DLS	Dynamic light scattering
DMEM:	Dulbecco´s Modified Eagle´s Medium-high glucose
DMPC:	1,2-Dimyristoyl-*sn*-glycero-3-phosphocholine
DMSO:	Dimethyl sulfoxide
DOPA:	4-dihydroxy-*L*-phenylalanine
DOPC:	1,2-Dioleoyl-*sn*-glycero-3-phosphocholine
DPPC:	1,2-dipalmitoyl-*sn*-glycero-3-phosphocholine
DSTAP:	1,2-stearoyl-3-trimethylammonium-propane (chloride salt)
EBM:	Endothelial Basal Medium
ECACC:	European Collection of Authenticated-Culture Collections
EDTA:	ethylenediaminetetraaceti c acid solution
EE:	Encapsulation efficiency
EGM-2:	Endothelial Growth Medium-2 Bullet kit
EMA:	European Medicines Agency
eNOS:	Endothelial nitric oxide synthase
FBS:	fetal bovine serum
FDA:	Food and Drug Administration
FI:	Fluorescence intensity
FI_0:	Fluorescence intensity at time zero
FI_t:	Fluorescence intensity at different time points
FITC:	Fluorescein isothiocyanate
FI_{TX}:	Fluorescence intensity after Triton-X addition
GA:	Gentamicin/amphotericin -B
GOx:	Glucose oxidase
GR:	Grafting ratio
GSH:	Glutathione
GSH-Px:	Glutathione peroxidases
GSSG:	Glutathione disulfide

H_2O_2:	Hydrogen peroxide
hEGF:	Human epidermal growth factor
HeLa:	Adenocarcinoma cell line
HEPES:	4-(2-hydroxyethyl) piperazine-1-ethane-sulfonic acid
HER2:	Human epidermal growth factor receptor 2
hFGF-β:	Human fibroblast growth factor-beta
HIV:	Human immunodeficiency virus
HRP:	Horseradish peroxidase
HUVEC:	Human umbilical vein endothelium cells
IgG-FITC:	Fluorescein isothiocyanate -labelled immunoglobulin G
KRAS:	Kristen Rat Sarcoma
L:	Unilamellar empty liposomes
L^{Cal}:	Calcein-loaded liposomes
L^{CAT}:	Catalase-loaded liposomes
$L^{CAT-FITC}$:	Fluorescent labelled catalase-loaded liposomes
$L^{F,CAT}$:	Catalase-loaded liposomes containing NBD-PC
L^{F}:	Unilamellar empty AND Fluorescently labelled liposomes
LSDs:	Lysosomal storage diseases
MB:	Methylene blue
Me-PEG-NHS:	α-Methoxy-ω-carboxylic acid succinimidyl ester poly(ethylene glycol)
MG/L/PDA/PEG:	PEGylated carriers containing empty and non- fluorescently labelled liposomes
MG/L/PDA:	Non PEGylated carriers containing empty non-fluorescently labelled liposomes
MG/L^{Cal}/PDA/PEG:	PEGylated carriers containing calcein-loaded liposomes
MG/L^{Cal}/PDA:	Non-PEGylated carriers containing calcein-loaded liposomes
$MG/L^{CAT-FITC}$/PDA:	Non-PEGylated microreactors containing FITC labelled catalase-loaded liposomes
$MG/L^{F,CAT}$/PDA/PEG:	PEGylated microreactors containing catalase-loaded fluorescent liposomes
$MG/L^{F,CAT}$/PDA:	Non-PEGylated microreactors containing catalase-loaded fluorescent liposomes
MG/L^{F}/PDA/PEG:	PEGylated carrier containing empty fluorescently labelled
MG/L^{F}/PDA:	Non PEGylated carriers containing empty fluorescently labelled
MG_{350}:	Microgels with ~350 nm in diameter
MG_{700}:	Microgels with ~700 nm in diameter
MG^{MB}/L/PDA/PEG:	PEGylated carriers containing Methylene blue-loaded microgels
MG^{MB}/L/PDA:	Non-PEGylated carriers containing Methylene blue-loaded microgels
MG^{MB}:	Methylene blue-loaded microgels
MGs:	Microgels
MPS:	Mononuclear phagocyte system
NaCl:	Sodium chloride
NADPH:	Nicotinamide adenine dinucleotide phosphate oxidase
$NaHCO_3$:	Sodium bicarbonate
NBD-PC	1-myristoyl-2-[12-[(7-nitro-2-1,3-benzoxadiazol-4-yl)amino]dodecanoyl]-*sn*-glycero-3-phosphocholine
nCMFI:	Normalised cell mean fluorescence intensity
NIPAM:	*N*-isopropylacrylamide

NIR:	Near infrared
nMFI:	Normalised mean fluorescence intensity
NO:	Nitric oxide
NOO-:	Peroxynitrite
$O_2^{\cdot-}$:	Superoxide radical
P(NIPAM):	Poly(*N*-isopropylacrylamide)
P(NIPAM)-*co*-AAc:	Poly(*N*-isopropylacrylamide-*co*-acrylic acid)
PBS:	Phosphate buffered saline
PDA:	Poly(dopamine)
PDI:	Polydispersity
PEG:	Poly(ethylene glycol)
PFA:	Paraformaldehyde
PFA:	Paraformaldehyde
phalloidin-TRITC:	Tetramethylrhodamine B isothiocyanate -labelled phalloidin
Phe:	Phenylalanine
PLGA:	Poly(lactic-*co*-glycolic acid)
PLGA:	poly(lactic-*co*-glycolic acid)
PLL:	Poly(*L*-lysine)
PLL-*g*-PEG:	Poly(*L*-lysine (20 kDa))-graft [3.5]-poly(ethylene glycol (2 kDa))
POEPC:	1-palmitoyl-2-oleoyl-*sn*-glycero-3-ethylphosphocholine (chloride salt)
POPC:	1-palmitoyl-2-oleoyl-phosphatidylcholine
PSMA:	Prostate-specific membrane antigen
Pt-NP:	Platinum nanoparticles
QCM-D:	Quartz crystal microbalance with dissipation monitoring
R3-IGF-1:	R3-insulin-like growth factor-1
RAW 264.7:	Macrophage cell line
ROS:	Reactive oxygen species
SDS:	sodium dodecyl sulfate
SEC:	Size Exclusion Chromatography
SEM:	Scanning electron microscopy
SOD:	Superoxide dismutase
t-ca:	Trans-cinnamic acid
T_m:	Transition temperature
Tris:	Tris(hydroxymehtyl)aminomethane
TRITC:	Tetramethylrhodamine B isothiocyanate
TRP:	Trypsin
Trx:	Thioredoxin
VEGF:	Vascular endothelial growth factor
VPTT:	Volume phase transition temperature
WST-8:	[2-(2-methoxy-4-nitrophenyl)-3-(4-nitrophenyl)- 5-(2,4-disulfophenyl)-2H-tetrazolium monosodium salt]
ζ-potential:	Zeta-potential
ΔD:	Dissipation changes measured by Quartz crystal microbalance with dissipation monitoring
Δf:	Frequency changes measured by Quartz crystal microbalance with dissipation monitoring
τ:	Shear stress
$\tau_{0.5}$:	0.5 dyn cm^{-2}
τ_0:	0 dyn cm^{-2}
τ_{20}:	20 dyn cm^{-2}
τ_4:	4 dyn cm^{-2}

List of schemes, figures and tables

Disposition

This thesis comprises six chapters, one introductory chapter (Chapter 1), which includes information from two review papers published in Colloids and Surfaces B: Biointerfaces (2017) and Advanced Healthcare Materials (2018), and three experimental chapters (Chapter 3, 4 and 5). Being Chapter 2 the aims of this PhD thesis. Chapter 3 describes the assembly and characterisation of the multicompartment carrier. Chapter 4 describes the functionality of the developed multicompartment carrier as a dual-cargo vehicle and its interaction with relevant cell lines in the absence and presence of physiological shear stress conditions. Chapter 3 and 4 include results from an experimental paper published in Colloids and Surfaces B: Biointerfaces (2018). Chapter 5 describes the functionality of the multicompartment carrier as a microreactor (envisioned to act extracellularly) able to scavenge reactive oxygen species. Finally, Chapter 6 presents the main conclusions based on the findings of this PhD thesis.

Papers included in this thesis:

York-Duran, M. J.; Godoy-Gallardo, M.; Labay, C.; Urquhart, A. J.; Andresen, T. L.; Hosta-Rigau, L. Recent Advances in Compartmentalized Synthetic Architectures as Drug Carriers, Cell Mimics and Artificial Organelles. *Colloids Surf., B* **2017**, *152*, 199–213.

Godoy-Gallardo, M.; **York-Duran, M. J.;** Hosta-Rigau, L. Recent Progress in Micro/Nanoreactors toward the Creation of Artificial Organelles. *Adv. Healthc. Mater.* **2018**, *7* (5), 1–35.
*First co-authorship

York-Duran, M. J; Ek, P. K.; Godoy-Gallardo M.; Hosta-Rigau L. Shear stress regulated uptake of liposome-decorated microgels coated with a poly(dopamine) shell. *Colloids Surf., B* **2018**, 171, 427-436.

Conference contributions:

York-Duran, M. J; Godoy-Gallardo M.; Ek, P. K.; Hosta-Rigau L. Flow cytometry as analytical technique to evaluate the influence of shear stress on the interaction of a novel drug delivery

vehicle. *Nordic Flow Cytometry Meeting, Copenhagen, Denmark*, **2017**. Oral and poster contribution.

York-Duran, M. J; Ek, P. K.; Godoy-Gallardo M.; Hosta-Rigau L. Impact of physiological shear stress on cell association/uptake with a novel multicompartment carrier. *Sustain 2017, Technical University of Denmark*, **2017**. Poster contribution.

Chapter I Introduction

1.1 Multicompartment carriers

Inspired by the natural compartmentalized structure of eukaryotic cells, the design of multicompartment platforms has risen increasing interest over the last few years due to its great potential in a wide range of fields such as biomedicine, drug delivery or biomimicry.[1] This strategy allows the cells to isolate and protect essential cellular activities required for living such as protein production in the ribosomes, digestion of unwanted materials in the lysosomes or energy production and cellular respiration in the mitochondria from external cytotoxic reactions.[2]

The most investigated and advanced multicompartment systems reported to date are divided in two groups depending on the composition of the sub-compartments and the carrier vessel (Figure 1.1): Single-component assemblies in which the nature of both the sub-compartments and the carrier vessel is the same (*i.e.*, liposomes-in-liposomes (vesosomes),[3,4] polymersomes-in-polymersomes[5] and capsules-in-capsules[6]) and dual-component assemblies in which the nature of the components differs (*i.e.*, polymersomes-in-liposomes,[7] cubosomes-in-polymer capsules[8,9] and liposomes embedded within a polymer capsule (so-called capsosomes)[10–14]).

Table 1.1 summarizes the advantages and disadvantages of each building block. Liposomes, spherical vesicles consisting of single or multiple phospholipid bilayers containing an aqueous core,[15] are the most studied drug delivery system to date, first reported in 1961[16] with a dozen liposomal drugs approved for clinical use.[17] The synthetic equivalent of liposomes are called polymersomes, in which the phospholipid bilayer is substituted by amphiphilic polymers.[18] Lastly, cubosomes are honeycombed structures formed by bicontinous lipid bilayers forming two internal aqueous channels.[19] Although liposomes and polymer capsules have been extensively used in the design of multicompartment systems, reports using polymersomes and cubosomes are scarce. This is probably due to main disadvantages of these systems, such as the low permeability of polymersomes which hinders the traffic of molecules required to perform enzymatic reactions (one of the main applications of multicompartment carriers) while the time-consuming and labour-intensive production of cubosomes limit their use.[2]

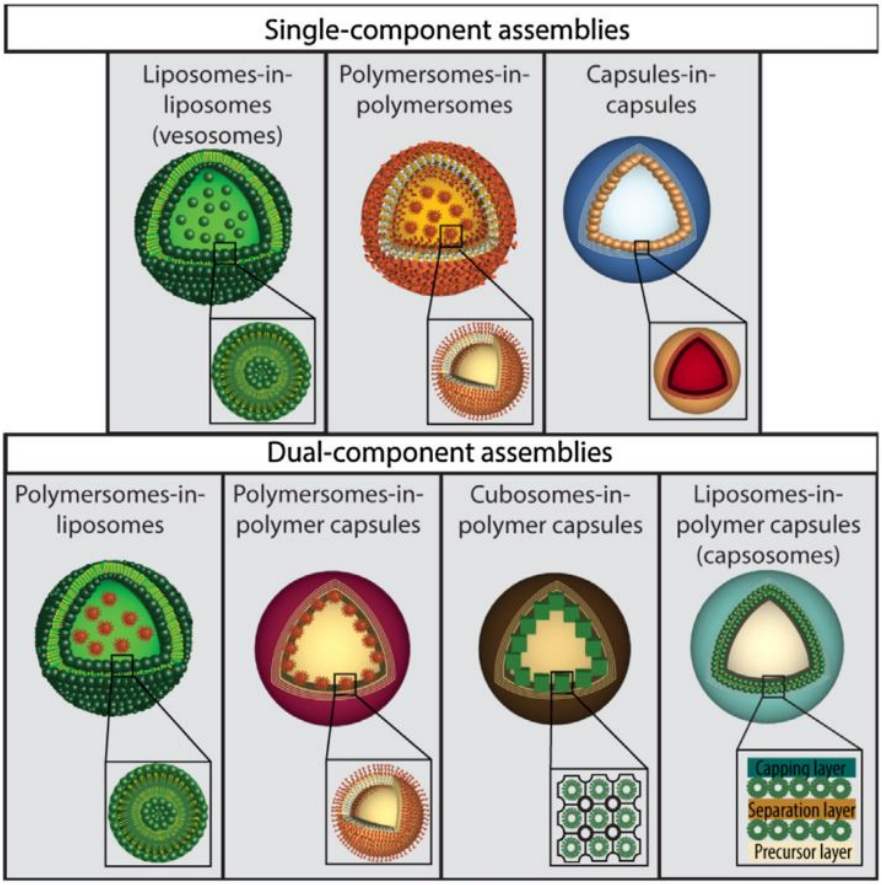

Figure 1.1 Schematic of the most studied multicompartment carriers to date. Reprinted from reference [2] with permission. Copyright (2017) by Elsevier.

Building block	Advantages	Disadvantages
Liposomes	- Formed *via* self-assembly - Encapsulation of both hydrophilic and hydrophobic cargo - Biocompatible - Biodegradable - Communication between the internal and external milieu readily achievable - Triggered release of cargo	- Premature cargo release - Lack of control over degradability
Polymersomes	- Formed *via* self-assembly - Encapsulation of both hydrophilic	- Lack of permeability for polar molecules

	and hydrophobic cargo - High hydrophobic loading capacity - High mechanical stability - Chemical versatility of the polymer building blocks - Biodegradable (by the right choice of the polymer building blocks) - Triggered release cargo	- Diminished ability for functionalisation with biological components (*i.e.*, protein pores, receptors or antibodies) - Made of amphiphilic polymers only - Low amounts of hydrophilic cargo
Polymer capsules	- Large variety of polymers can be employed - Precise control over size, shape and wall thickness - Triggered release of cargo	- Aggregation issues - Time-consuming, labour-intensive assembly process - Difficult to encapsulate small hydrophilic cargo
Cubosomes	- High mechanical stability - Biodegradable - Larger loading capacity compared to liposomes	- Time-consuming, labour intensive assembly process

Table 1.1 Advantages and disadvantages of building blocks used in the assembly of multicompartment carriers. Reprinted from reference [2] with permission. Copyright (2017) by Elsevier.

1.2 Multicompartment carriers: applications

The compartmentalized structured of the multicompartment carriers offers the possibility to independently load each sub-compartment with incompatible therapeutic molecules and to perform enzymatic reactions in separated sub-compartments in a parallel and/or cascade manner (similar to the organization of a eukaryotic cell).[2] Therefore, the main applications of multicompartment systems to date are as drug delivery vehicles,[2] and extracellular[20] or intracellular (the so-called artificial organelles)[11,12,21] microreactors.

1.2.1 Multicomparment carriers as drug delivery vehicles

Regarding their application as drug delivery vehicles, the multicompartment platforms guarantee the co-localization of therapeutically relevant molecules, which could be potentially incompatible in terms of solubility and or stability,[2] at the target site. The principle is based on the loading of therapeutic molecules in independent sub-compartments leading to their co-encapsulation within the same carrier. This approach is particularly relevant in many diseases such as cancer,[22] immune-associated diseases,[23] type 2 diabetes[24] or rheumatoid arthritis[25] in which a cocktail of drugs is required. The achievement of a homogeneous spatial and temporal co-delivery of therapeutic molecules at the target site is highly unlikely if administered separately, due to the different pharmacodynamic and pharmacokinetic properties.[22] Multiple compartment drug delivery carriers are envisioned to improve therapeutic efficacy while reducing side effects.[2] However, depending on the specific application the different building blocks that conform the multicompartment platform will vary. For applications where the tandem release of multiple drugs is desired, building blocks with different release profiles are needed. For this, hydrogels coated with liposomes (hydrogel-liposome complexes) are particularly suitable due to the combination of two inherently different systems with intrinsically different release kinetics (*i.e.*, while hydrogels generally exhibit a fast release profile due to their large pore size, the liposomes offer a slower release profile).[26]

1.2.2 Multicompartment carries as microreactors

In addition to their application as drug delivery vehicles, great efforts have been reported regarding the application of multicompartment systems as extra or intracellular (*i.e.*, artificial organelles) microreactors. The principle is based on the encapsulation and protection of enzymes in separated sub-compartments in order to perform cascade and/or parallel enzymatic reactions. When these reactions are envisioned to be performed at an intracellular level the microreactor acts as an artificial organelle, normally replacing missing or lost natural metabolic activities.[11]

In order to function as a reactor there are specific requirements that need to be satisfied: (i) to possess a compartmentalized structure in order to encapsulate and protect the enzymes, (ii) to retain enzymatic activity required for functionality, (iii) to control the permeability of the carrier to ensure the entry of substrates and the escape of the products, (iv) depending on the application in mind, cell internationalization is desired to be able to enter (artificial organelles) target cells or not in the case of extracellular microreactors and (v) to be biodegradable and biocompatible.[27]

1.2.2.1 Intracellular microreactors

The multicompartment platforms that fulfil the aforementioned requirements hold promising potential in enzymatic replacement therapy of, for example, lysosomal storage diseases (LSDs), in which the substitution of a missing or malfunctioning enzyme(s) is needed acting as an artificial organelle.[28] More than 50 LSDs have been reported to date and they are caused by genetic mutations that encode different lysosome enzymes leading to accumulation of harmful molecules resulting in organ damage.[29] Another example of enzymatic replacement therapy in which multicompartment carriers are useful is acting as an artificial peroxisome. A peroxisome is a natural organelle with multiple functions including the regulation of the intracellular levels of reactive oxygen species (ROS) through enzymatic reactions.[30] The ROS overproduction has been linked to several vascular diseases such as arthritis, cancer, hypercholesterolemia, etc.[31] Their natural regulation is based on an enzymatic cascade reaction in which different enzymes (*i.e.*, superoxide dismutase (SOD), catalase (CAT), glutathione peroxidase, etc.) keep the ROS level constant.[32] Therefore, the intracellular implantation of a multicompartment system acting as a reusable microreactor offers great advantages over the administration of free enzymes such as protection from external environment (*i.e.*, degradative enzymes, pH, immunogenicity, etc.) and the possibility to perform cascade[11] and/or parallel[12] enzymatic reactions at the target site. Numerous studies have addressed the application of multicompartment carriers as microreactors in test tubes.[15] For example, vesosomes are able to conduct parallel enzymatic reactions (*i.e.*, encapsulating alkaline phosphatase and two different substrates) by using temperature due to the different T_m of the sub-

compartments,[33] or cascade reactions (*i.e.*, encapsulating lactase, glucose oxidase (GOx) and horseradish peroxidase (HRP)) using transmembrane protein pores to allow communication between the compartment.[34]

Polymersomes-in-polymersomes have also been employed as microreactors. Specifically, they have being designed to encapsulate three different enzymes (*i.e.*, phenyl acetone monooxygenase, *Candida antarctica* lipase B and alcohol dehydrogenase) to convert a non-fluorescent molecule into a fluorescent one,[35] or to encapsulate GOx and HRP in order to transform β-D-glucose into a final fluorescent product using transmembrane channel proteins to allow the communication between the compartments.[36]

Lastly, extensive efforts have been devoted to the development of capsosomes,[14,37–41] being the only multicompartment system with a confirmed intracellular functionality.[11,12,21] In particular, Thingholm *et al.*,[21] first reported the intracellular conversion of β-D-glucose into cytotoxic H_2O_2 , leading to cell death, by GOx-loaded liposomes embed in poly(dopamine) (PDA) coated capsosomes-like platforms decorated with RGD targeting moieties. PDA is a bioinspired polymer that has attracted great attention over the years due to the possibility to coat virtually any surface as result of the self-polymerisation of dopamine (DA) under slightly basic conditions , biocompatibility and easy post-functionalisation due to its reactivity towards amines and thiols.[42] Later on, Godoy *et al.*,[12] reported the ability of capsosomes to perform intracellular parallel enzymatic reactions by encapsulating trypsin (TRP) and HRP in different compartments in order to transform a non-fluorescent substrate into a green fluorescent product by TRP while a red fluorescent product was generated by HRP at the same time. On a follow up study,[11] the authors performed an intracellular cascade reaction using GOx and HRP as tandem enzymes to transform β-D-glucose into a fluorescent molecule in an intracellular two-step cascade reaction.

1.2.2.2 Extracellular microreactors

More relevant for this PhD thesis is the design of multicompartment systems that meet the requirements to act as a microreactor (*i.e.*, (i) compartmentalized structure (ii) to retain

enzymatic activity, (iii) to control the permeability of the carrier, (iv) avoid internalisation (v) to be biodegradable and biocompatible) but that are envisioned to act extracellularly.

Although the assembly of sub-compartmentalized systems has gain great interest over the last few years, only few reports exploit this application. The first report, published by Hosta-Rigau *et al*.,[20] is based on the construction of capsosomes containing non-human phenylalanine ammonia lyase loaded liposomes in order to convert the amino acid phenylalanine (Phe) into trans-cinnamic acid (t-ca) as a potential treatment for phenylketonuria disease in which the enzyme responsible to transform Phe into tyrosine is missing. The system is envisioned to deplete Phe from the gastrointestinal track which would eventually lead to a decrease of Phe level in plasma. The extracellular functionality was confirmed by the successful transformation of Phe into t-ca in the presence of human intestinal epithelial cells in both culture plates and peristalsis-like motions mimicking the intestinal movement. The cellular uptake is avoided probably due to the large size of the microreactor, of approximately 5 µm. In a more recent report, Itel *et al*.,[43] developed a 50 µm alginate microreactor equipped with alkaline phosphatase-loaded liposomes or SaOS-2 (bone-like osteoblast cells) derived matrix vesicles (which contains alkaline phosphatase among other components) followed by co-assembly with SaOS-2 cells in order to form a spheroid. The principle is based on the hydrolysis of inorganic pyrophosphates into inorganic phosphate which generates calcium phosphate precipitates leading to bio mineralization. The results demonstrated that only when the matrix vesicles were present the bio mineralization was improved for at least 10 days. Zhang *et al*.,[44] assembled 10 µm silica PDA coated particles containing bovine liver CAT-loaded liposomes in order to remove ROS (*i.e.*, H_2O_2) from the cell culture mimicking the liver function. The extracellular functionality was successfully confirmed by the improved cell viability upon exposure H_2O_2 for at least 34 h while non-inherent cytotoxicity was found for the microreactors for up to 10 days. In a different study, Zhang *et al*.,[45] demonstrated improved cell viability of planar cultures and cell aggregated of hepatocytes upon removal of H_2O_2 by a 40 µm alginate microreactor containing CAT-loaded liposomes.

1.2.2.3 Reactive oxygen species: Importance and antioxidant solutions

As illustrated by the studies reported by Zhang *et al*.,[44,45] the extracellular ROS detoxification using compartmentalized systems has attracted attention recently. The equilibrium of beneficial and detrimental effects of ROS is maintained in the body by endogenous enzymes such as SODs, CAT, glutathione peroxidases, peroxiredoxins, etc. (Figure 1.2).[32] ROS, including superoxide radical ($O_2^{\cdot -}$), hydrogen peroxide (H_2O_2), hydroxyl radical ($^{\cdot}OH$) and peroxynitrite (NOO^-) are naturally produced by several enzymes such as nicotinamide adenine dinucleotide phosphate oxidase, xanthine oxidase, mitochondrial electron transport chain, cytochrome p450 monoxygenases, etc. (Figure 1.2),[31] being essential for cellular function, signalling and as a line of defence.[46] However, when the production of ROS exceeds the endogenous antioxidant capacity, oxidative stress is generated leading to several diseases due to the high reactivity of these species. This high reactivity lies on the unpaired electron in the outer orbital of $O_2^{\cdot -}$, and $^{\cdot}OH$ and the ability to exchange electron with other molecules exhibited by non-radical species such as H_2O_2.[31]

A wide range of diseases have been associated to the overproduction of ROS in the human physiology, such as hypercholesterolemia, hypertension, diabetes, aging and sickle disease, among others.[31]

The most dangerous ROS is $O_2^{\cdot -}$ due to its ability to generate other ROS. It easily reacts with nitric oxide generating NOO^-, leading to hypertension, or it is subjected to dismutation by SOD yielding H_2O_2 which is involved in cell damage (Figure 1.3). Nowadays several studies have investigated the use of antioxidant molecules to scavenge ROS diminishing their damaging effects and therefore reduce the oxidative stress. The most investigated antioxidant molecules include vitamin C (ascorbic acid) which is obtained through the diet, vitamin E (tocopherol), vitamin A (retinoids), coenzyme Q10 and lycopene and β-carotene (catoinoids). However, these antioxidant molecules exhibit a lower efficacy in

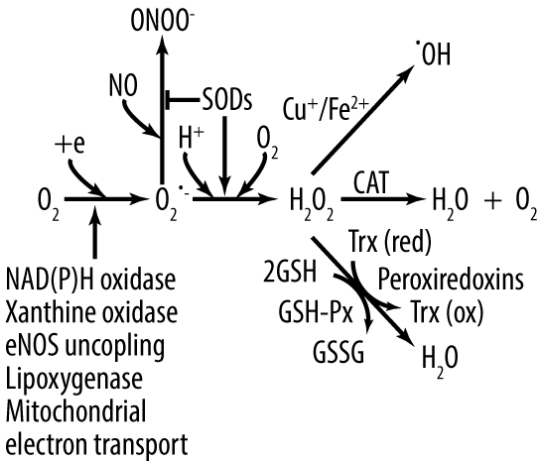

Figure 1.2 Biological production and metabolism of reactive oxygen species. Superoxide ($O_2^{\cdot-}$) is naturally produced by several pathways including nicotinamide adenine dinucleotide phosphate oxidase (NADPH) and endothelial nitric oxide synthase (eNOS). $O_2^{\cdot-}$ is converted in hydrogen peroxide (H_2O_2) , by superoxide dismutases (SODs), which is then either transformed into H_2O by catalase (CAT) or by glutathione peroxidases (GSH-Px) (oxidizing GSH into glutathione disulfide (GSSG)) and peroxiredoxins (oxidizing thioredoxin (Trx)). $O_2^{\cdot}$ can rapidly react with nitric oxide (NO) yielding peroxynitrite (NOO-) which can be inhibited by SODs. Lastly, H_2O_2 can spontaneously be transformed in hydroxyl radical ($^{\cdot}OH$). Adapted from reference [32] with permission. Copyright (2011) by Mary Ann Liebert, Inc.

ROS scavenging compared to the natural antioxidant enzymes (*i.e.*, SOD and CAT)[47] and what is more, the efficacy of vitamin E has been centre of debate since some studies reported that vitamin E has harmful effects.[31]

The specificity and high efficacy of SOD and CAT make their use a promising approach to reduce oxidative stress. SODs are metalloenzymes responsible for the conversion of $O_2^{\cdot-}$ into H_2O_2 having three different human isoforms, SOD containing cooper and zinc found in the cytosol, SOD containing manganese found in the mitochondria and extracellular copper-containing SOD.[48] On the other hand, CAT transforms H_2O_2 into H_2O and O_2 being highly active in kidney, erythrocytes and mostly in the liver.[49]

However, the administration of bare SOD and CAT remains an unviable strategy due to the short half-life of both enzymes *in vivo,* [50], immunogenicity,[51] and deactivation by plasma proteases. Therefore, the encapsulation of the enzymes arises as a tool for their use in ROS scavenging.

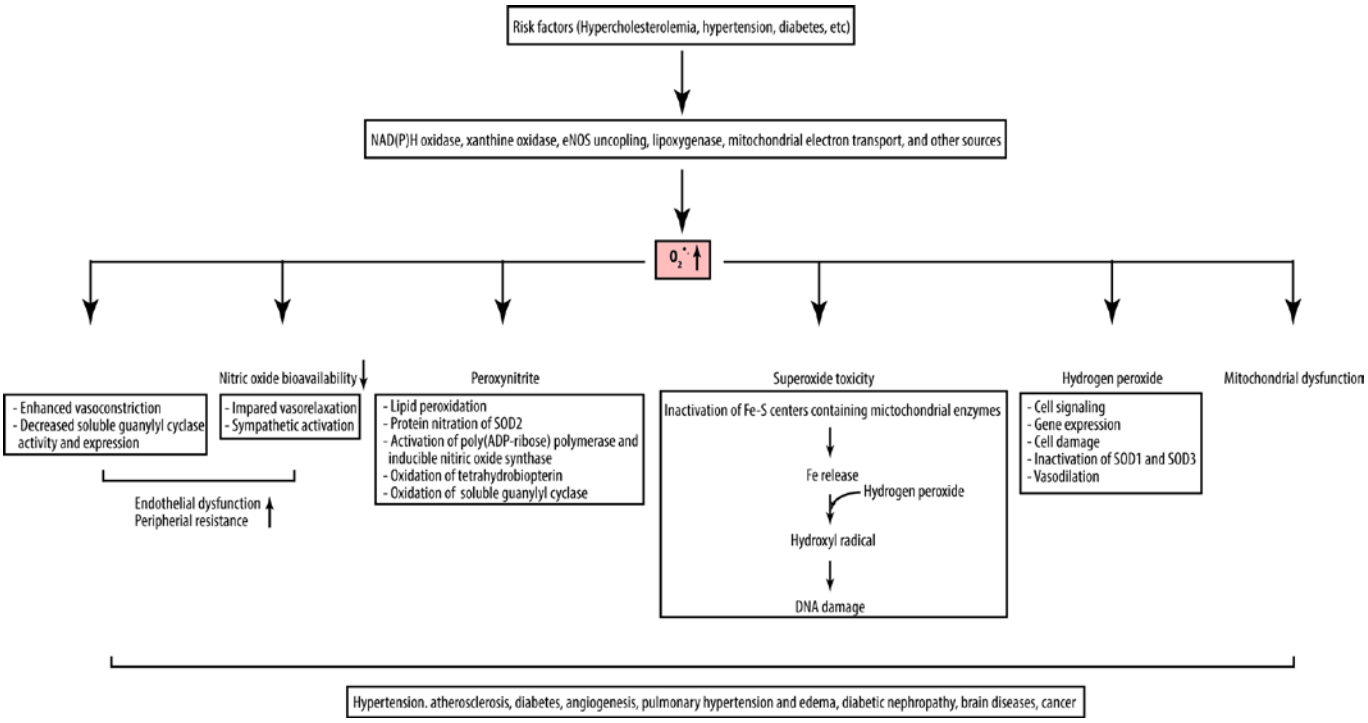

Figure 1.3 Production and role of superoxide radical ($O_2^{\cdot-}$) in pathological and physiological pathways. SOD1: superoxide dismutase localized in the cytosol, SOD2: superoxide dismutase localized in mitochondria matrix and SOD3: extracellular superoxide dismutase. Adapted from reference [32] with permission. Copyright (2011) by Mary Ann Liebert, Inc.

Few reports have developed a platform that encapsulates both enzymes acting as a tandem micro/nanoreactor rather than as an enzyme delivery vehicle to detoxify ROS (*i.e.*, in the micro/nanoreactor the enzymes are always confined and the substrate diffuses into the reactor in order to performed their enzymatic activity while in a delivery vehicle they are released for the enzymatic reaction to take place elsewhere).[30,52] However, all these SOD-CAT-containing reactors act intracellularly (resulting in promising results by improving cell viability upon ROS exposure), rather than extracellularly.

Some ROS (*i.e.*, H_2O_2) are able to cross the cell membrane while others (*i.e.*, $O_2^{\cdot-}$) are able to use the chloride channels to enter and exit the cells.[53] This means that, while the ROS are originally generated intracellularly they can easily escape the cell and reach distant organs (through the systemic circulation) leading to severe pathologies.[54] Therefore, the removal of ROS from the blood stream (extracellularly) is of outmost importance.

Inspired by the promising results obtained with the tandem activity of SOD-CAT in previous studies,[30,52] this PhD thesis presents a different approach for ROS detoxification, as proof of concept, by assembling a PDA-coated microreactor containing CAT-loaded liposomes. The principle relies on taking advantage of the SOD-like activity of a bioinspired polymer named PDA (*i.e.*, PDA possess several catechol groups which react with $O_2^{\cdot-}$ to yield H_2O_2 and a mix of products)[55] combined with the scavenging activity of CAT envisioned to act as an extracellular microreactor. By doing so, the delicate enzyme related work (*i.e.*, encapsulation and purification) is simplified while expanding the knowledge about PDA antioxidant activity towards the depletion of $O_2^{\cdot-}$ radical. Considering that PDA exhibits a structure similar to that of melanin, it shares some of its properties such as the antioxidant activity.[56] Although it has been previously shown that PDA particles are able to scavenge radicals *(i.e.*, 1,1-Diphenyl-2-picrylhydrazyl radical and 2,2-Azio-bis(3-ethylbenzthiazoline-6-sulfonic acid))[57,58] their antioxidant activity has not been extensively evaluated by means of their ability to scavenge the most dangerous ROS, named $O_2^{\cdot-}$ radical. In a very interesting study, Huang *et al*.,[59] coated selenium particles with PDA and demonstrated the antioxidant activity of PDA towards $O_2^{\cdot-}$ and $^{\cdot}OH$ and selenium particles towards H_2O_2 in test tubes, *in vitro* studies and *in vivo* studies using a lung inflammation model.

1.3 Developed multicompartment carrier: Building blocks

In this PhD thesis, a hydrogel-liposome complex coated with PDA and further functionalised with poly(*L*-lysine- grafted poly(ethylene glycol) (PLL-*g*-PEG) is designed, characterised an tested *in vitro* as a multicompartment carrier for dual-cargo drug delivery and extracellular microreactor (Figure 1.4). In the following sub-sections an in depth explanation of each building block is provided.

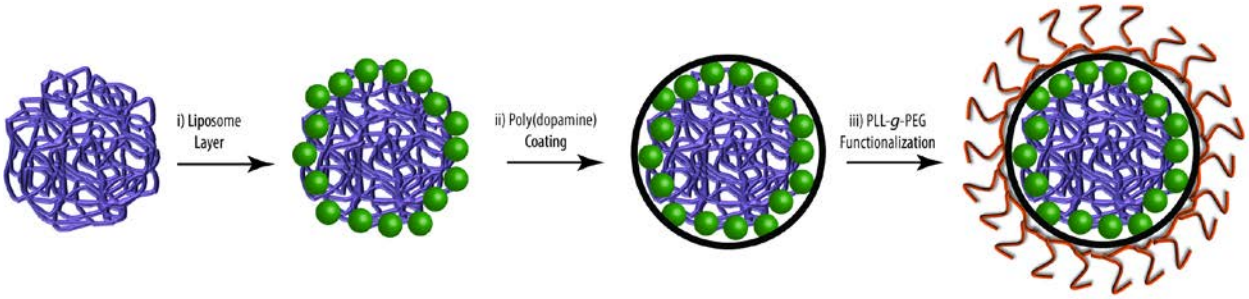

Figure 1.4 Schematic of the assembly of the multicompartment carrier. First a poly(*N*-isopropylacrylamide-*co*- acrylic acid) (P(NIPAM)-*co*-AAc) microgel is decorated with a liposome layer (i) through electrostatic interactions. Next, a poly(dopamine) (PDA) layer (ii) is deposited on the surface by self-polymerisation of dopamine. Finally, the PDA surface is functionalised with poly(*L*-lysine)-grafted poly(ethylene glycol (PLL-*g*-PEG) (iii) through covalent bonds between the *o*-quinones of the PDA and the amine groups of PLL. Adapted from reference [60] with permission. Copyright (2018) by Elsevier.

1.3.1 Poly(*N*-isopropylacrylamide) microgels

Poly(*N*-isopropylacrylamide) (P(NIPAM)) microgels (MGs) are the most investigated and well known MGs which were first reported in 1986.[61] The extensive usage of P(NIPAM) MGs in a wide range of fields such as drug delivery,[62] biosensors,[63] tissue engineering[64], and photonics[65] has attracted great attention over the years due to their several advantages such as simple synthesis,[62] ability to encapsulate hydrophobic and hydrophilic cargo,[66] and the possibility of being biodegradable depending on the cross linker used on their synthesis,[67] amongst others.

P(NIPAM)-*co*-AAc MGs are typically synthesised by precipitation polymerisation using persulfates (*i.e.*, potassium or ammonium persulfate (APS)) as initiators (Figure 1.5).[68] The synthesis is based on the fact that NIPAM monomers polymerise to form P(NIPAM) polymer chains upon reaction with the initiator (forming oligoradicals). Once the polymer chains have grown long enough they precipitate forming nuclei that can be stabilise by either the addition of stabilizing agents such as surfactants avoiding aggregation within the nuclei (which will lead to a smaller MG) or by continuous growing of the nuclei due to aggregation leading to larger MGs (this synthesis is known as surfactant free precipitation polymerisation) (Figure 1.5). The size can also be modified by controlling the decomposition rate of the initiators at different temperatures, meaning

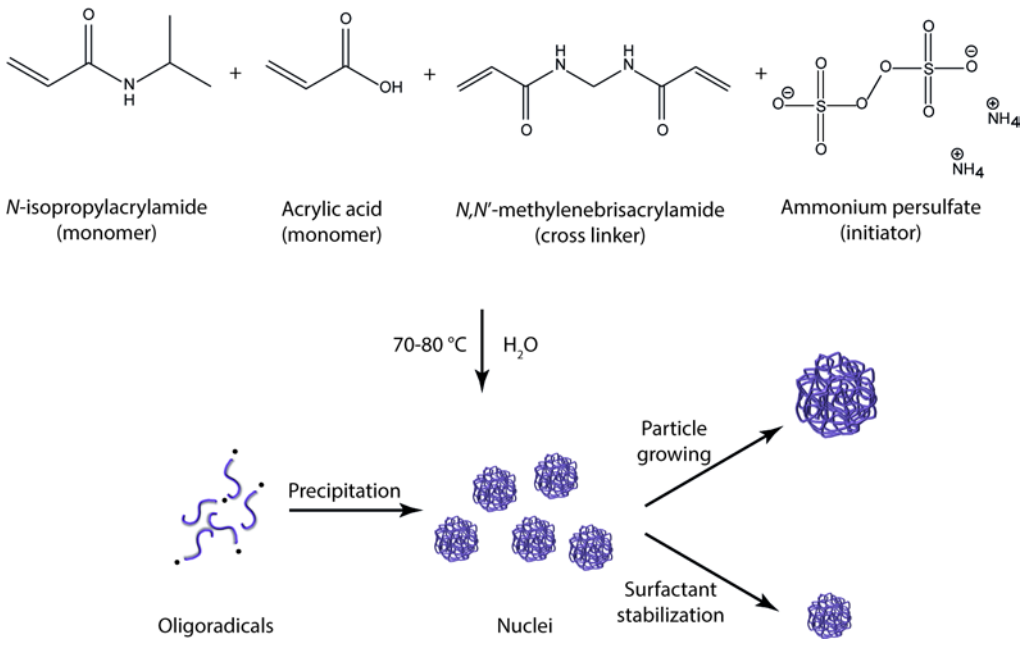

Figure 1.5 Schematic illustration of poly(N-isopropylacrylamide-*co*-acrylic acid) microgel (MG) synthesis using surfactant free precipitation polymerisation or precipitation polymerisation. The reaction starts with the generation of oligoradicals of monomers and cross linker upon reaction with the initiator following by their precipitation forming nuclei. These nuclei can grow to form larger MGs or can be stabilise to form smaller MGs.

that larger particles will result from lower temperatures as the initiator will decompose at a lower rate.[68]

The polymeric network is hold in place using a cross linker. Depending on the election of the cross linker the resulting MG can be biodegradable under the intracellular reducing environment (*i.e.*, using *N,N´*-bis(acryloyl)cystamine)[67] or not (*i.e.*, using *N,N'*-methylenebiscarylamide (BA)). Due to their straight forward synthesis, the possibility to fine-tune their size, their properties and their general fast release profile due to the large pores exhibited by the MGs, they are promising candidates for tandem release.[26]

1.3.2 Liposomes

Liposomes are spherical vesicles consisting of single or multiple phospholipid bilayers enclosing an aqueous core.[15] Due to their resemblance to cellular membranes the liposomes have been the material of choice for several applications (*i.e.*, drug delivery,

cosmetics, etc.).[2] Their membrane is formed by single (according to their size could be small, ~ 100 nm, large, ~200 nm – 800 nm[69] or giant, ~1-100 μm,[70] unilamellar vesicles) or multiple (multilamellar) phospholipid bilayer. Phospholipids are made of four components: fatty acids, glycerol or sphingosine backbone, a phosphate group, and an alcohol.[71] The fatty acids (tails) represent the hydrophobic part of the phospholipids while the glycerol, the phosphate group and the alcohol represents the hydrophilic part (head). This dual composition (hydrophobic and hydrophilic) confers amphiphilic properties to the phospholipids which is responsible for the self-assembly of the lipids into liposomes once they are exposed to aqueous media, orientating the head facing the water and the tails facing each other to avoid water interaction (Figure 1.6).[72]

Each phospholipid exhibits a specific transition temperature (also known as melting temperature or T_m) at which the phospholipids transition from solid-gel phase to liquid phase. In the solid-gel phase the lipid bilayer is tightly packed while in the liquid phase the lipid bilayer is disorganized increasing the permeability of the membrane.[73]

This temperature is highly affected by the nature of the hydrophilic groups, length of hydrocarbon chains (the longer the hydrocarbon chain the higher the T_m) and the degree of saturation of the hydrocarbon chains (saturated phospholipids have a higher T_m than unsaturated phospholipid with the same hydrocarbon chain length and hydrophilic group).[71]

Several techniques have been reported to assemble liposomes such as thin-film hydration, solvent injection, reverse-phase evaporation, sonication, etc. The thin-film hydration method is the most widely used to prepare liposomes. It consists in dissolving the lipids in an organic solvent (*i.e.*, chloroform), evaporation of the organic solvent to generate a thin-film of lipids followed by the hydration of the film with an aqueous solution containing the drug to be encapsulated. This simple and robust method, yields multilamellar liposomes that can be transformed into unilamellar liposomes by extrusion through a fixed pore membrane (small or large unilamellar liposomes can be obtained depending on the pore size) or by sonication (typically sonication yields small unilamellar liposomes). The solvent injection technique consists in the injection of lipids dissolved in ethanol into an aqueous phase leading to small unilamellar liposomes. Lastly, the addition of a detergent to

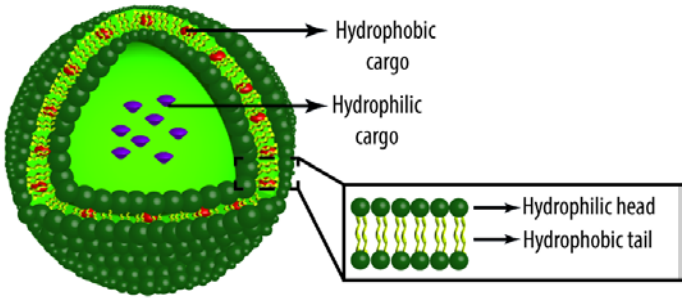

Figure 1.6 Schematic of the structure of a liposome.

the lipid mixture could also be used, followed by detergent dialysis leading to large unilamellar liposomes.[72] However, solvent injection and detergent are not suitable when the molecule to be encapsulated is an enzyme since it could lead to enzyme denaturation.

Due to the amphiphilic character of the phospholipids both hydrophobic and hydrophilic drugs can be encapsulated inside of the liposomes, in the membrane and in the core, respectively (Figure 1.6). The drug release from the liposomes can be controlled, by easily tailoring their compositions. For example, by increasing the temperature above the T_m (*i.e.*, using local hyperthermia or high intensity focused ultrasound) the drug release of a specific drug can be triggered at the target tissue since above T_m the membrane is more permeable.[74] The T_m can be easily tailored depending on the phospholipids that conform the liposome. The pH can also control the drug release since the pH sensitive liposomes are designed to be stable at physiological pH 7.4 while the phospholipid membrane is destabilised at acidic pH leading to the release of the encapsulated drug in tumours, endosomes and lysosomes)[75]. The liposomes can also respond to redox potential by including a disulfide bond in their composition that can be cleaved by intracellular glutathione which concentration is much higher in the cytosol, mitochondria and cell nucleus compared to blood, making possible to release the drug at specific places).[76] Lastly, specific enzymes overexpressed in the tumour environment (*i.e.*, secretory phospholipase A_2 and matrix metalloproteases, etc.) can also trigger the instability of the liposomes leading to drug release.[77]

All the versatile properties described above make the liposomes the most used platform in drug delivery field with multiple liposomal based drug approved for clinical use and several in clinical trials.[78] However, since liposomes possess some drawbacks such as low stability or lack of control over degradability,[79] surface modification of liposomes with polymers has emerged as the golden standard to enhance their stability.[80] While incorporating PEGylated lipids is the typical way to increase their circulation time by protecting the liposomes from the adhesion of plasma proteins and opsonins,[81] other strategies include the adsorption of chitosan, polysaccharides[82] or the sequential deposition of the interacting polymer pair consisting of PLL and poly(*L*-aspartic acid).[83] One of the most recent strategies in order to improve their stability is based on the liposome coating with PDA.[80]

1.3.3 Poly(dopamine)

PDA is a bioinspired polymer that in the last decade has attracted considerable interest.[84] Mussels are able to adhere to virtually any surface (inorganic and organic) due to the *mytilus* foot proteins-3 and -5 which exhibit high concentration of 4-dihydroxy-*L*-phenylalanine (DOPA), high catechol (3,4-dihydroxybenzene) amount and high content of primary and secondary amines by means of lysine and histidine residues. Therefore, the speculation that the combination of catechol and DOPA are essential for the mussel attachment led the researches to develop PDA as a simple and powerful tool for surface modification.[84]

The simplicity of the method relies on the self-oxidative polymerisation of DA into PDA under slightly basic pH (higher than 7.5) using the dissolved oxygen as oxidation agent and being able to attach onto virtually any type and shape of surface.[85] However, the polymerisation mechanism and the structure of PDA have been the centre of debate for years due to the different intermediates formed during the reaction.[42] Nevertheless, three main structures have been proposed in the last years (Figure 1.7).[42] The first theory suggests a covalent oxidative polymerisation of DA yielding PDA and a self-assembly trimeric complex formed by two molecules of unreacted DA and one molecule

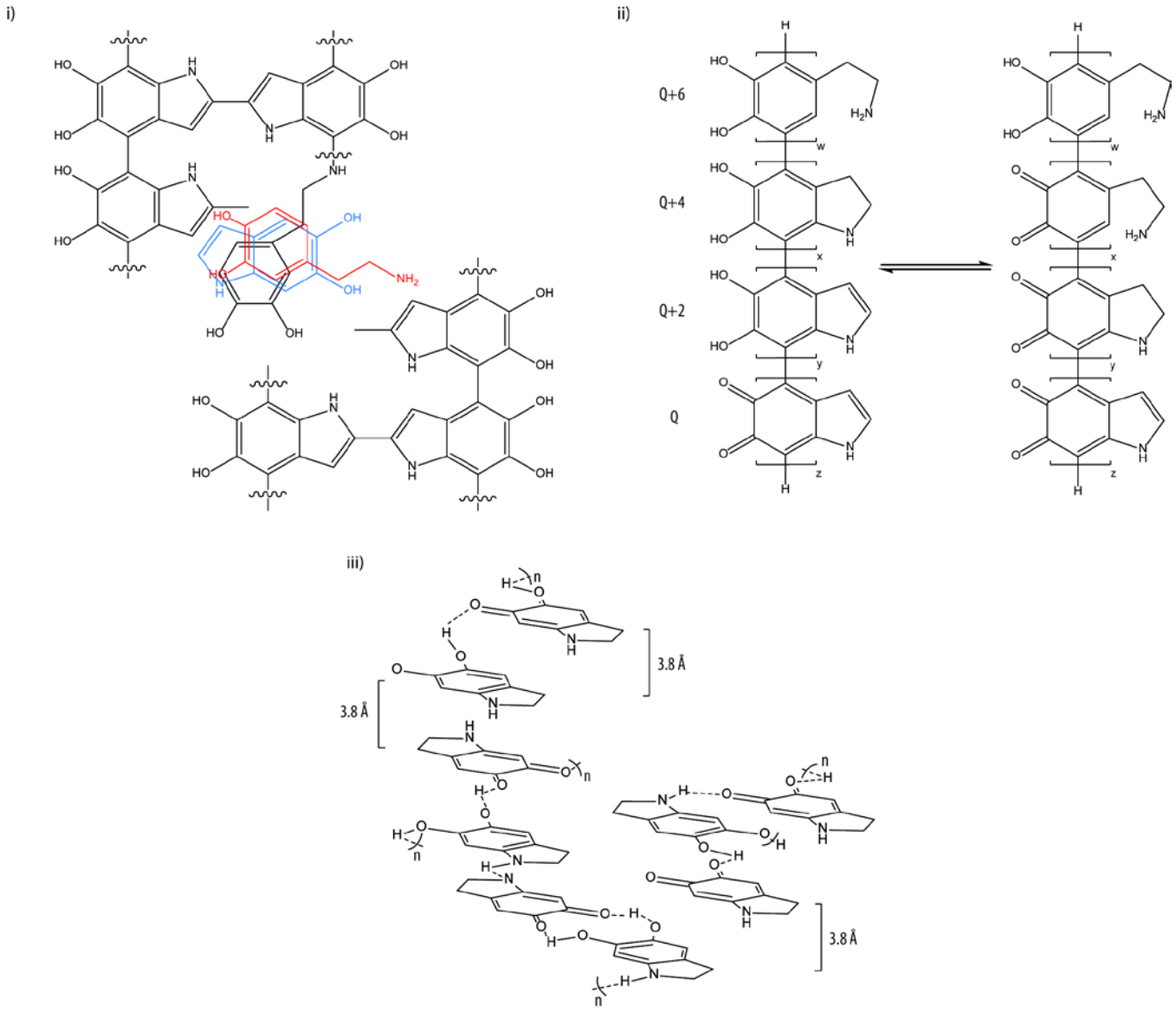

Figure 1.7 Suggested poly(dopamine) (PDA) structures in the last years. i) Covalent and non-covalent interactions between the trimeric complex and PDA. Reprinted with permission from reference [86], Copyright (2018) by John Wiley and Sons ii) Covalently linked dihydroxyindole and indoledione with different degrees of (un) saturation (*i.e.*, Q+6, Q+4, Q+2,Q). Reprinted with permission from reference[87], Copyright (2018) by American Chemical Society. iii) Aggregates of indole monomers held together by non-covalent interactions. Reprinted with permission from reference[88], Copyright (2018) by American Chemical Society.

of dihydroxyindole. Such complex is then incorporated within the PDA structure leading to a mixture of covalent and non-covalent interactions (Figure 1.7i).[86] The second theory proposes that the structure of PDA is based on a heteropolymer composed by covalently linked (C-C bonds between the benzene rings) dihydroxyindole and

indoledione units with different degrees of (un)saturation arranged in a parallel or anti-parallel manner through quinone-hydroquinone interactions (Figure 1.7ii).[87] Lastly, it has also been proposed that PDA is formed by aggregates of indole monomers (*i.e.*, dihydroxyindoline, indolinedione) and DA held together by intra- and interchain non-covalent forces such as Π-stacking, hydrogen bonding and charge transfer (Figure 1.7iii).[88]

The wide range of PDA applications such as antimicrobial surfaces,[89] tissue engineering,[90] bio imaging,[91] drug delivery,[92] biosensors,[93] among others,[42,85] are a consequence of the great advantages displayed by this material. Such advantages include biocompatibility,[42] biodegradation (PDA breaks down in acidic environments)[94], simple and less time consuming method to cover any surface compared to more labour-intensive methods such as the layer-by-layer technique (based on the deposition of sequential interacting polymers) that has been commonly used to assemble other multicompartment carriers,[11,12] and reactivity towards nucleophiles such as amines and thiols. The reactivity of the *o*-quinone groups present in the PDA structure renders this material with one of the most important properties which is the straightforward functionalisation of any surface with amine or thiol containing molecules through Michael and/or Schiff base reactions.[42]

This easy functionalisation has been exploited by attaching specific ligands on the surface of particles pre coated with PDA in order to target nano/microparticles, for example, to the folate receptor overexpressed in cancer cells,[95] integrin receptors overexpressed in macrophages and endothelial cells[21,95] or to confer the particles with antifouling properties by functionalisation with PLL-*g*-PEG.[21,96]

1.3.4 Poly(ethylene glycol)

As stated in the previous sub-section PDA can be easily functionalised, to confer the surface anti-fouling properties, using polymers such as PLL-*g*-PEG. First reported in 1977,[97] PEG is the most used polymer to confer stealth or antifouling properties highly needed in drug delivery carriers. Its use has been approved by the Food and Drug Administration (FDA) and the European Medicines Agency (EMA) in food, cosmetic and

pharmaceutical industries (Table 1.2 summarizes a list of PEGylated drug delivery carriers clinically approved or undergoing clinical trials).[98]

Name (Company)	Particle type	Application	Approval/Clinical trial
Doxil/Caelyx (Janssen)	Liposomal doxorubicin	Ovarian cancer, HIV-associated Kaposi´s sarcoma, multiple myeloma	Approved by FDA in 1995 and EMA in 1996
Onivyde MM-398 (Merrimack)	Liposomal irinotecan	Metastatic pancreatic cancer	Approved by FDA in 2015
PROMITIL (Lipomedix Pharmaceuticals)	Liposomal mitomycin-C	Solid tumours	Clinical trials phase I
MM-302 (Merrimack Pharmaceuticals)	HER2- targeted liposomal doxorubicin	Brest cancer	Clinical trials phase I,II and III
Nanocort (Enceladus in collaboration with Sun Pharma Global)	Liposomal Prednisolone	Rheumatoid arthritis and haemodialysis fistula maturation	Clinical trials phase II and III
BIND-014 (BIND Therapeutics)	PSMA targeted docetaxel PLGA particle	Prostate, metastatic non-small cell lung, cervical, head and neck, or KRAS positive lung cancers	Clinical trials phase I and II
NC-6004 Nanoplatin (Nanocarrier)	Polyamino acid, PEG, and cisplatin derivative micellar nanoparticle	Advanced solid tumour or lymphomas	Clinical trials phase I
NC-4016 DACH-Platin micelle (Nanocarrier)	Polyamino acid, PEG, and oxaliplatin micellar nanoparticle	Advanced solid tumours or lymphomas	Clinical trials phase I
RadProtect (Original BioMedicals)	PEG, iron, and amifostine micelle Transferrin-mediated	Dose escalation and	Clinical trials phase I

	chelation for amifostine release	safety for acute radiation syndrome	
AuroLase (Nanospectra Biosciences)	PEG-coated silica-gold nanoshells for near infrared light facilitated thermal ablation	Thermal ablation of solid primary and/or metastatic tumours	Clinical trials unknown phase
Cornell Dots	Silica nanoparticles with a NIR fluorophore, PEG coating and a ^{124}I radiolabelled cRGDY targeting peptide	Imaging of melanoma and malignant tumours	Clinical trials unknown phase

Table 1.2 Summary of poly(ethylene glycol) functionalised (PEGylated) drug delivery carriers clinically approved or undergoing clinical trials by 2016. HIV: Human immunodeficiency virus; HER2: Human epidermal growth factor receptor 2; PSMA: Prostate-specific membrane antigen; PLGA: Poly(lactic-*co*-glycolic acid); KRAS: Kristen Rat Sarcoma; NIR: Near infrared; cRGDY: Cyclic arginine-glycine-aspartic acid Adapted from reference [99] with permission. Copyright (2016) by John Wiley and Sons.

Once exposed to the human physiology, drug delivery carriers encounter multitude of proteins (*i.e.*, albumin, lipoproteins, apolipoproteins, proteins of complement, immunoglobulins, etc.) that can easily interact and bind to their surfaces influencing their circulation time in the body. The non-specific protein deposition can increase (opsonins) or decrease (dysopsonins) the removal of the particles by the mononuclear phagocyte system (MPS).[100] The MPS is a crucial line of defence that protects the body against foreign agents by rapidly eliminating them from the blood stream. It consists of dendritic cells, granulocytes, monocytes and tissue-resident macrophages in the liver, spleen and lymph nodes.[101]

Although albumin exhibits an initial dysopsonic effect, it can be easily replaced by other opsonins, such as apolipoproteins, leading to higher chances of being phagocytosed by the MPS cells. What is more, lipoproteins and apolipoproteins can displace phospholipids in the liposomal membrane leading to its destabilisation and therefore releasing the cargo prematurely. The proteins of the complement system can also increase the macrophage recognition particularly on charged, highly hydrophobic and irregular surfaces.[100] Therefore, the coating of the surface with biocompatible, inert, neutral, hydrophilic

polymers such as PEG would sterically hinder, depending on its length and density, the protein/surface interaction leading to an increase in circulation time (stealth properties).[101]

1.3.5 Hydrogel-liposome complexes

The hydrogel-liposome complexes represent a promising approach for controlled tandem release of the therapeutic cargo by combining two inherently different systems. Regarding the combination of P(NIPAM)-*co*-AAc MGs and intact liposomes to conceive a drug delivery platform that combines different kinetic release profiles, little has been reported. To date, the efforts have been focused on controlling the release kinetics of the liposomes by combining them with P(NIPAM)-*co*-AAc MGs rather than studying the system as a dual-cargo carrier. MacKinnon *et al*.,[102] assembled a hydrogel-liposome complex by binding liposomes, composed by 1-palmitoyl-2-oleoyl-phosphatidylcholine (POPC) and biotin- derived phosphatidylethanolamine, to biotinylated P(NIPAM)-*co*-AAc MGs through avidin-biotin conjugation. The authors showed that the liposomes remained intact upon binding with the MGs exhibiting a slow release of the fluorescent cargo over time at room temperature while, at high temperatures (~ 50 °C), the release was found to be slightly faster. However, such increase in release rate is expected to be due to thermal destabilisation of the liposomes rather than changes in size of MGs as response to the temperature since the volume phase transition temperature (VPTT, temperature above which the MGs shrink) is predicted to be quite high due to the high AAc content. In a follow up study, the authors modified the composition of P(NIPAM)-*co*-AAc MGs in order to decrease their VPTT and, thus, be able to evaluate the effect of MG changes, above VPTT, on the lipid bilayer integrity. However, the control over the release kinetics of the liposomes was not investigated.[103] A more recent study reports the immobilization of liposomes, consisting of 1,2-dipalmitoyl-*sn*-glycero-3-phosphocholine (DPPC), inside a poly (2-methacryloyloxyethyl phosphorylcholine) particle´s matrix. This approach allows controlling the release kinetics of a drug from the liposomes by controlling the matrix viscosity leading a slow and sustained release.[104] On the other hand, a solitary study investigates the suitability of hydrogel-liposomes complexes composed by P(NIPAM)-*co*-AAc MGs and liposomes (made of POPC and functionalised with 3-O (2-

aminoethoxyethyloxyethyl)-carbamoyl cholesterol) as dual-drug carriers.[26] The authors demonstrated that the liposomes structure is not compromised upon binding to the MGs and that the liposomes exhibited a slower release of the fluorescent cargo compared to the MGs release kinetics regardless of the temperature.

1.4 Influence of shear stress on carrier-cell interaction

So far, this introductory chapter has covered the different multicompartment carriers, applications and building blocks of the multicompartment carrier presented in this PhD thesis. Nevertheless, a crucial aspect to be considered when designing a drug delivery vehicle and/or a microreactor is the dynamics of the human physiology. Once entering into the body the carrier and/or microreactor is exposed to the fluids of the body. Therefore, it is not only important to investigate its interaction with the fluid components (*i.e.*, proteins) and cell populations (*i.e.*, endothelial cells lining the blood vessels, circulating macrophages or target cells) but also how this interaction and its efficacy is affected by the dynamics of the blood flow and/or the interstitial fluid flow in case it is designed to reach tumour tissue.

Among the mechanical forces exerted as consequence of the dynamic environment (Figure 1.8), the impact of shear stress (force experienced by the cells due to friction of fluid across their surface)[105] has been extensively investigated in endothelial cells[106] and with less extent in cancer cells.[107]

So far, most of the studies have been focused on morphology changes, receptor expression, cell function, vasculature remodelling, vascular diseases (*i.e.*, atherosclerosis), cell migration, metastasis, etc.[106,107] However, the study of cell-carrier interaction under the presence of shear stress is not commonly considered in the *in vitro* set-ups.

In the last few years, it has been shown that shear stress has great influence on the cell-carrier interaction in terms of therapeutic efficacy,[108] carrier cytotoxicity,[109] PEGylation effect,[96] targeting efficiency,[21,110] cellular uptake[109] and cellular

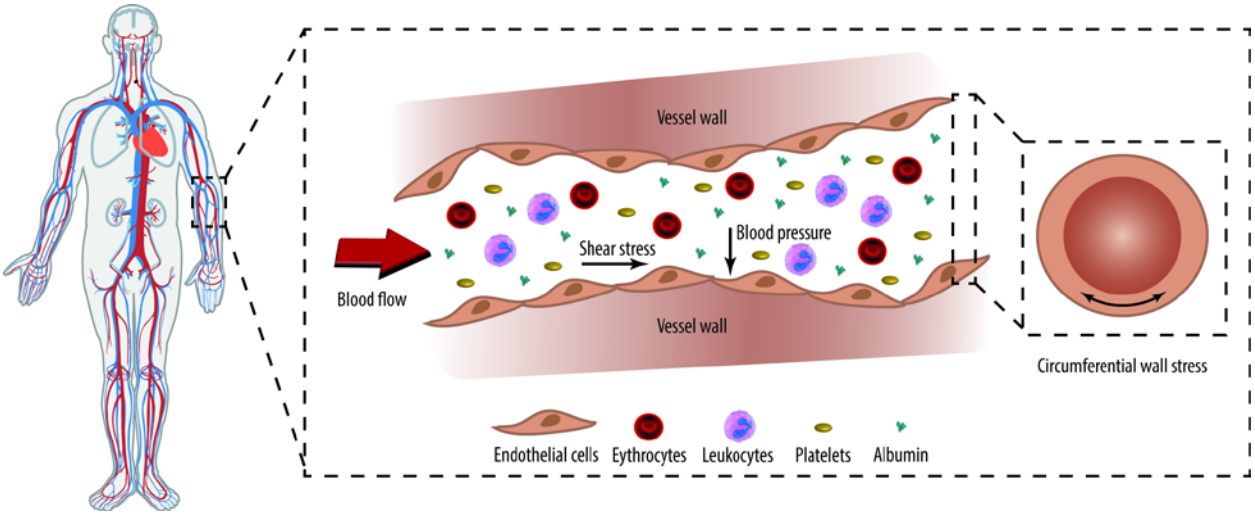

Figure 1.8 Major mechanical forces due to blood flow. Shear stress is the force resulting from the friction of the parallel blood flow and the cellular surface, the blood pressure is the force applied perpendicular to the vessel wall and the circumferential wall stress results from the stretching of the vessel wall as consequence of the pressure gradient across the vessel wall.[111]

uptake pathway [112,113] This influence is a consequence of cellular morphology changes in cells cultured under shear stress, changes in the diffusion of the carrier towards the cells and different dispersion of the carrier compared to the gravitational settling of the static cultures.[109] Unfortunately, these effects vary depending on the size, particle type, charge, magnitude of shear stress, functionalisation and cell type, meaning that the effect of shear stress must be carefully evaluated for each specific carrier and cell line.[109,114]

Considering that the field of drug delivery has been extensively investigated for decades but only few formulations have been able to reach the market, the translation of *in vitro* to preclinical studies could potentially benefit from *in vitro* set-ups that better mimic *in vivo* conditions such as the inclusion of shear stress.

Chapter II Aims of the thesis

The focus of this PhD thesis is the assembly and characterisation of a multicompartment carrier in the submicron range able to act as a dual-cargo vehicle and as an extracellular microreactor in order to scavenge ROS which are associated with severe vascular diseases. The results presented in this PhD thesis aim to represent a step forward in the multicompartment carriers field and help to expand the knowledge of hydrogel-liposome complexes.

The three main objectives of the present PhD thesis are:

i) The development of a multicompartment carrier in the submicron range (**Chapter 3**)

ii) To prove its potential as a dual-cargo carrier with different release profiles which could be beneficial for diseases where a cocktail of drugs is necessary (*i.e.*, cancer, immune-associated diseases, type 2 diabetes or rheumatoid arthritis). And, to demonstrate the importance of including shear stress on *in vitro* set ups by evaluating its influence on protein deposition and PEGylation effect upon incubation with relevant cell lines macrophages (RAW 264.7), endothelial cells (HUVEC) and cancer cells (HeLa) and cellular uptake pathway (**Chapter 4**)

iii) To prove its functionality as a microreactor able to scavenge the most dangerous ROS named $O_2^{\cdot -}$ by combining the SOD-like activity of PDA and the scavenging activity of CAT-loaded liposomes (**Chapter 5**)

To achieve the aforementioned objectives a number of aims have been set:

i) To identify a suitable MG size (with a diameter of 700 nm or 350 nm) in terms of colloidal stability, PEGylation effect and facile assembly.

ii) To characterise and optimise the multicompartment carriers assembly regarding the amount of lipids per MG core, PDA deposition, liposomal integrity and PEG coating to confer stealth properties (*i.e.*, PEGylation effect) and storage stability.

iii) To evaluate the application of the chosen multicompartment carrier as a dual-cargo vehicle by encapsulation of model molecules in the core of the MGs and liposomes followed by the study of the release profile of each molecule

iv) To study the influence of physiologically relevant shear stress conditions on the PEGylation effect by means of protection against relevant protein deposition (*i.e.*, immunoglobulin G and albumin)

v) To evaluate the influence of shear stress on the PEGylation effect upon incubation with three relevant cell lines: macrophages (RAW 264.7), endothelial cells (HUVEC) and cancer cells (HeLa).

vi) To elucidate the influence of shear stress on the cellular uptake pathway followed by non-functionalised and functionalised multicompartment carrier upon incubation with RAW 264.7, HUVEC and HeLa cells using chemical inhibitors.

vii) To encapsulate active CAT inside liposomes, followed by purification and quantification of the encapsulated protein

viii) To prove the CAT reactivity upon microreactor assembly together with the SOD-like activity of PDA (in both, non-PEGylated an PEGylated assemblies)

ix) To evaluate the recyclability of both CAT and PDA (in both, non-PEGylated an PEGylated assemblies)

Chapter III Assembly and Characterisation of Multicompartment carriers

Summary

This chapter involves the development of a multicompartment carrier consisting of P(NIPAM)-*co*-AAc MGs as a core decorated with unilamellar liposomes. The whole assembly is then protected by a PDA layer that can be further functionalised with PLL-*g*-PEG to confer anti-fouling properties to the system. For this, two different diameter-sized MGs (*i.e.*, small and large) will be tested for its suitability as the core of the multicompartment carrier in terms of colloidal stability upon optimisation of the amount of liposomes per MG, PDA coating and surface functionalisation. For this different techniques were used, including flow cytometry, dynamic light scattering (DLS), ξ-potential measurements, scanning electron microscopy (SEM) images, differential interference contrast (DIC) microscopy images and quartz crystal microbalance with dissipation monitoring (QCM-D) measurements. Importantly, the *in vitro* performance, by means of PEGylation effect, is evaluated upon incubation with three relevant cell lines namely RAW 264.7 (macrophages), HUVEC (endothelial) and HeLa (model cancer) cells.

The results concerning the larger MG have been adapted from the following publication:

York-Duran, M. J; Ek, P. K.; Godoy-Gallardo M.; Hosta-Rigau L. Shear stress regulated uptake of liposome-decorated microgels coated with a poly(dopamine) shell. *Colloids Surf., B* **2018**, 171, 427-436.

3.1 Introduction

The development of carriers containing multiple compartments has gained great attention over the years due to their large potential as biomedical tools. Aiming to expand the applications of the classical architectures (*i.e.*, liposomes, polymersomes, capsules), the combination of building blocks, of the same or different nature, opens the possibility to approach some diseases in a more efficient way.

Although the most investigated multicompartment systems to date are composed of building blocks of the same nature (*i.e.*, liposomes-in-liposomes, polymersomes-in-polymersomes and capsules-in-capsules) a more interesting alternative has emerged by combining building blocks of different nature (*i.e.*, polymersomes-in-liposomes, polymersomes-in polymer capsules, cubosomes-in-polymer capsules and capsosomes) since the latter strategy allows to join advantages while minimizing the drawbacks.[2]

The majority of the multicompartment systems developed so far are in the micron range[9,115–124] which limits their *in vivo* application and therefore, their therapeutic potential. For example, upon intravenous injection the particles are first subjected to the lung capillaries selection filter. With a diameter between 2-15 μm, only particles smaller than 3 μm are able to circulate through the lung capillaries and therefore circumvent pulmonary retention, reaching the systemic circulation.[100]

Therefore, aiming to develop a multicompartment system with a final diameter below the micron range, two different MGs with different diameters (*i.e.*, ~700 nm, MG_{700} and ~ 350 nm, MG_{350}) are evaluated as the core.

For this, the carrier is assembled by the deposition of positively charged unilamellar liposomes onto the negatively charged surface of P(NIPAM)-*co*-AAc MGs (Scheme 3.1). Next, the liposomes are protected from rupture and displacement by the polymerisation of DA creating a layer of PDA onto the MG/L surface. Depending on the desired application, the functionalisation of the carrier´s surface is crucial (*i.e.*, targeting or long circulating properties). In this PhD thesis, the PDA layer is easily functionalised with PLL-*g*-PEG conferring the carrier antifouling properties.

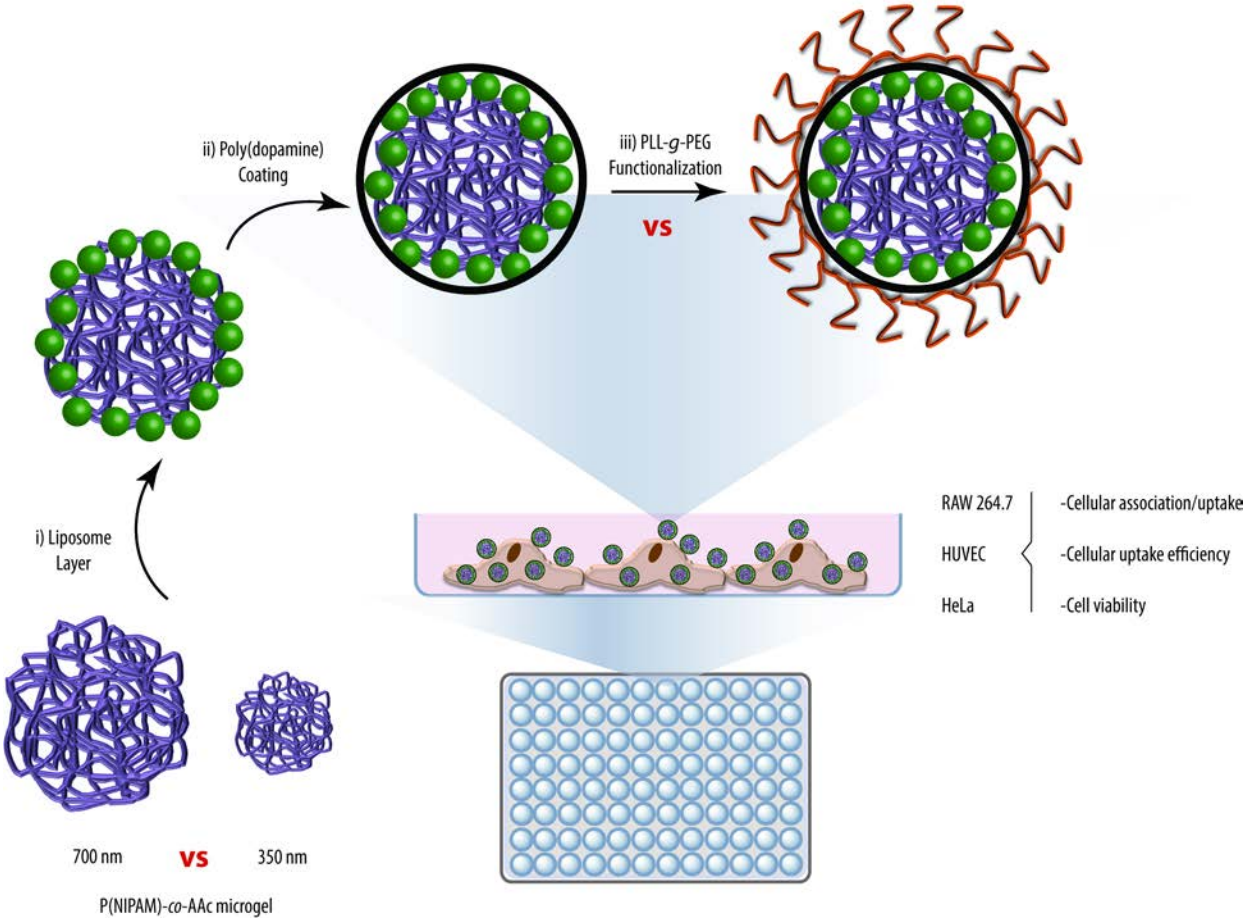

Scheme 3.1 Schematic of the assembly of the multicompartment carrier. First a poly(*N*-isopropylacrylamide-*co*- acrylic acid) (P(NIPAM)-*co*-AAc) microgel (with a diameter of 700 nm or 350 nm) is decorated with a liposome layer (i) through electrostatic interactions. Next, a poly(dopamine) (PDA) layer (ii) is deposited on the surface by self-polymerisation of dopamine. Finally, the PDA surface is functionalised with poly(*L*-lysine)-grafted poly(ethylene glycol (PLL-*g*-PEG) (iii) through covalent bonds between the *o*-quinones of the PDA and the amine groups of PLL. The PEGylation effect of non-functionalised and functionalised carrier is evaluated in terms of cellular association/ uptake, cellular uptake efficiency and cell viability upon incubation with macrophages (RAW 264.7), endothelial cells (HUVEC) and cancer cells (HeLa). Adapted from reference [60] with permission. Copyright (2018) by Elsevier.

It is worth to note that each selected building block offers different advantages to the overall system. The P(NIPAM)-*co*-AAc MGs are a well-known hydrogel with a simple preparation method,[62] that offer the possibility to encapsulate hydrophilic and hydrophobic cargo[66] while being biodegradable by choosing the appropriate cross

linker.[67] The liposomes have been the other material of choice due to its extensive use in different fields such as drug delivery and cosmetics due to their biocompatibility [2] and ability to encapsulate both hydrophobic and hydrophilic cargo. What is more, their composition is easily tailored, and they offer protection to the fragile cargo (*i.e.*, model molecules and enzymes) while allowing small molecules (*i.e.*, substrates and products) to diffuse across their membrane (if they are exposed to a temperature higher than their T_m) which is particularly important when they are use as reactors.[125] The PDA offers both, protection to the compartments and straightforward functionalisation with amine and thiols due to the presence of *o*-quinones in its structure. PDA is also biodegradable and offers an effortless assembly of the carrier compared to other techniques such as LbL due to its ability to self-polymerise under slightly basic pH and cover virtually any surface.[42,85] Finally, the steric hindrance towards blood and plasma protein deposition on the carrier surface offered by PEG, together with its biocompatibility make this polymer an ideal tool to increase the circulation time *in vivo*.[101]

Herein, a thoroughly characterisation and optimisation of the assembly is presented followed by the evaluation of the PEGylation effect of both MGs (*i.e.*, MG_{700} and MG_{350}) with relevant cell lines, macrophages (RAW 264.7) which are the first line of defence of the human body against pathogens, endothelial cells (HUVEC) which cover the interior surface of the blood vessel and a model cancer cell line as a therapeutic target (HeLa).

3.2 Materials and Methods

3.2.1 Materials

NIPAM, AAc, BA, APS, sodium dodecyl sulfate (SDS), tris(hydroxymehtyl)aminomethane (Tris), sodium chloride (NaCl), 4-(2-hydroxyethyl) piperazine-1-ethane-sulfonic acid (HEPES), dopamine hydrochloride, chloroform anhydrous (> 99%), phosphate buffered saline (PBS), Dulbecco´s Modified Eagle´s Medium-high glucose (DMEM D5796), sodium pyruvate, penicillin/streptomycin, fetal bovine serum (FBS), [2-(2-methoxy-4-nitrophenyl)-3-(4-nitrophenyl)- 5-(2,4-disulfophenyl)-2H-tetrazolium monosodium salt] (WST-8) counting cell kit,

adenocarcinoma cell line HeLa and endothelial cell line HUVEC were purchased from Sigma-Aldrich (Saint Louis, MO, USA). POPC, 1-palmitoyl-2-oleoyl-*sn*-glycero-3-ethylphosphocholine (chloride salt) (POEPC), 1-myristoyl-2-[12-[(7-nitro-2-1,3-benzoxadiazol-4-yl)amino]dodecanoyl]-*sn*-glycero-3-phosphocholine (NBD-PC) were obtained from Avanti Polar Lipids (Alabaster, AL, USA). Poly(*L*-lysine (20 kDa))- graft [3.5]-poly(ethylene glycol (2 kDa)) (PLL-*g*-PEG) was obtained from SuSoS AG (Dübendorf, Switzerland). Endothelial Growth Medium-2 Bullet kit (EGM-2) was purchased from Lonza (Basel, Switzerland). The EGM-2 is composed of Endothelial Basal Medium (EBM), human epidermal growth factor (hEGF), vascular endothelial growth factor (VEGF), R3-insulin-like growth factor-1 (R3-IGF-1), ascorbic acid, hydrocortisone, FBS, human fibroblast growth factor-beta (hFGF-β), heparin and gentamicin/amphotericin-B (GA). The macrophage cell line RAW 264.7 was obtained from European Collection of Authenticated-Culture Collections (ECACC, Wiltshire, UK). Tris 1 buffer is composed of 10 mM Tris (pH 8.5); Tris 2 is composed of 10 mM Tris and 150 mM NaCl (pH 7.4); HEPES is composed of 10 mM HEPES and 150 mM NaCl (pH 7.4). All buffers were made with ultrapure water (Milli-*Q*, gradient A 10 system, TOC < 4 ppb, resistance 18 MV cm, EMD Millipore, USA).

3.2.2 Methods

3.2.2.1 MGs synthesis and characterisation

The MG_{700} were synthesised by surfactant free precipitation polymerisation (Figure 1.5, Chapter 1).[68] First, the monomers were purified in order to remove any potential impurities that could affect the polymerisation. NIPAM was recrystallised in n-hexane while AAc was purified by filtration through an aluminium oxide column. Upon purification, the monomers and cross-linker (3.97 mmol NIPAM, 0.69 mmol AAc and 0.097 mmol BA) were dissolved in 30 mL Milli-*Q* and filtered through 0.22 µm cellulose acetate filters into a 100 mL three-neck round-bottom flask equipped with an argon inlet and outlet. Upon purging the reaction mixture with an argon flow for 1 h at 80 °C and 1000 rpm stirring speed, the polymerisation was initiated by addition of 0.024 mmol APS

and allowed to proceed overnight under argon atmosphere at 80 °C. For purification, the turbid product was first filtered through glass wool and purified by five centrifugation cycles at 6 °C (17 100 g, 45 min) using a Thermo Scientific SL16R high speed centrifuge.

The MG_{350} were synthesised using the precipitation polymerisation technique employing surfactants to stabilise the nuclei and therefore promote the formation of small MG (Figure 1.5, Chapter 1).[126] Specifically, 3.97 mmol of recrystallised NIPAM, 0.69 mmol AAc, 0.097 mmol BA and 0.069 mmol SDS were dissolved in 74 mL Milli-*Q* water followed by filtration into a 250 mL three-neck round-bottom flask equipped with an argon inlet and outlet. Next, the reaction mixture was purged with argon for 1 h at 70 °C and at stirring rate of 450 rpm. The reaction was initiated by the addition of APS (0.105 mmol dissolved in 1.5 mL Milli-*Q*) and allowed to proceed overnight under argon atmosphere at 70 °C. Finally, the product was purified for seven days by dialysis against Milli-*Q* water in order to remove monomers, oligomers and surfactant.

The size, polydispersity (PDI) and ζ-potential of the MG_{350} and MG_{700} were determined by dynamic light scattering (DLS), using a ZetaPALS ζ-potential analyser (Brookhaven Instruments Corporation, Holtsville, NY, USA), adding 100 µg of MG_{700} or MG_{350} to Tris 1 buffer (2 mL) or to Milli-*Q* water (1.5 mL).

The concentration of the MG suspension was determined by weighting out several freeze-dried aliquots.

3.2.2.2 Liposomes assembly and characterisation

The liposomes were assembled by the lipid film hydration method.[72] Specifically, 1.75 mg POPC and 0.75 mg POEPC were dissolved in chloroform followed by the formation of the lipid film using a nitrogen flow. Next, the lipid film was exposed to vacuum for at least 1 h in order to completely evaporate the organic solvent. Upon rehydration in Tris 1 buffer (1 mL), the 3.2 mM liposomes solution was extruded through 50 nm nucleopore polycarbonate filters (drain disc 10 mm PE, Whatman, Maidstone, UK) 11 times at room temperature in order to yield unilamellar empty liposomes (L). To prepare fluorescently labelled liposomes (L^F), 2 wt% of NBD-PC was added to the lipid mixture prior to the lipid

film formation. The size and PDI of the liposomes (L, L^F) was determined by DLS and their charge by ζ-potential measurements. Only L and L^F, with a PDI below 0.14 were used for the experiments.

3.2.2.3 Optimisation of the amount of liposomes per MG

In order to optimise the amount of liposomes per MG (MG_{700} and MG_{350}), a suspension of 479 µg of MG_{700} or MG_{350} was washed 2× in HEPES buffer for 15 min at 13 500 rpm, using a bench top centrifuge (MiniSpin, Eppendorff, AG, Germany). Due to the small size and low density of MG_{350}, the washing steps were performed in an amicon Ultra centrifugal filter (100 kDa). Next, the MGs were incubated with increasing amounts of L^F keeping the total volume constant for 1.5 h at room temperature in a tube rotator. Upon incubation, the MG_{700} suspension was washed 2× in HEPES buffer for 6 min at 10 000 rpm while the MG_{350} suspension was diluted 20 times in order to minimize further interaction between MG_{350} and L^F. Finally, the saturation of the MGs surface by L^F deposition was monitored by flow cytometry using a BD Accuri C6 flow cytometer (BD Biosciences, Sparks, MD, USA) equipped with a 488 nm laser and an emission detection of 530 nm. At least 20 000 events were recorded and two independent experiments were carried out.

3.2.2.4 Assembly of multicompartment carriers

The non-PEGylated carriers (MG/L/PDA) were prepared by washing a suspension containing 958 µg MG_{700} or 1916 µg MG_{350} in Tris 1 buffer for 14 min at 8500 rpm followed by incubation with liposomes (L, L^F) (0.25 mg or 0.35 mg lipids, respectively) for 1.5 h at room temperature in a tube rotator. Next, in order to coat the MG/L surface with PDA the suspension was concentrated to a volume of 100 µL followed by exposure to a DA solution in Tris 1 buffer (1 mg mL^{-1} or 2 mg mL^{-1} for MG_{700} or MG_{350}, respectively) for 16 h at room temperature in a tube rotator. Finally, the unreacted DA and PDA were washed away by 2× washing cycles in Tris 2 for 7 min at 10 000 rpm for the MG_{700} assemblies or 12 min at 13 000 rpm for the MG_{350} assemblies. In order to decrease the material loss all the steps before PDA deposition were performed in an amicon ultra centrifugal filter (100 kDa).

3.2.2.5 DIC and fluorescence microscopy

The DIC images and fluorescent images of the carrier were taken with an Olympus Inverted IX83 microscope equipped with a 60× oil-immersion objective. The diameter of the MG and MG/L/PDA particles was determined measuring at least 200 particles making use of an imaging software (Image J) using at least five independent images per sample.

3.2.2.6 SEM images

The samples were first coated with gold (0.9 nm thickness) using a Q150T ES Turbo-Pumped Sputter Coater (Quorum Technologies, UK) for MG_{700} and a Cressington 208HR High Resolution Sputter Coater (Cressington Scientific Instruments Ltd., UK) for MG_{350}. The samples were imaged using a FEI Quanta 200 ESEM FEG Scanning Electron Microscope (FEI-Company, USA) at an accelerating voltage of 5 kV and working distance of 22.9 mm for MG_{700} and 20 kV and 9.6 mm for MG_{350} (at least six images were acquired per sample).

3.2.2.7 Surface functionalisation

For the PEGylated carriers (MG/L/PDA/PEG), the MG/L/PDA suspensions (4.8 mg mL^{-1} MG_{700} or MG_{350}) were incubated with PLL-*g*-PEG 1 mg mL^{-1} , 5 mg mL^{-1} or 7 mg mL^{-1} in Tris 1 for 1 h at room temperature in a tube rotator, followed by washing the PLL-*g*-PEG excess by 2× washing cycles in Tris 2 in the case of MG_{700} (7 min, 10 000 rpm) or by 3 h dialysis against Tris 2 in the case of MG_{350}.

3.2.2.8 QCM-D measurements

QCM-D is a highly sensitive technique that measures changes in mass down to the nanogram scale in real-time. Briefly, its principle is based on the oscillation of a piezoelectric quartz-crystal, situated between two electrodes, at its resonance frequency by applying an AC voltage.[127] The changes in the frequency (Δf) of oscillation are related to the changes of mass on the crystal surface, meaning that a decrease in Δf translates into mass being adsorbed onto the crystal's surface. This Δf/mass relationship is

described as linear by the Sauerbrey equation (Equation 3.1) only when the deposited mass is a rigid layer, meaning that the equation is violated by the layers containing high amount of water due to the damping of the crystal oscillation.[128] In order to describe highly hydrated systems (*i.e.*, considering the viscosity) an extra parameter is necessary, this parameter is known as dissipation change (ΔD). ΔD is determined by measuring the energy dissipation from the crystal by means of the decay rate of the oscillation after the AC voltage is turned off.[127] Therefore, rigid films will exhibit a low ΔD while soft films (*i.e.*, liposomes) will exhibit a high ΔD.[127] It is worth mentioning that in this PhD thesis both Δf and ΔD are used to qualitatively asses the assembly of the carrier (*i.e.*, to confirm the binding of each layer and the integrity of the liposomes). Mass quantification is out of the scope of this PhD thesis.

$$\Delta m = -C \frac{\Delta f}{n}$$

Equation 3.1 Sauerbrey equation. Δm: mass adsorbed; C: mass sensitivity constant = ~17.7 nm cm^{-2} Hz^{-1} for a 5 MHz quartz crystal. n: number of overtones = 1,3,5, etc.[128]

The assembly of the carrier on a planar set up was assessed by monitoring the deposition of the layers on a silica crystal (QSX300, Q-sense) using a Q-sense E1 instrument (Biolin Scientific, Sweden). The crystals were first cleaned by rinsing with ethanol and blow-drying with compressed air followed by plasma treatment. Except when indicated otherwise, the layer deposition was performed at 0.2 mL min^{-1} flow rate.

Due to the negatively charged surface of the MG_{350} a positively charged layer was first deposited onto the silica crystals. For this, upon Tris 1 buffer baseline stabilisation, a PLL solution (1 mg mL^{-1} in Tris 1) was injected into the flow module and allowed to reach saturation. Next, the unbound PLL was washed away with Tris 1 buffer until baseline stabilisation. A suspension of MG_{350} (7.2 mg mL^{-1} in Tris 1) was then injected to the flow module for 35 min until surface saturation. Similar to PLL, the excess of MG_{350} was washed away with Tris 1 buffer until the baseline stabilisation was achieved. The negatively charged MG_{350} layer was exposed to a positively charged liposome solution (2.5 mg mL^{-1}) for 40 min, reaching saturation and followed by a washing step. For the PDA coating, the flow rate was

decreased to 0.05 mL min^{-1} and a DA solution was loaded in the flow module for 1 h. The short DA polymerisation time was chosen to avoid potential clogging of the chambers. In order to ensure the availability of enough DA monomers on the surface, a freshly prepared DA solution was loaded after 30 min of incubation.[14] The surface was functionalised with a PLL-*g*-PEG solution (1 mg mL^{-1} in Tris 1) reaching surface saturation. The experiments were carried out at 23 ± 0.02 °C. Normalised Δf and ΔD values using the third harmonic are reported. At least two independent experiments were carried out.

3.2.2.9 Cell experiments

The adenocarcinoma HeLa and mouse macrophage RAW 264.7 cells lines were cultured in DMEM supplemented with 2% (v/v) HEPES, 1% sodium pyruvate, 10% (v/v) FBS and 1% (v/v) penicillin/streptomycin (10 000 U/mL and 10 µg/mL, respectively) at 37°C in a humidified incubator with 5% CO_2 level. The endothelial HUVEC cell line was cultured in EBM-2 supplemented with 0.1% (v/v) hEGF, 0.1% (v/v) VEGF, 0.1% (v/v) R3-IGF-1, 0.1% (v/v) ascorbic acid, 0.04% (v/v) hydrocortisone, 0.4% (v/v) hFGF-β, 0.1% (v/v) heparin, 2% (v/v) FBS and 0.1% (v/v) GA. The cell media was renewed every 2-3 days and only passages between 14-20, 3-9 and 1-4 of HeLa cells, RAW 264.7 cells and HUVEC cells were used in all the experiments. The cells were allowed to proliferate up to ~80% confluency before being detached from the culture flask using trypsin (3 mL, 0.5 mg mL^{-1}) in the case of HeLa and HUVEC cells and a cell scraper for RAW 264.7 cells. Next, the trypsin was removed by centrifugation (1000 rpm, 5 min) and the cells were resuspended in new cell culture media.

In order to ensure that the cells are exposed to the same amount of carrier, the concentration of the carrier solution was determined by fluorescence measurements of MG/L^F/PDA or MG/L^F/PDA/PEG followed by serial dilutions to achieve the desired concentration. At least three independent experiments were carried out and the data was analysed using one-way ANOVA with a confidence level of 95% ($\alpha = 0.05$) followed by Tukey´s multiple comparison posthoc test (*$p \leq 0.05$; **$p \leq 0.01$; ***$p \leq 0.001$; ****$p \leq 0.0001$) in a GraphPad Prism 7 software.

3.2.2.10 Cell viability

The maximum amount of carriers that can be administered to the cells without generating cytotoxicity was determined by seeding 30 000 cells (RAW 264.7) or 15 000 cells (HeLa or HUVEC) in 96-well plate in 200 µL of cell culture media and allowed to attach to the surface of the wells for 24 h at 37°C, 5% CO_2. Next, the cells were incubated with increasing amounts of carrier per cell (MG_{700}/L/PDA or MG_{350}/L/PDA) in 200 µL cell culture media for 4 h at 37°C, 5% CO_2 followed by washing 2× in 200 µL pre-warmed PBS and 1× in a solution containing cell culture media: WST-8 kit reagent (1:10) in order to remove the non-associated/internalised carriers. Upon washing, the cells were incubated with 100 µL cell culture media and 10 µL WST-8 kit reagents for 70 min at 37 °C, 5% CO_2. Finally, 100 µL were transferred to a new 96-well plate and the formazan salt generated by the reduction of WST-8 by dehydrogenases in cells was detected at 450 nm (Victor 3-1420 Multilabel Counter plate reader, PerkingElmer, Waltham, MA, USA). Cell culture media without cells or carriers was used to determine the background signal while untreated cells (cells without carriers exposure) were used to determine the maximum formation of formazan. The following equation was utilised to calculate the percentage of cell viability:

$$\text{Cell viability } (\%) = \frac{\text{treated or untreated cells-cell culture media}}{\text{untreated cells-cell culture media}} \text{ x } 100$$

Once the maximum amount of carrier per cell had been determined, the following experiments were performed using 3.7 ng MG_{700}/L/PDA or MG_{700}/L/PDA/PEG per cell and 18.5 ng MG_{350}/L/PDA or MG_{350}/L/PDA/PEG.

3.2.2.11 Cell association/uptake experiments

In order to ensure the maximum cellular uptake efficiency (CUE, defined as the percentage of cells with a mean fluorescence intensity higher than the auto fluorescent

level of the cells due to the association/internalisation of the fluorescent carrier), 30 000 cells (RAW 264.7) or 15 000 cells (HeLa or HUVEC) were seeded in 96-well plate in 200 µL cell culture media and allowed to attach to the surface for 24 h at 37°C, 5% CO_2. Next, the cells were incubated with 3.7 ng MG_{700}/L^F/PDA or 18.5 ng MG_{350}/L^F/PDA per cell for 3, 4 and 5 h at 37°C, 5% CO_2, followed by washing 2× in 200 µL pre-warmed PBS in order to remove non-internalised/associated carriers. Finally, the cells were harvested from the wells (using 60 µL trypsin for HeLa and HUVEC cells or a scrapper for RAW 264.7 cells) and analysed by flow cytometry (at least 2000 events were analysed). As controls, carriers without exposure to the multicompartment carriers were employed.

3.3 Results and Discussion

3.3.1 MGs synthesis and characterisation

In order to evaluate the best candidate as core for the multicompartment carrier in terms of facile production, colloidal stability and PEGylation effect two different MGs sizes were synthesised.

MG_{700} was synthesised by surfactant free precipitation polymerisation,[68] while MG_{350} was synthesised by precipitation polymerisation[126] using SDS as surfactant in order to favour the production of the small MG size.

First, both MGs were characterised in terms of size, ξ- potential and PDI (Table 3.1).

MG	Size (nm)	ξ- potential (mV)	PDI
MG_{700}	740.5 ± 17.9	-45.8 ± 5.7	0.116 ± 0.08
MG_{350}	375.2 ± 19.8	-34.8 ± 1.2	0.068 ± 0.001

Table 3.1 MG characterisation. Size, zeta- potential (ξ- potential) and polydispersity (PDI) of the synthesised MGs. Mean values ± Standard deviation. Adapted from reference [60] with permission. Copyright (2018) by Elsevier.

The size and PDI values obtained by DLS were confirmed by DIC images by means of particle homogeneity and non- present aggregates (Figure 3.1).

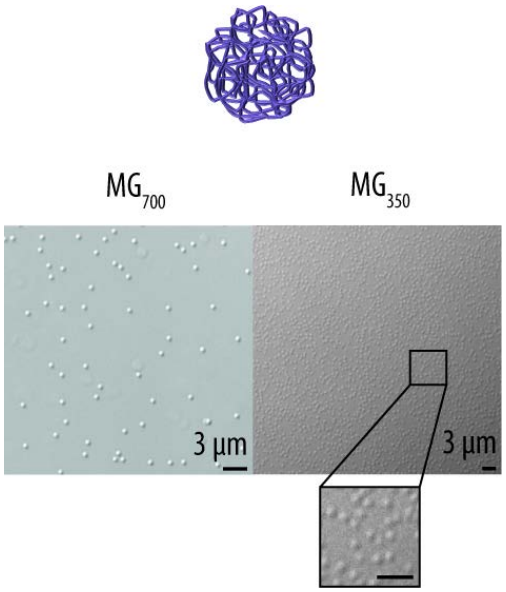

Figure 3.1 MGs characterisation. Differential interference contrast microscopy images of larger microgel (MG_{700}) and smaller microgel (MG_{350}). Inset scale bar: 2 µm. Adapted from reference [60] with permission. Copyright (2018) by Elsevier.

3.3.2 Multicompartment carrier assembly and characterisation

3.3.2.1 Liposome deposition

The first step in the assembly of the multicompartment carrier is the liposome deposition. For this, the maximum amount of L^F that could be adsorbed onto the MGs without causing aggregation was determined by incubating the MGs with increasing amounts of L^F followed by monitoring the normalised mean fluorescence intensity (nMFI) of the MG/L^F assemblies. The negatively charged MGs (see Table 3.1) are expected to interact with the positively charged L^F (31.5 ± 5 mV with a diameter of 102.8 ± 0.6 nm) through electrostatic interactions.

As shown in Figure 3.2, the results were normalised to the highest amount of lipids that did not cause aggregation of any of the MGs. Both MGs showed an approximately linear trend between the amount of lipids added and the nMFI. However, according to DIC images, while MG_{700} aggregated at 0.175 mg of lipids (Figure 3.2a, inset 2), MG_{350} exhibited better colloidal stability since none of the tested amount of lipids caused aggregation for this MG (Figure 3.2b, inset).

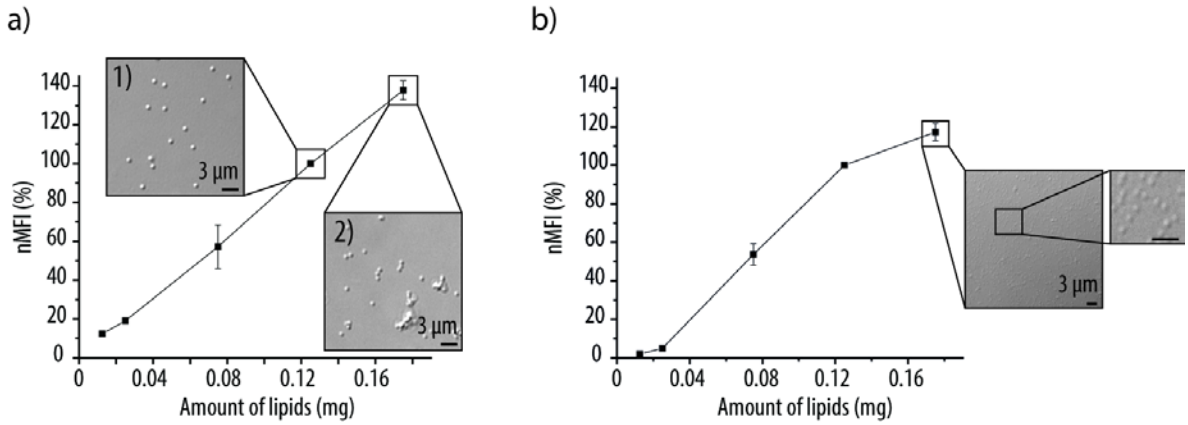

Figure 3.2 Liposomes deposition. Normalised mean fluorescence intensity (nMFI) of a) MG_{700} and b) MG_{350} upon incubation with increasing amount of lipids. a) Inset 1: Differential interference contrast (DIC) microscopy images of non-aggregated MG_{700} decorated with fluorescently labelled liposomes (L^F). Inset 2: DIC images of aggregated MG_{700}/ L^F. b) Inset: DIC images of non-aggregated MG_{350}/ L^F, scale bar: 2 µm. Adapted from reference [60] with permission. Copyright (2018) by Elsevier.

The deposition of L^F onto the MG was further corroborated by the strong green signal in fluorescence microscopy images (Figure 3.3) upon incubation with the highest amount of lipids that did not promote aggregation of the system, namely 0.125 mg and 0.175 mg of lipids for MG_{700} and MG_{350}, respectively.

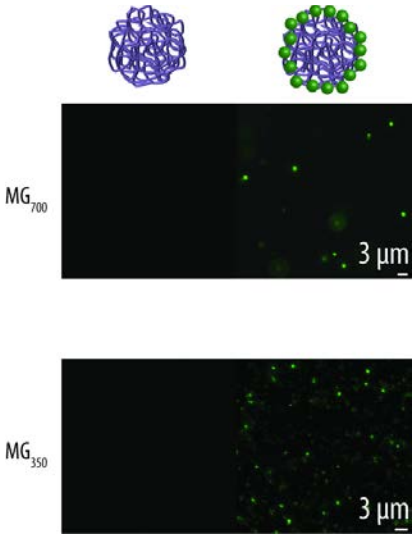

Figure 3.3 Liposome deposition. Fluorescence microscopy image of non-aggregated microgels (MG) decorated with fluorescently labelled liposomes (L^F) showing a green signal arising from the L^F. Adapted from reference [60] with permission. Copyright (2018) by Elsevier.

3.3.2.2 Prime-coating with PDA

Once the liposome deposition had been optimised, the DA polymerisation onto the MG/L^F surface was next characterised in terms of colour change of the solution upon DA polymerisation, colloidal stability and diameter increase.

In order to create the PDA coating, the MG/L^F assemblies were incubated with a DA solution in Tris 1 buffer for approximately 16 h at room temperature, followed by extensive washing in order to remove the unreacted DA and unbound PDA. The PDA coating processed resulted in a black suspension indicating the successful deposition of PDA on the MG/L^F surface (Figure 3.4a).[129] Next, the good colloidal stability (absence of aggregation) of the MG_{700}/L^F assemblies upon PDA deposition was confirmed by DIC and fluorescence microscopy images (Figure 3.4b). For the MG_{350}/L^F assemblies, aggregates were observed upon PDA deposition.

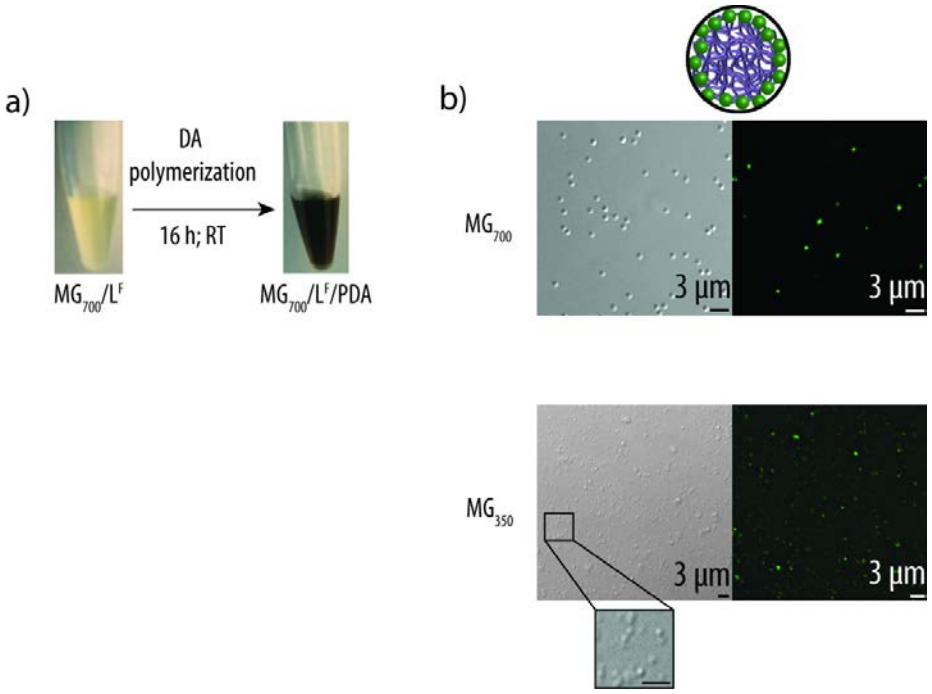

Figure 3.4 Poly(dopamine) (PDA) deposition. a) Dopamine (DA) polymerisation into PDA, for 16 h at room temperature, on MG/fluorescent liposomes (L^F) resulting in a black suspension. b) Differential interference contrast microscopy image and fluorescence microscopy images of MG/L^F/PDA carriers. Inset scale bar: 2 µm. Adapted from reference [60] with permission. Copyright (2018) by Elsevier.

The MG/L^F/PDA assemblies were further characterised by SEM and compared to bare MG and MG/L^F (Figure 3.5a). The images did not show any noticeable differences between the samples for MG_{700} or MG_{350} (*i.e.*, MG, MG/L^F or MG/L^F/PDA) which indicates the absence of PDA aggregates on the surface of the carriers.

Finally, the size of the MG/L^F/PDA was determined by DIC images. The size distribution histograms (Figure 3.5b), show an increase of the diameter from ~750 nm for bare MG_{700} to ~950 nm for the MG_{700}/L^F/PDA assemblies (Figure 3.5bi) and ~390 nm for bare MG_{350} to ~ 580 nm for the MG_{350}/L^F/PDA assemblies. All in all, these results suggest the successful deposition of PDA onto MG/L^F.

3.3.2.3 PEGylation

Although the PDA structure is still highly debated,[42] PDA coatings can be functionalised in a straightforward manner due to the reactivity of the *o*-quinone groups

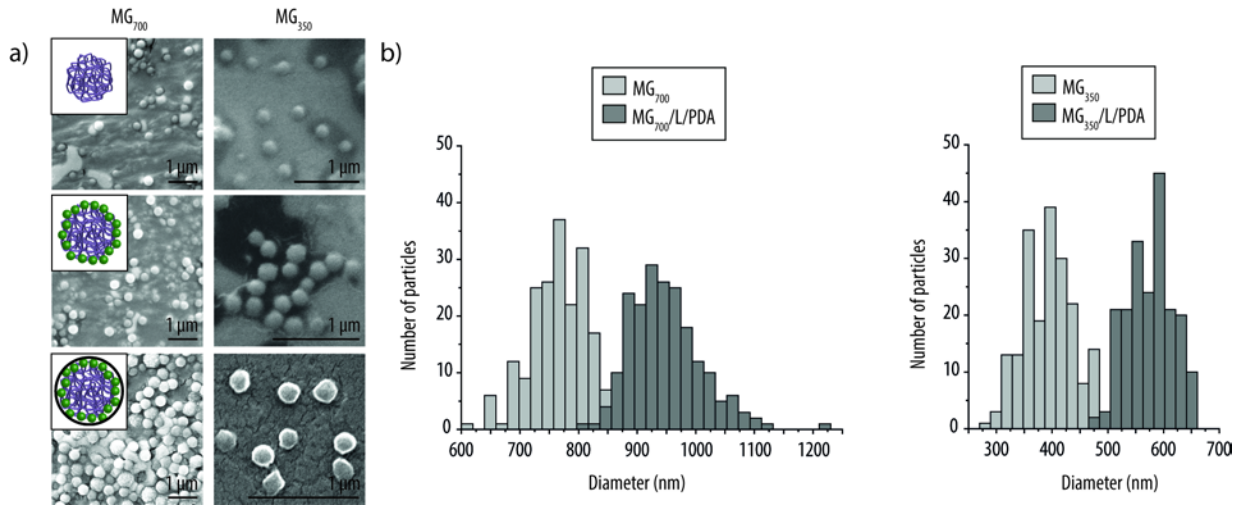

Figure 3.5 MG/L^F/PDA characterisation. a) Scanning electron microscopy images of bare MGs (top), MG/L^F (middle) and MG/L^F/PDA (bottom). b) Size-distribution histogram of i) bare MG_{700} and MG_{700}/L^F/PDA and of ii) bare MG_{350} and MG_{350}/L^F/PDA. Adapted from reference [60] with permission. Copyright (2018) by Elsevier.

(present in the PDA structure) towards amines and thiols via Schiff base and/or Michael addition reactions.[130] Therefore, taking advantage of the PDA reactivity towards amines the surface of MG/L^F/PDA was functionalised with PLL-*g*-PEG in order to confer anti-fouling properties (*i.e.*, diminished cellular uptake) to the multicompartment carrier.

For this, MG/L/PDA assemblies were incubated with a PLL-*g*-PEG solution in Tris 1 buffer for 1 h at room temperature followed by extensive washing. The PDA functionalisation was first assessed by ξ-potential measurements (Figure 3.6) resulting in an increase from -45.8 ± 5.7 mV for bare MG_{700} to -35.8 ± 6.1 mV upon incubation with a positively charged L solution, thus confirming the L deposition onto the MG_{700} (Figure 3.6ai). Upon DA polymerisation into PDA, another increase in the ζ-potential was observed (-27.8 ± 3.4 mV). Although unaltered[95,96] ζ-potential or slightly decreased[21,131,132] ζ-potential upon PDA deposition onto PLGA particles,[95] positively charged liposomes,[96] mesoporous silica particles [131,132] and PLL-coated silica particles [21] have been previously reported, the increase in ζ-potential observed in the developed carrier could be due to a larger deposition of PDA (of 16 h) since the reported incubation times varied from 15 min to 6 h for DA concentrations from 0.5 to 1 mg mL^{-1}.

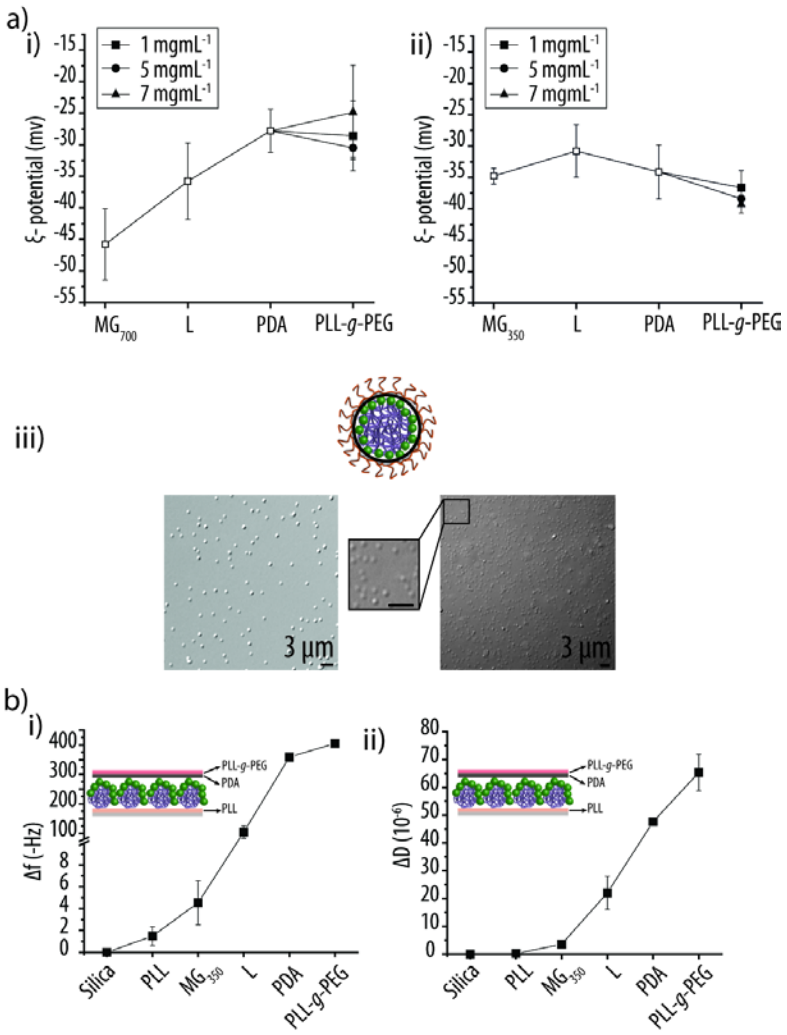

Figure 3.6 Poly(dopamine) (PDA) functionalisation with poly(*L*-lysine)- grafted poly(ethylene glycol (PLL-*g*-PEG) (PLL-*g*-PEG). a) ξ- potential measurements of microgels (MGs) i) MG_{700} and ii) MG_{350} after each deposition step: liposomes (L), PDA and PLL-*g*-PEG. iii) Differential interference contrast image of the MG/L/PDA/PEG carrier. Inset scale bar: 2 µm. b) i) Frequency (Δf) and ii) dissipation (ΔD) changes measure by quartz crystal microbalance with dissipation monitoring after each incubation step. Adapted from reference [60] with permission. Copyright (2018) by Elsevier.

In order to optimise the PLL-*g*-PEG coating conditions, the PDA-coated multicompartment carrier (MG_{700}/L/PDA) was incubated at three different concentrations (*i.e.*, 1, 5 and 7 mg mL^{-1}) of PLL-*g*-PEG. All three tested concentrations resulted in a slight changes in ʒ-potential, which is in agreement with previous reports of PDA functionalisation with PLL-*g*-PEG[96] or with amino PEG.[95] This slight change in ʒ-potential upon incubation with the positively charge PLL-*g*-PEG is speculated to be due

to the reaction of most of the amino groups present in PLL-*g*-PEG with the PDA quinones.[133] The three tested concentrations resulted in a very similar change in ζ-potential, suggesting already a saturation of the surface when employing 1 mg mL^{-1} of PLL-*g*-PEG, therefore this concentration was selected for further experiments.

The L deposition onto MG_{350} (Figure 3.6aii) also resulted in an increase in ζ-potential from -34.8 ± 1.2 mV for bare MG_{350} to -30.79 ± 4.2 mV upon incubation with the positively charged L solution. Interestingly, the PDA deposition resulted in a slight drop in ζ-potential (to -34.1 ± 4.3 mV), in agreement with literature[21,95,96,131,132] but contrary to MG_{700}. Considering that the MG mg/ DA mg was kept constant for both MG the larger surface to volume ratio of MG_{350}, compared to MG_{700}, could lead to a different PDA deposition resulting in different ζ-potential results. However, upon DA incubation the MG_{350} suspension also turned black, indicating the deposition of the PDA on the surface of the MG_{350}/L assemblies. Similar to MG_{700}, all tested PLL-*g*-PEG concentrations resulted in slight ζ-potential changes. Therefore, 1 mg mL^{-1} of PLL-*g*-PEG was selected for further experiments.

The colloidal stability of MG/L/PDA/PEG was confirmed by DIC images showing the absence of aggregates upon incubation of MG/L/PDA with PLL-*g*-PEG (Figure 3.6aiii).

In order to draw stronger conclusions on the PDA functionalisation and to evaluate the physical integrity of the L upon the PDA deposition, the assembly of the MG_{350}/L/PDA/PEG was characterised by QCM-D (Figure 3.6b). As previously explained, QCM-D measures Δf (related to mass changes, it decreases when mass is being loaded on the crystal) and ΔD in real-time (related to structural changes, layers with low water content such as a lipid bilayer will have a low ΔD, while highly hydrated layers such as intact liposomes will have a large ΔD).

Due to the negative charge exhibited by the MGs, the silica sensors were first coated with a positively charged polymer (*i.e.*, PLL) resulting in a Δf of -1.48 ± 0.74 Hz (Figure 3.6bi). This new positively charged surface allowed for the deposition of negatively charged MG_{350}, via electrostatic interactions, as indicated by a Δf of -3.13 ± 1.20 Hz. The QCM-D experiments were carried out only with MG_{350} in order to avoid potential

compromise of the sensitivity due to the loading of larger particles. Next, the deposition of the L layer yielded a Δf of -100.60 ± 16.69 Hz and a ΔD of 18.44 × 10^{-6} ± 5.07 × 10^{-6} (Figure 3.6bii), thus suggesting the adsorption of intact L rather than a lipid bilayer.[134] In order to confirm that the deposition of L was due interaction with the negatively charged MG_{350}, a control experiment without MG_{350} was conducted and the results demonstrated that, when adsorbing L onto a PLL-coated silica sensor, negligible Δf and ΔD were detected (Δf of -0.23 ± 0.55 Hz and ΔD of 0.09 × 10^{-6} ± 0.04 × 10^{-6}). Upon PDA deposition, a further increase in Δf of -259.94 ± 6.52 Hz together with a ΔD of 27.90 × 10^{-6} ± 1.37 × 10^{-6} was observed, which indicates that the deposition of PDA did not displaced or ruptured the L from the surface. Finally, an increase in Δf of -46.41 ± 1.57 Hz upon PLL-*g*-PEG deposition, suggests a successful functionalisation of the PDA coating. Therefore, the results confirmed the deposition of L onto the MG surface without rupture, as well as the successful functionalisation of the PDA surface with PLL-*g*-PEG, thus ensuring an intact bilayer membrane for the protection of fragile cargo.

3.3.2.4 Storage stability

The stability of MG_{700}/L/PDA and MG_{700}/L/PDA/PEG, in terms of aggregations, was evaluated upon storage at 4 °C in PBS for up to 14 days (Figure 3.7).

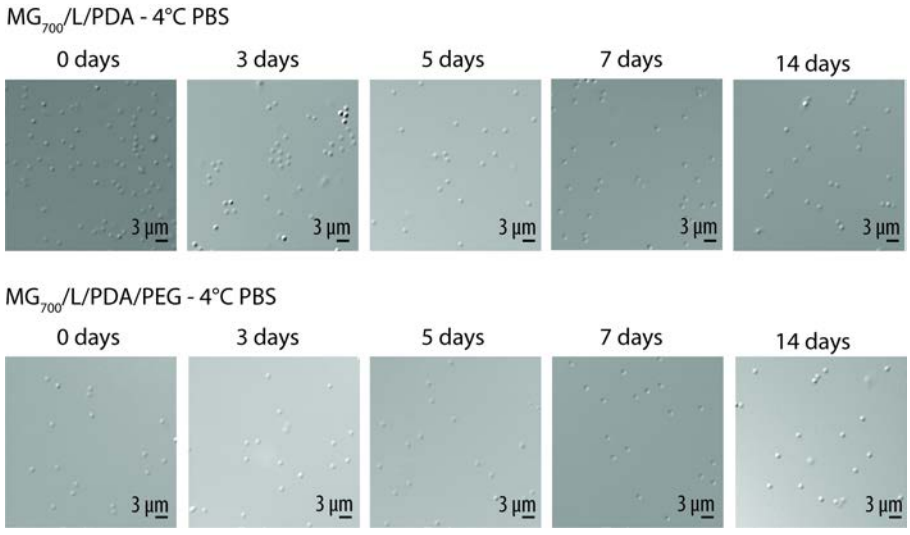

Figure 3.7 Storage stability. Differential interference contrast microscopy images MG_{700}/L/PD) functionalised with PLL-*g*-PEG (MG_{700}/L/PDA/PEG) stored at 4 °C in PBS for up to 14 days. Adapted from reference [60] with permission. Copyright (2018) by Elsevier.

The DIC images revealed the absence of aggregates during the whole time-frame. Only MG_{700} was studied due to the difficulties in imaging small MGs such as MG_{350}.

3.3.3 Interaction of non-functionalised (MG/L/PDA) and PEGylated (MG/L/PDA/PEG) carriers with cells

Drug delivery carriers designed to be administered intravenously are directly exposed to the cell populations in the circulatory system. Therefore, the assessment of the interaction of the as-prepared multicompartment carrier (in terms of cell association/uptake and cell viability) with relevant cell lines is of outmost importance. For this, its performance is evaluated in the presence of macrophages (RAW 264.7) which are the first line of defence of the human body against pathogens and are part of the MPS,[100] and endothelial cells (HUVEC) which are the cells lining the interior surface of blood vessels. In order to evaluate the therapeutic potential of the novel carrier its interaction with a model cancer cell (HeLa) is also evaluated.

3.3.3.1 Biocompatibility

A crucial requirement of every drug delivery system is to avoid inherent toxicity. Therefore, the maximum amount that could be administered to the different cell lines was first determined by incubating the cells with increasing amount of MG/L/PDA per cell for 4 h at 37°C, 5% CO_2 [12] followed by extensive washing and cell viability measurements (by means of formazan formation due to the activity of cellular dehydrogenases) (Figure 3.8). As shown in Figure 3.8a, the maximum amount of MG_{700}/L/PDA assemblies that can be administered without significantly decreasing the cell viability is 11.1 ng per cell for RAW 264.7 cells (Figure 3.8ai) while 3.7 ng per cell is the maximum amount that can be administered to HUVEC (Figure 3.8aii) and 6.1 ng for HeLa cells (Figure 3.8aiii). Therefore, 3.7 ng per cell was selected to conduct the subsequent experiments. Interestingly, the three cell lines showed an overall higher tolerability towards MG_{350}/L/PDA as compared to MG_{700}/L/PDA (Figure 3.8b). In particular, only the cell

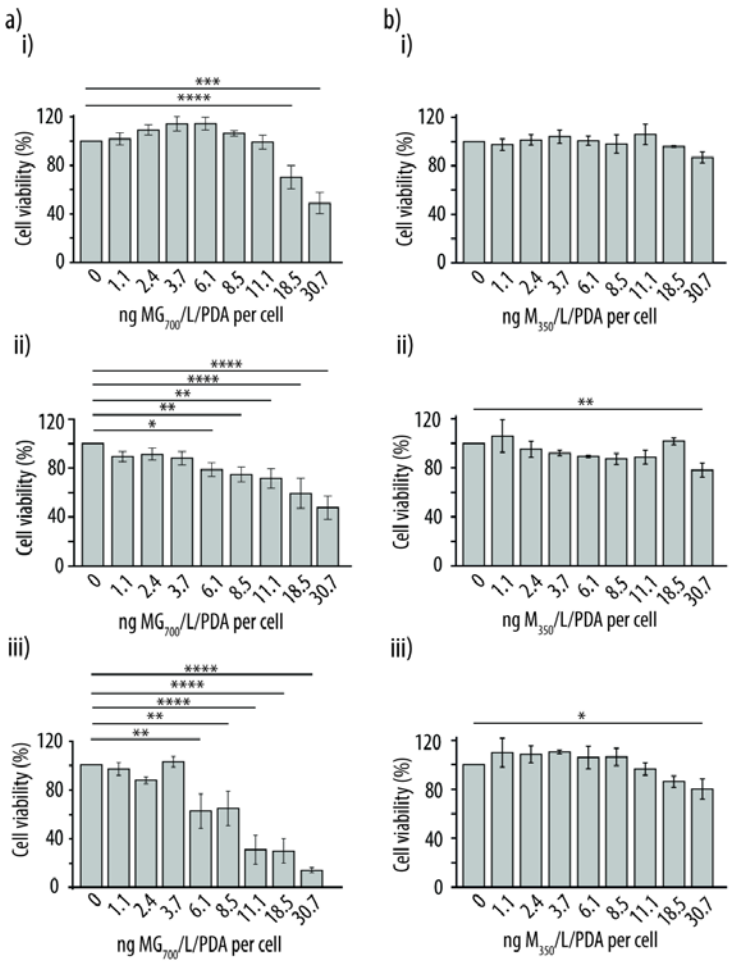

Figure 3.8 Biocompatibility. a) Cell viability of i) RAW 264.7 cells, ii) HUVEC cells and iii) HeLa cells upon incubation with increasing amount of MG_{700}/L/PDA. b a) Cell viability of i) RAW 264.7 cells, ii) HUVEC cells and iii) HeLa cells upon incubation with increasing amount of MG_{350}/L/PDA. n=3; ns > 0.05 *p ≤ 0.05; **p ≤ 0.01; ***p ≤ 0.001; ****p ≤ 0.0001. Adapted from reference [60] with permission. Copyright (2018) by Elsevier.

viability of HUVEC (Figure 3.8bii) and HeLa (Figure 3.8biii) was significantly reduced upon exposure to the highest amount of MG_{350}/L/PDA tested (*i.e.*, 30.7 ng). Therefore, the maximum amount that can be administered to the three cell lines without significantly decrease the cell viability is 18.5 ng of MG_{350}/L/PDA, being the selected amount for subsequent experiments.

In order to ensure maximum CUE the different cell lines were incubated with 3.7 ng MG_{700}/L^{F}/PDA per cell for 0.5, 1, 2, 3, 4, 5 or 24 h at 37°C, 5% CO_2 followed by extensive washing and flow cytometry analysis. The results (Figure 3.9a) demonstrated

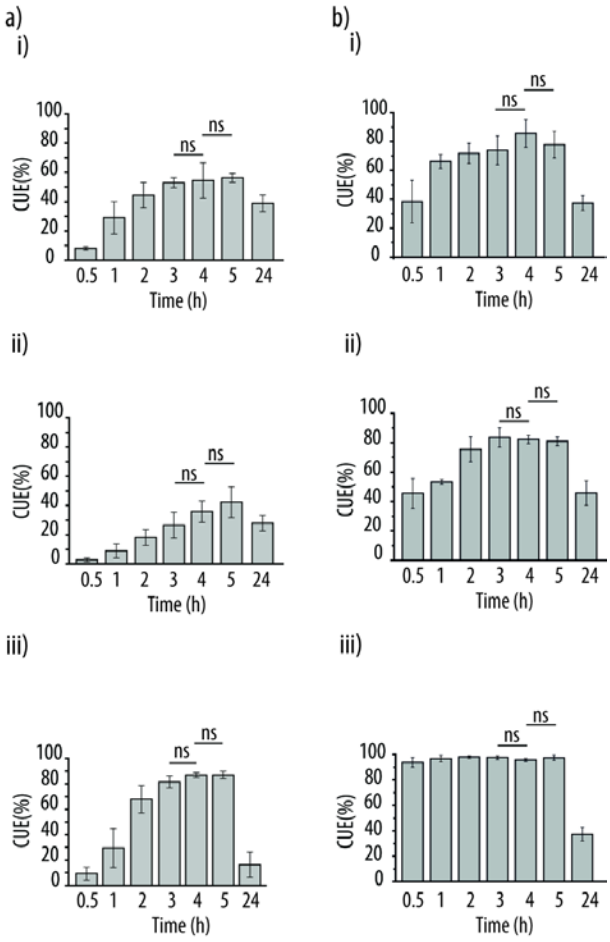

Figure 3.9 Incubation time optimisation. a) Cellular uptake efficiency (CUE) of i) RAW 264.7 cells, ii) HUVEC cells and iii) HeLa cells upon incubation with 3.7 ng of MG_{700}/L^F/PDA at different time points. b) CUE of i) RAW 264.7 cells, ii) HUVEC cells and iii) HeLa cells upon incubation with 18.5 ng of MG_{350}/L^F/PDA at different time points n=3; ns > 0.05. Adapted from reference [60] with permission. Copyright (2018) by Elsevier.

that the maximum cell uptake is reached after 3 h for RAW 264.7 (Figure 3.9ai) and HeLa (Figure 3.9aiii) cells and 5 h for HUVEC (Figure 3.9aii) cells. Importantly, non-significant differences were found for any of the cell lines after 3, 4 or 5 h incubation. Therefore, 4 h incubation time was selected for following experiments.

Similar to MG_{700}/L^F/PDA, the different cell lines were incubated with 18.5 ng MG_{350}/L^F/PDA per cell for 0.5, 1, 2, 3, 4, 5 or 24 h at 37°C, 5% CO_2 followed by extensive washing and flow cytometry analysis. The maximum CUE (Figure 3.9b) was achieved after 4, 3 h and 0.5 h incubation with RAW 264.7 (Figure 3.9bi), HUVEC

(Figure 3.9bii) and HeLa (Figure 3.9biii) cells, respectively. Importantly, non-significant differences were found for any of the tested cell lines after 5 h. Therefore, 4 h was chosen as the incubation times for the next experiments.

Importantly, the formation of aggregates did not take place upon incubation of MG_{700}/L/PDA and MG_{700}/L/PDA/PEG at 37 °C for up to 5 h in cell culture media (Figure 3.10).

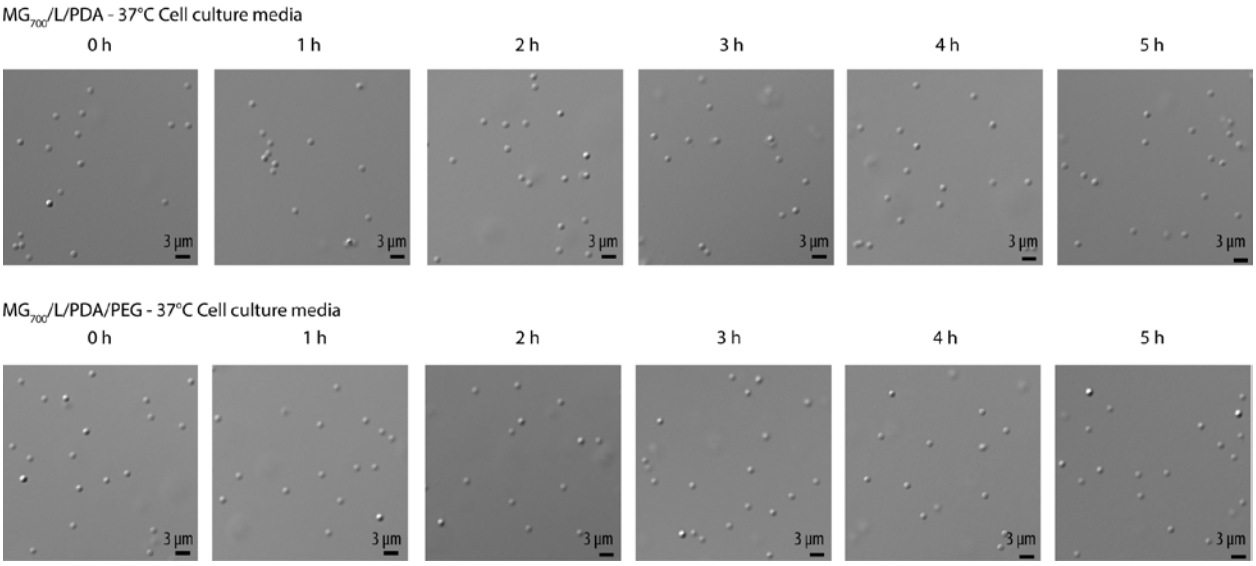

Figure 3.10 Stability upon cell culture media exposure. Differential interference contrast microscopy images of MG_{700}/L/PDA or functionalised MG_{700}/L/PDA/PEG incubate in cell culture media at 37 °C for different time points. Adapted from reference [60] with permission. Copyright (2018) by Elsevier.

3.3.3.2 Cellular uptake/association of MG/L/PDA and MG/L/PDA/PEG assemblies

Once the optimal conditions for both MGs and each cell line were determined, the PEGylation effect in terms of cellular uptake/association was evaluated.

A comparison of the PEGylation effect was assessed employing the maximum amount of MGs tolerated per cell (3.7 ng/cell for MG_{700}/L/PDA and 18.5 ng/cell for MG_{350}/L/PDA) upon incubation for 4 h at 37 °C, 5% CO_2.

RAW 264.7 cells: As shown in Figure 3.11a, the exposure of macrophages to the PEGylated assemblies of both MGs resulted in a significant decrease in cell mean fluorescence intensity (CMFI) (by ~2.5 fold for MG_{700}/L^F/PDA/PEG, black bar, and ~1.5 fold for MG_{350}/L^F/PDA/PEG, grey bar) compared to the non-functionalised carriers. Although only MG_{700}/L^F/PDA/PEG resulted in a significant decrease in CUE (by ~2.4 fold) compared to MG_{700}/L^F/PDA (Figure 3.11b, black bar). Therefore, for this cell line the most efficient system by means of PEGylation effect is MG_{700}/L^F/PDA/PEG.

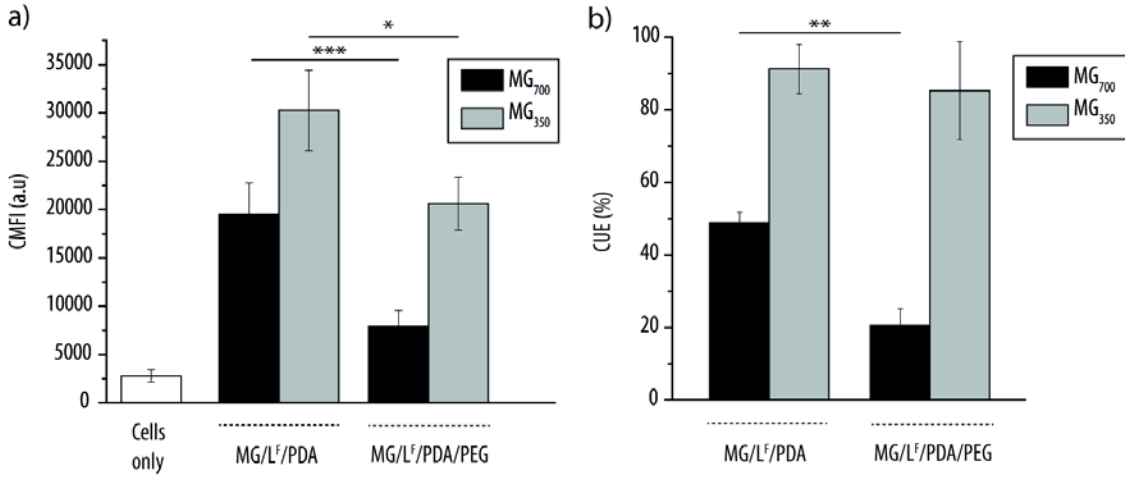

Figure 3.11 Cellular uptake/association of MG/ L^F /PDA and functionalised MG/L^F/PDA/PEG with RAW 264.7 cells. a) Cell mean fluorescence intensity (CMFI) upon incubation with MG/L^F/PDA and MG/L^F/PDA/PEG. b) Cellular uptake efficiency (CUE) upon incubation with MG/L^F/PDA and MG/L^F/PDA/PEG. n=3; *$p \leq 0.05$; **$p \leq 0.01$. Adapted from reference [60] with permission. Copyright (2018) by Elsevier.

HUVEC cells: Different from the RAW 264.7 cells, the PEGylation effect is only seen upon exposure to MG_{350}/L^F/PDA/PEG respect to the MG_{350}/L^F/PDA, resulting in a significant decrease in CMFI by ~1.3 fold (Figure 3.12a, grey bar). Such reduction is comparable with the one observed in RAW 264.7 cells for the same system. However, the CUE (Figure 3.12b) remained unaltered regardless of the surface functionalisation or the MGs core being the CUE of the MG_{350}/L^F/PDA and MG_{700}/L^F/PDA slightly lower than the CUE observed for macrophages (~ 10% lower for both MG).

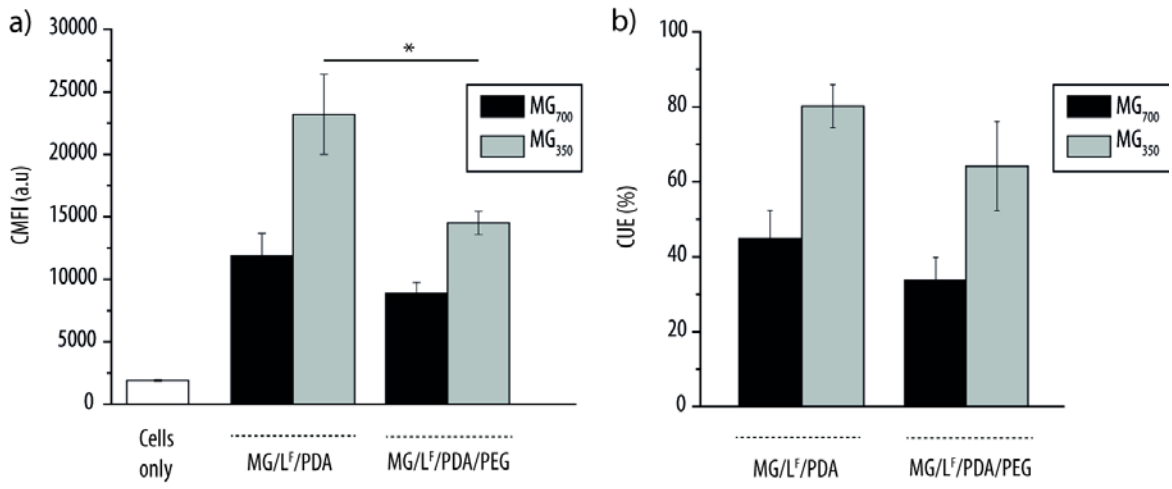

Figure 3.12 Cellular uptake/association of MG/ L^F /PDA and functionalised MG/L^F/PDA/PEG with HUVEC cells. a) Cell mean fluorescence intensity (CMFI) upon incubation with MG/L^F/PDA and MG/L^F/PDA/PEG. b) Cellular uptake efficiency (CUE) upon incubation with MG/L^F/PDA and MG/L^F/PDA/PEG. n=3; *$p \leq 0.05$. Adapted from reference [60] with permission. Copyright (2018) by Elsevier.

HeLa cells: For this cell line, the PEGylation effect was not observed for any of the MGs (Figure 3.13a). The higher CUE (Figure 3.13b), for both MGs, as compared to RAW 264.7 and HUVEC cells demonstrates a preferential association/internalisation of the carriers by this cell line compared to RAW 264.7 and HUVEC cells which makes the multicompartment carrier an interesting candidate for cancer therapy.

Although the results suggest that the PEGylation effect of the MG_{350}/L^F/PDA/PEG was better than MG_{700}/L^F/PDA/PEG (*i.e.*, significantly decrease either CMFI or CUE in two out of three cell lines), aiming to keep the CUE with macrophages and endothelial cells to the minimum possible while still being high in cancer cells and the difficulty in producing the MG_{350}/L^F/PDA or MG_{350}/L^F/PDA/PEG at high quantities , the MG_{700} was selected as a core for the chapter 4 and 5 of this PhD thesis.

Importantly, the PEGylation of the surface did not resulted in any inherent cytotoxicity for any of the tested cell lines (Figure 3.14).

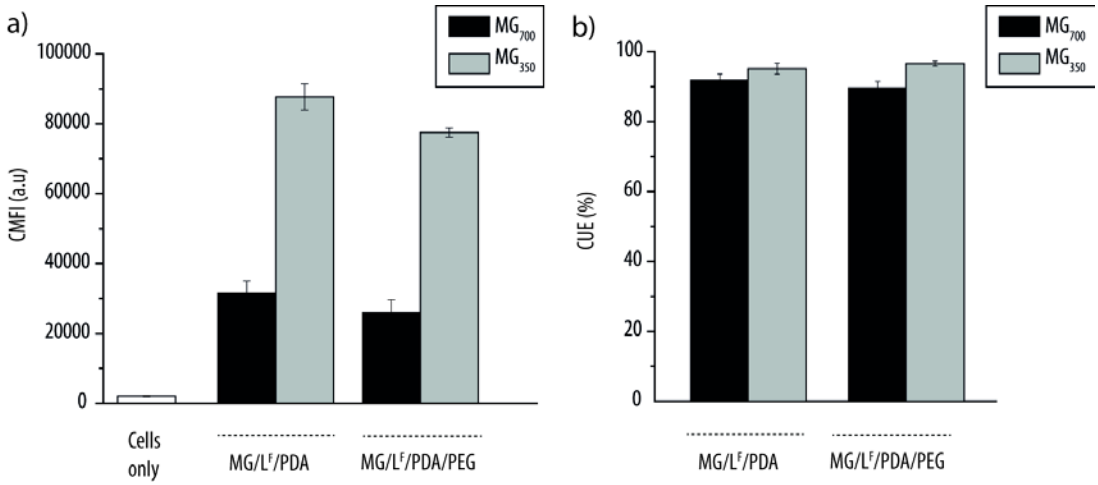

Figure 3.13 Cellular uptake/association of MG/ L^F /PDA and functionalised MG/L^F/PDA/PEG with HeLa cells. a) Cell mean fluorescence intensity (CMFI) upon incubation with MG/L^F/PDA and MG/L^F/PDA/PEG. b) Cellular uptake efficiency (CUE) upon incubation with MG/L^F/PDA and MG/L^F/PDA/PEG. n=3. Adapted from reference [60] with permission. Copyright (2018) by Elsevier.

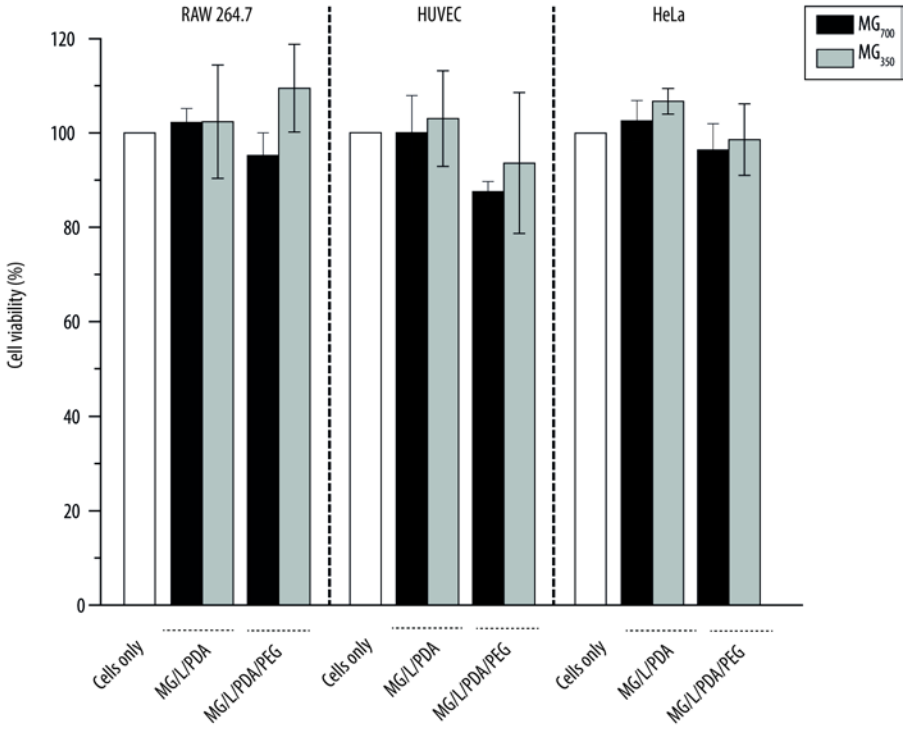

Figure 3.14 Cell viability of RAW 264.7, HUVEC and HeLa cells upon incubation with MG/L/PDA or MG/L/PDA/PEG. n=3. The results were normalised to cells only. Adapted from reference [60] with permission. Copyright (2018) by Elsevier.

3.4 Conclusions

In this chapter, an in depth characterisation of the assembly of a multicompartment carrier in the submicron range is described and discussed using to different MGs (*i.e.*, MG_{700} and MG_{350}) as the core.

Based on the results presented above, both MGs exhibited a good colloidal stability along the assembly process, including incubation with the liposomes, DA polymerisation into PDA (being better the MG_{700} compared to MG_{350}) and PDA functionalisation with

PLL-*g*-PEG, without being compromised upon storage conditions for up to 14 days (only assessed for MG_{700}).

The integrity of the liposomes was confirmed upon PDA and PLL-*g*-PEG deposition, ensuring protection for the potential cargo encapsulated within the liposomes (*i.e.*, therapeutic molecules, enzymes, etc.).

Importantly, a PEGylation effect was observed, by significant decrease in CMFI and/or CUE upon cellular incubation with the PEGylated carrier compared to the non-functionalised counterpart, in macrophages (*i.e.*, MG_{700}/L^F/PEG and MG_{350}/L^F/PEG) and endothelial cells (*i.e.*, MG_{350}/L^F/PEG) but not in the model cancer cell line. Although MG_{350} showed a slightly better performance in terms of PEGylation effect, compared to MG_{700}, the difficulties in producing large amounts of carrier necessary for more advanced experiments (*i.e.*, shear stress conditions) and the high CUE compared to MG_{700} (for both macrophages and endothelial cells), make MG_{700} a better candidate for further experiments.

Therefore, although it is worth to invest efforts in optimizing the large production of the MG_{350} due to their small size making them good candidates for intracellular delivery, size and cellular performance the following experimental chapters of this PhD thesis will include only multicompartment carriers assembled making use of MG_{700} as the core.

Chapter IV Shear stress regulated uptake of liposome-decorated microgels with a poly(dopamine) shell

Summary

Since, in this chapter all the multicompartment carriers are assembled with MG_{700}, MG_{700} will be referred, from now on, as MG.

This chapter involves the evaluation of the PEGylation effect by means of protection towards protein adsorption on the carrier´s surface upon exposure to albumin and immunoglobulin G in the absence or presence of shear stress, using flow cytometry, DIC and fluorescence imaging. Next, the potential functionality as a dual-cargo carrier is evaluated by studying the different kinetic release profiles of model molecules offered by the two components of the system (*i.e.*, P(NIPAM)-*co*-AAc MGs and liposomes). Importantly, the effect of the physiological dynamics, by exposure to relevant shear stress conditions (*i.e.*, due to blood flow and interstitial fluid in the tumour environment), on the cellular association/uptake and PEGylation effect (*i.e.*, diminished cell uptake/association) are extensively investigated. For this, three relevant cell lines (*i.e.*, RAW 264.7, HUVEC and HeLa cells) are studied using flow cytometry and confocal laser microscopy (CLSM). Finally, the influence of shear stress is further investigated regarding the cellular uptake pathway followed by the multicompartment carrier to enter the different cell lines using chemical inhibitors and flow cytometry (Scheme 4.1).

The results presented in this chapter have been adapted from the following publication:

York-Duran, M. J; Ek, P. K.; Godoy-Gallardo M.; Hosta-Rigau L. Shear stress regulated uptake of liposome-decorated microgels coated with a poly(dopamine) shell. *Colloids Surf., B* **2018**, 171, 427-436.

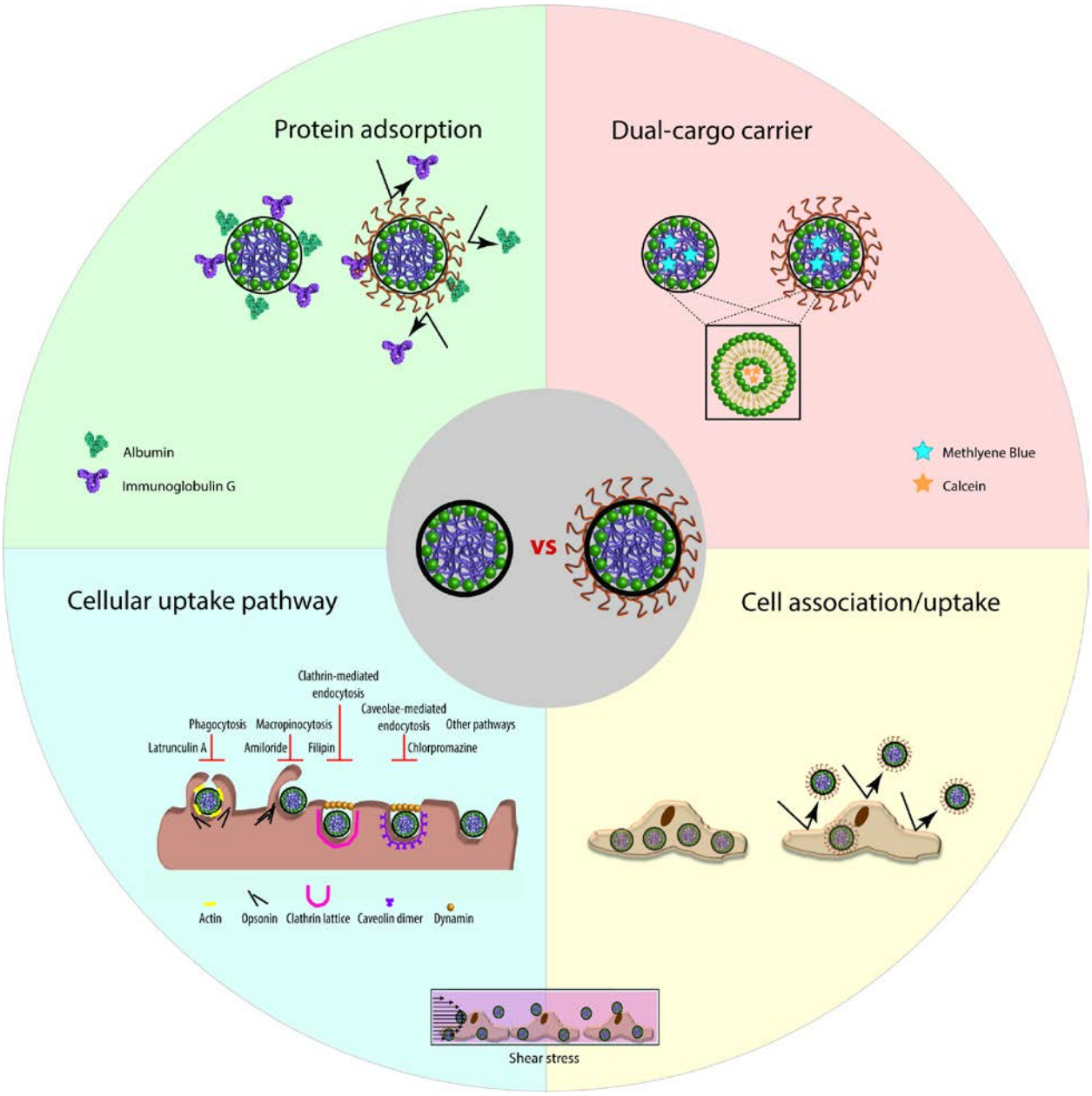

Scheme 4.1 Overview of the topics covered by this chapter. PEGylation effect by means of protection towards protein adsorption in the presence and absence of shear stress. Evaluation of its functionality as a dual-cargo carrier. Study of the influence of shear stress in the cell association/uptake by three different cell lines (*i.e.*, RAW 264.7, HUVEC and HeLa cells) and cellular uptake pathway using chemical inhibitors (*i.e.*, latrunculin A, amiloride, filipin and chlorpromazine). Adapted from reference [60] with permission. Copyright (2018) by Elsevier.

4.1 Introduction

One of the numerous advantages offered by carriers containing multiple compartments is the possibility to co-encapsulate several (incompatible) molecules within the same carrier ensuring their co-localization at the target site, improving the safety and the efficacy of the therapeutic outcome.[2]

An interesting approach to achieve a control release of the encapsulated cargo is creating a carrier using building blocks with different properties and therefore different kinetic profiles such as P(NIPAM)-*co*-AAc MGs and liposomes.

Although both building blocks have been extensively investigated separately, only one report investigates their combination as a dual-cargo carrier, showing that the MGs exhibit a faster release profile compared to liposomes due to their large pore size.[26] Herein, the concept is taken to the next level by creating a multicompartment carrier that can be easily functionalised (due to PDA protective layer which exhibits reactivity towards amines and thiols) with relevant molecules (such as PLL-*g*-PEG) while maintaining the different kinetic of the building blocks. It is worth to note that the assembly of the multicompartment carrier is the same as the one explained in Chapter 3 of this PhD thesis.

From a different perspective, the carriers administered intravenously are directly exposed to not only proteins and different cell populations present in the blood and vasculature but also to the dynamic nature of the physiological environment. This means, that the carrier/cell interaction will be subjected to different mechanical forces such as shear stress that can vary from 0.5 to 30.0 dyn cm^{-2} in the vasculature and be as low as 0.1 dyn cm^{-2} in the tumour microenvironment due to the interstitial flow.[135,136]

Although it has been previously reported that physiological shear stress conditions can influence the therapeutic efficacy,[108] carrier cytotoxicity,[109] PEGylation effect,[96] targeting efficiency,[21,110] cellular uptake,[109] and cellular uptake pathway,[112,113] it is still rarely seen in *in vitro* set-ups when a carrier is being investigated, especially when it comes to cancer cell lines. Therefore, *in vitro* studies in which a more *in vivo*-like

environment is not contemplated could translate into a poor transition of the developed carrier from *in vitro* to preclinical studies. This difficult transition could potentially reduce its chances to reach clinical studies.

An easy way to include shear stress in *in vitro* set-ups is making use of microfluidic devices. They offer the possibility to study the interactions between carriers and biological systems in depth by accurately controlling the fluidic conditions.[137] Their relevance has been demonstrated by the *in vivo* validation of the findings previously observed using microfluidic devices.[138] Therefore, the integration of microfluidics in *in vitro* set-ups is envisioned to assist the design of carriers, to better understand the interaction with its biological target and to improve the screening of potential drug delivery vehicles before moving to *in vivo* models. Although the microfluidic devices can be home-built the use of validated commercial microfluidic devices (Scheme 4.2) makes possible the investigation of the influence of shear stress conditions on carrier/cell interaction for everyone.

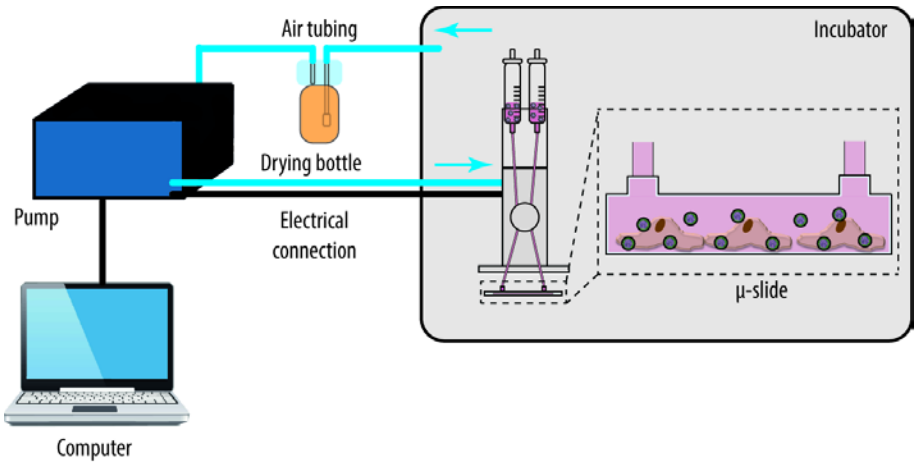

Scheme 4.2 Schematic representation of the commercial microfluidic device used to accurately control the shear stress. Adapted from reference [60] with permission. Copyright (2018) by Elsevier.

Herein, an in depth comparison between non-functionalised (MG/L/PDA) and functionalised carrier (MG/L/PDA/PEG), by means of (i) protection towards protein adsorption in the absence and presence of shear stress, (ii) suitability as dual-cargo

carriers and (iii) evaluation of the influence of physiological shear stress on the cellular uptake/association, cellular uptake efficiency and cellular uptake pathway, compared to conventional well plate *in vitro* experiments, is presented.

4.2 Materials and Methods

4.2.1 Materials

Tris, NaCl, calcein (Cal), methylene blue (MB), fluorescein isothiocyanate (FITC), FITC-labelled immunoglobulin G (IgG-FITC), bovine serum albumin (BSA), PBS, DMEM D5796, sodium pyruvate, penicillin/streptomycin, FBS, trypsin, paraformaldehyde (PFA), tetramethylrhodamine B isothiocyanate (TRITC)-labelled phalloidin (phalloidin-TRITC), WST-8 counting cell kit, adenocarcinoma cell line HeLa, endothelial cell line HUVEC, dimethyl sulfoxide (DMSO), sodium bicarbonate ($NaHCO_3$), chlorpromazine hydrochloride, amiloride hydrochloride hydrate, filipin complex from Streptomyces filipinensis, latrunculin A and PLL (Mw 15 000-30 000 Da) were purchased from Sigma-Aldrich (Saint Louis, MO, USA). POPC, POEPC and NBD-PC were obtained from Avanti Polar Lipids (Alabaster, AL, USA). PLL-*g*-PEG was obtained from SuSoS AG (Dübendorf, Switzerland). EGM-2 was purchased from Lonza (Basel, Switzerland). The EGM-2 is composed of EBM, hEGF, VEGF, R3-IGF-1, ascorbic acid, hydrocortisone, FBS, human hFGF-β, heparin and GA. The macrophage cell line RAW 264.7 was obtained from ECACC, Wiltshire, UK. α-Methoxy-ω-carboxylic acid succinimidyl ester poly(ethylene glycol) (Me-PEG-NHS, Mw_{PEG} = 2000 Da) was purchased from Iris Biotech GmbH (Marktredwitz, Germany). Tris 1 buffer is composed of 10 mM Tris (pH 8.5); Tris 2 is composed of 10 mM Tris and 150 mM NaCl (pH 7.4); HEPES is composed of 10 mM HEPES and 150 mM NaCl (pH 7.4). All buffers were made with ultrapure water (Milli-*Q*, gradient A 10 system, TOC < 4 ppb, resistance 18 MV cm, EMD Millipore, USA).

4.2.2 Methods

4.2.2.1 MB-loaded MGs (MG^{MB}) assembly

In order to encapsulate MB within the MGs core, a suspension containing 958 µg MG was incubated with 0.055 µmols of MB dissolved in Tris 1 buffer (100 µL) and incubated overnight at room temperature in a tube rotator. After the incubation time, the sample was washed 3× in Tris 1 in order to remove non-encapsulated MB using a bench top centrifuge (MiniSpin, Eppendorf, AG, Germany).

4.2.2.2 Cal-loaded liposomes (L^{Cal}) assembly

The liposomes were assembled by the lipid film hydration method. Specifically, 1.75 mg POPC and 0.75 mg POEPC were dissolved in chloroform followed by the formation of the lipid film using a nitrogen flow. Next, the lipid film was exposed to vacuum for at least 1 h in order to completely evaporate the organic solvent. In order to encapsulate Cal within the liposome core, the lipid film was rehydrated with 1 mL of Cal 20 mM in Tris 1 yielding a final lipid concentration of 32 mM. Upon rehydration, the solution was extensively vortexed every 15 min for 1 h to ensure the maximum Cal encapsulation followed by extrusion and dilution to a final concentration of 3.2 mM. The L^{Cal} were purified from non-encapsulated Cal by Size Exclusion Chromatography (SEC) using an Illustra Nap-10 column (GE Healthcare Life Science, Brondby, Denmark). The size and PDI of the L^{Cal} was determined by DLS. Only L^{Cal} with a PDI below 0.14 were used for the experiments. For empty fluorescent liposomes (L^{F}) 2 wt% of NBD-PC was added to the lipid mixture prior to the lipid film formation.

4.2.2.3 Assembly of multicompartment carriers

The MG^{MB}/L/PDA, MG/L^{Cal}/PDA or MG/L^{F}/PDA carriers were prepared by washing a suspension containing 958 µg MGs or MG^{MB} in Tris 1 1× buffer for 14 min at 8500 rpm followed by incubation with liposomes (L^{F} or L^{Cal}) (0.25 mg lipids) for 1.5 h at room temperature in a tube rotator. Next, in order to coat the surface with PDA the suspension

was concentrated to a volume of 100 µL followed by exposure to a DA 1 mg mL^{-1} for 16 h at room temperature in a tube rotator. Finally, the unreacted DA and PDA were washed away by 2× washing cycles in Tris 2 for 7 min at 10 000 rpm. In order to decrease the material loss all the steps before PDA deposition were performed in an amicon ultra centrifugal filter (100 kDa). The MG^{MB}/L/PDA, MG/L^{Cal}/PDA or MG/L^{F}/PDA carriers were PEGylated (MG^{MB}/L/PDA/PEG, MG/L^{Cal}/PDA/PEG or MG/L^{F}/PDA/PEG) by incubating MG^{MB}/L/PDA, MG/L^{Cal}/PDA or MG/L^{F}/PDA suspensions with PLL-*g*-PEG 1 mg mL^{-1} in Tris 1 for 1 h at room temperature in a tube rotator, followed by washing the PLL-*g*-PEG excess by 2× washing cycles in Tris 2 (7 min, 10 000 rpm).

4.2.2.4 Protein adsorption

Synthesis of BSA-FITC: BSA was fluorescently labelled (BSA-FITC) following a previously published protocol.[139] A FITC solution (3.7 mg of FITC in 300 µL DMSO) was added dropwise to a BSA solution containing 30 mg of protein in 6 mL of $NaHCO_3$ 0.05 M pH 10) under vigorous shaking followed by overnight incubation at room temperature in a tube rotator. Upon incubation, the excess of FITC was removed by two days dialysis against Milli-*Q* water using a cellulose dialysis membrane with a cut-off of 12.4 kDa. Finally, the fluorescently labelled protein was freeze-dried.

A suspension containing 0.47 mg MG/L/PDA or MG/L/PDA/PEG in 0.2 mL was incubated at 37 °C for 4 h with 0.5 mg mL^{-1} IgG-FITC or BSA-FITC solutions in PBS followed by extensive washing in PBS in order to remove unbound proteins. Next, in order to assess the extent of protein adsorption on the carrier´s surface the fluorescence intensity of the carriers containing the fluorescent proteins was measured by flow cytometry (BD Biosciences, Sparks, MD, USA). For protein adsorption under the presence of shear stress (τ), syringes containing 17.6 mg of carriers and 0.5 mg mL^{-1} IgG-FITC or BSA-FITC solutions in PBS (7.5 mL) were connected to a chamber (µ-slide $VI^{0.4}$, tissue culture treated, Ibidi GmbH. Munich, Germany) in order to apply two different shear stresses ($\tau_{0.5}$ = 0.5 dyn cm^{-2} and τ_4 = 4 dyn cm^{-2}) with an Ibidi Pump System (Ibidi GmbH, Munich, Germany). After 4 h of incubation at 37 °C, the samples were washed 2× in PBS (5 min, 8500 rpm) and analysed by flow cytometry. At least 20 000 events were analysed in two independent experiments. In all the experiments, the

ratio between MG/L/PDA or MG/L/PDA/PEG and IgG-FITC or BSA-FITC (in mg) was kept constant.

4.2.2.5 Release Kinetics

MB release kinetics: MG^{MB}/L/PDA or MG^{MB}/L/PDA/PEG multicompartment carriers (56.2 mg mL^{-1} in Tris 2 buffer) were incubated at 37 °C under constant shaking using a PMHT thermoshaker (Grant Bio, Cambridge, United Kingdom). At different time-points, the samples were centrifuged for 5 min at 8500 rpm and the absorbance (A) of the supernatants was analysed at 664 nm employing a Tecan Spark multimode plate reader. Carriers without MB (MG/L/PDA or MG/L/PDA/PEG) were used as controls. The results were normalised to the A at the maximum incubation time:

$$\text{Release of MB } (\%) = \frac{A_t - A_0}{A_\infty - A_0} \text{ x } 100$$

Being A_t: A at different time points; A_0: A at time zero; A_∞: A at maximum incubation time. At least two independent experiments were carried out.

Cal release kinetics: MG/L^{Cal}/PDA or MG/L^{Cal}/PDA/PEG carriers (28.1 mg mL^{-1} in Tris 2 buffer) were incubated at 37 °C under constant shaking using a thermoshaker. Similar to MB release experiments, at specific time-points the samples were centrifuge for 5 min at 8500 rpm and the supernatants were analysed using black 96-well plates and an excitation and emission wavelengths of 485 nm and 535 nm, respectively in a multimode plate reader (Victor3-1420 Multilabel Counter, PerkingElmer, Waltham, MA, USA). In order to achieve the maximum Cal release, 0.1% (v/v) Triton-X was added to the suspensions. As controls, multicompartment carriers with empty liposomes (MG/L/PDA or MG/L/PDA/PEG) were employed. The results were normalised to the fluorescence intensity (FI) after Triton-X addition:

$$\text{Release of Cal } (\%) = \frac{FI_t - FI_0}{FI_{TX} - FI_0} \text{ x } 100$$

Being FI_t: FI at different time points; FI_0: FI at time zero; FI_{TX}: FI after Triton-X addition. At least two independent experiments were performed.

4.2.2.6 Cell experiments

The adenocarcinoma HeLa and mouse macrophage RAW 264.7 cell lines were cultured in DMEM supplemented with 2% (v/v) HEPES, 1% sodium pyruvate, 10% (v/v) FBS and 1% (v/v) penicillin/streptomycin (10 000 U/mL and 10 µg/mL, respectively) at 37°C in a humidified incubator with 5% CO_2 level. The endothelial HUVEC cell line was cultured in EBM-2 supplemented with 0.1% (v/v) hEGF, 0.1% (v/v) VEGF, 0.1% (v/v) R3-IGF-1, 0.1% (v/v) ascorbic acid, 0.04% (v/v) hydrocortisone, 0.4% (v/v) hFGF-β, 0.1% (v/v) heparin, 2% (v/v) FBS and 0.1% (v/v) GA. The cell media was renewed every 2-3 days and only passages between 14-20, 3-9 and 1-4 of HeLa cells, RAW 264.7 cells and HUVEC cells were used in all the experiments. The cells were allowed to grow up to ~80% confluency before being detached from the culture flask using trypsin (3 mL, 0.5 mg mL^{-1}) in the case of HeLa and HUVEC cells and a cell scraper for RAW 264.7 cells. Next, the trypsin was removed by centrifugation (1000 rpm, 5 min) and the cells were resuspended in new cell culture media.

In order to ensure that the cells are exposed to the same amount of carrier, the concentration of the carrier solution was determined by fluorescence measurements of MG/L^F/PDA or MG/L^F/PDA/PEG followed by serial dilutions to achieve the desired concentration. At least three independent experiments were carried out and the data was analysed using one-way ANOVA with a confidence level of 95% ($\alpha = 0.05$) followed by Tukey´s multiple comparison posthoc test (*$p \leq 0.05$; **$p \leq 0.01$; ***$p \leq 0.001$; ****$p \leq 0.0001$) in a GraphPad Prism 7 software.

4.2.2.7 Cell viability

Static conditions (96 well-plates): 30 000 cells (RAW 264.7) or 15 000 cells (HeLa or HUVEC) were seeded in 96-well plate in 200 µL cell culture media and allowed to attach

to the surface for 24 h at 37°C, 5% CO_2. Next, the cells were incubated with 3.7 ng carrier per cell (MG/L/PDA or MG/L/PDA/PEG) in 200 µL cell culture media for 4 h at 37°C, 5% CO_2 followed by washing 2× in 200 µL pre-warmed PBS and 1× in a solution containing cell culture media: WST-8 kit reagent (1:10) in order to remove the non-associated/internalised carriers. Upon washing, the cells were incubated with 100 µL cell culture media and 10 µL WST-8 kit reagents for 70 min at 37°C, 5% CO_2. Finally, 100 µL were transferred to a new 96- well plate and the formazan generated by the reduction of WST-8 by dehydrogenases in cells was detected at 450 nm.

Dynamic conditions (shear stress): 54 000 cells (RAW 264.7) or 27 000 cells (HeLa or HUVEC) were seeded into closed perfusion chambers (µ-slide $VI^{0.4}$) in 150 µL cell culture media and allowed to attach to the surface for 24 h at 37°C, 5% CO_2. Next, the cells were exposed to 3.7 ng MG/L^F/PDA or MG/L^F/PDA/PEG per cell in syringes containing 7.5 mL media (for HUVEC and RAW 264.7) or 9 mL media (for HeLa cells) for 4 h at 37 °C and 5% CO_2 at specific shear stress conditions (τ_4 or τ_{20} = 20 dyn cm^{-2}). Upon incubation, the channel was washed 2× in 200 µL pre-warmed PBS and 1x in a solution containing cell culture media: WST-8 kit reagent (1:10) followed by incubation for 70 min at 37°C, 5% CO_2 with 100 µL cell culture media and 10 µL WST-8 kit reagents. Finally, 100 µL were transferred to a new 96- well plate and the formazan generated by the reduction of WST-8 by dehydrogenases in cells was detected at 450 nm.

In all the experiments cells without exposure to carriers and cell culture media were used as controls. The cell viability was calculated using the following equation:

$$\text{Cell viability (\%)} = \frac{\text{treated or untreated cells-cell culture media}}{\text{untreated cells-cell culture media}} \text{ x } 100$$

4.2.2.8 Cell association/uptake experiments

Static conditions (96 well-plates): 30 000 cells (RAW 264.7) or 15 000 cells (HeLa or HUVEC) were seeded in 96-well plate in 200 µL cell culture media and allowed to attach to the surface for 24 h at 37°C, 5% CO_2. Next, the cells were incubated with 3.7 ng carrier

per cell (MG/L/PDA or MG/L/PDA/PEG) in 200 µL cell culture media for 4 h at 37°C, 5% CO_2 followed by washing 2× in 200 µL pre-warmed PBS in order to remove non-internalised/non-associated carriers. Then, the cells were detached from the wells by scrapping (RAW 264.7 cells) or by trypsinization with 60 µL trypsin (0.5 mg mL^{-1}) (HeLa or HUVEC). Finally, the cell association/uptake of the carriers was evaluated by measuring the CMFI and CUE of at least 2000 cells by flow cytometry.

Dynamic conditions (shear stress): 54 000 cells (RAW 264.7) or 27 000 cells (HeLa or HUVEC) were seeded into closed perfusion chambers (µ-slide $VI^{0.4}$) in 150 µL cell culture media and allowed to attach to the surface for 24 h at 37°C, 5% CO_2. Next, the cells were exposed to 3.7 ng MG/L^F/PDA or MG/L^F/PDA/PEG per cell in syringes containing 7.5 mL media (for HUVEC and RAW 264.7) or 9 mL media (for HeLa cells) for 4 h at 37 °C and 5% CO_2 at specific shear stress conditions ($\tau_{0.5}$, τ_4 or τ_{20}). Upon incubation, the channel was washed 2× in 200 µL pre-warmed PBS and all cell lines were harvested (using trypsinization) for flow cytometry analysis (CMFI and CUE) of at least 2000 cells.

In all the experiments cells without exposure to carriers were used as control.

4.2.2.9 Cell imaging

Synthesis of PFA: In order to synthesise 8% (wt/v) PFA 16 mg PFA were dissolved in 80 mL Milli-*Q* water under constant stirring and nitrogen atmosphere at 60-70°C for 1 h. Then, two drops of 5 M NaOH were added in order to fully dissolve the PFA. Next, the pH was adjusted to 7.0 and the reaction mixture was allowed to cool down to room temperature followed by the addition of 20 mL Milli-*Q* water (final volume 100 mL). Finally, the solution was filtered through 0.45 µm cellulose acetate filters and mixed with 100 mL of PBS.

In order to confirm the successful internalisation of the carriers (MG/L^F/PDA or MG/L^F/PDA/PEG) rather than being associated with the cellular surface the cells were fixed and stained.

Static conditions (48 well-plate): 40 000 cells (RAW 264.7) and 25 000 cells (HUVEC or HeLa) were seeded in a 48-well plate containing a previously sterilized cover glass in each well in 500 µL media. Upon cell attachment, for 24 h at 37 °C and 5% CO_2, the cells were incubated with 3.7 ng MG/L^F/PDA or MG/L^F/PDA/PEG per cell for 4 h at 37 °C and 5% CO_2. Next, the non-internalised/non-associated carriers were removed by washing 2× in PBS followed by fixation with 4% PFA solution for 30 min at room temperature and extensively washed in PBS to remove the PFA. The actin filaments of the cellular membrane were stained with phalloidin-TRITC (0.003 mg mL^{-1}) for 1 h at room temperature followed by extensive washing in PBS in order to remove the excess of phalloidin-TRITC. Finally, the cells were imaged using CLSM (Leica Microsystems GmbH, Wetzlar, Germany) equipped with a 63× water-immersion objective. The macrophage cell line (RAW 264.7) was imaged using a Zeiss LSM700 CLSM (Carl Zeiss AG, Oberkochen, Germany) equipped with a 20× objective.

Dynamic conditions (shear stress): 54 000 cells (RAW 264.7) or 27 000 cells (HeLa or HUVEC) were seeded into closed perfusion chambers (µ-slide $VI^{0.4}$) in 150 µL cell culture media and allowed to attach to the surface for 24 h at 37°C, 5% CO_2. Next, the cells were exposed to 3.7 ng MG/L^F/PDA or MG/L^F/PDA/PEG per cell in syringes containing 7.5 mL media (for HUVEC and RAW 264.7) or 9 mL media (for HeLa cells) for 4 h at 37 °C and 5% CO_2 at specific shear stress conditions ($\tau_{0.5}$, τ_4 or τ_{20}). Upon incubation, the channel was washed 2× in 200 µL pre-warmed PBS and fixated with 4% PFA solution for 30 min at room temperature. Upon washing, the actin filaments of the cellular membrane were stained with phalloidin-TRITC (0.003 mg mL^{-1}) for 1 h at room temperature and washed in PBS. The cells were imaged inside of the channels using a CLSM and 63× water-immersion objective. The macrophage cell line (RAW 264.7) was imaged using a Zeiss LSM700 CLSM equipped with a 20× objective.

In all the experiments cells without exposure to multicompartment carriers were used as control.

4.2.2.10 Cell uptake pathway

Synthesis of PLL-*g*-PEG: For the cellular uptake pathway experiments, PLL-*g*-PEG was synthesised as previously reported.[140] Specifically, 0.038 mmol Me-PEG-NHS were dissolved in cold HEPES buffer and added to a solution composed by 0.143 mmol PLL in cold HEPES buffer followed by 4 h incubation at 4 °C under constant shaking. Next, the reaction mixture was purified by two days dialysis using a cellulose dialysis membrane with a cut-off of 14 kDa. Nuclear magnetic resonance analysis was used in order to confirm the grafting ratio (GR) of 2.9. GR is defined as the ratio of the number of lysine monomers to the number of PEG side chains

Static conditions (96 well-plate): 30 000 cells (RAW 264.7) or 15 000 cells (HeLa or HUVEC) were seeded in 96-well plate in 200 µL cell culture media and allowed to attach to the surface for 24 h at 37°C, 5% CO_2. Next, the RAW 264.7 cells were pre-incubated with either 1 µg mL^{-1} filipin, 50 µM amiloride or 1 µM lantrunculin A as previously reported.[11] While HeLa and HUVEC cells were pre-incubated with 20 µM chlorpromazine, 2 µg mL^{-1} filipin or 100 µM amiloride for 30 min at 37°C and 5% CO_2 in cell culture media without antibiotics in order to avoid deactivation of the inhibitor. Then, 3.7 ng of MG/L^F/PDA or MG/L^F/PDA/PEG per cell were added in the presence of the inhibitors, in order to avoid the restoration of the pathway during the exposure to the multicompartment carriers,[141] and incubated for 4 h at 37°C and 5% CO_2. Finally, the cells were washed in PBS, harvested by trypsinization or scrapping and analysed by flow cytometry (at least 2000 cells were analysed).

Dynamic conditions (shear stress): 54 000 cells (RAW 264.7) or 27 000 cells (HeLa or HUVEC) were seeded into closed perfusion chambers (µ-slide $VI^{0.4}$) in 150 µL cell culture media and allowed to attach to the surface for 24 h at 37°C, 5% CO_2. Next, the RAW 264.7 cells were pre-incubated with either 1 µg mL^{-1} filipin, 50 µM amiloride or 1 µM lantrunculin A as previously reported.[11] While HeLa and HUVEC cells were pre-incubated with 20 µM chlorpromazine, 2 µg mL^{-1} filipin or 100 µM amiloride for 30 min at 37°C and 5% CO_2 in cell culture media without antibiotics. Then, the cells were exposed to 3.7 ng MG/L^F/PDA or MG/L^F/PDA/PEG per cell in syringes containing 7.5

mL media (for HUVEC and RAW 264.7) or 9 mL media (for HeLa cells) and the inhibitors for 4 h at 37 °C and 5% CO_2 at specific shear stress conditions ($\tau_{0.5}$, τ_4 or τ_{20}). Finally the cells were washed in PBS, trypsinized from the channels and analysed by flow cytometry.

In all the experiments, cells without MG/L^F/PDA, MG/L^F/PDA/PEG and inhibitor exposure and cells exposed to either MG/L^F/PDA or MG/L^F/PDA/PEG without inhibitor exposure where used as controls.

4.3 Results and Discussion

4.3.1 Protein adsorption

Once a drug delivery carrier is intravenously administered it is exposed to the human physiology including blood components (*i.e.*., albumin, lipoproteins, apolipoproteins, proteins of complement, immunoglobulins, etc.) that can interact with the surface of the carrier leading to the accumulation of opsonins which translates into higher recognition and clearance by MPS.[100] Therefore, PEGylation of the carriers has been widely used in the drug delivery field as a strategy to protect the surface from opsonins binding and therefore, to improve their circulation time in the body.[101]

Albumin and IgG are the most abundant protein in plasma (30-45 g L^{-1}) and the most abundant immunoglobulin in blood (7-16 g L^{-1}) respectively. Therefore, the assessment of the PEGylation effect of the multicompartment system in the presence of these proteins is of outmost importance.

Another crucial aspect regarding the effect of human physiology on drug delivery carriers administered intravenously is the shear stress generated due to blood flow or interstitial fluid in tumour tissue (when targeting to tumour tissue is the aim). Therefore, it is not only important to evaluate the performance of the multicompartment carrier in the

presence of relevant proteins but also under conditions closer to the physiological dynamic environment.

For this, non-PEGylated (MG/L/PDA) and PEGylated (MG/L/PDA/PEG) carriers were incubated with either IgG-FITC or BSA-FITC in the absence (τ = 0 dyn cm^{-2} (τ_0)) or presence of shear stress found in vasculature ($\tau_{0.5}$ and τ_4) for 4 h at 37 °C followed by extensive washing and analysed by flow cytometry.

As shown in Figure 4.1 the results have been normalised to MFI of MG/L/PDA carriers incubated with either IgG-FITC or BSA-FITC at τ_0. An overall slight decrease in nMFI can be observed due to PEGylation of the carrier. However, this decrease in nMFI differs depending on both the studied protein as well as the shear stress conditions. For IgG-FITC binding, when exposing the carriers to both τ_0 and τ_4, there was only a 37 ± 5% and 26 ± 3% decrease, respectively, in nMFI as a result of PEGylation (Figure 4.1ai). Interestingly, a dramatic decrease in nMFI can be observed for MG/L/PDA/PEG carriers at the lowest shear stress condition ($\tau_{0.5}$, 117 ± 63%). For BSA-FITC incubation, in agreement with the IgG-FITC results, the largest reduction in nMFI (64 ± 12%) is also observed for the lowest shear stress conditions of $\tau_{0.5}$ (Figure 4.1aii). It is also worth mentioning that the presence of shear stress seems to promote protein deposition ($\tau_{0.5}$ in the case of IgG-FITC and $\tau_{0.5}$ and τ_4 in the case of BSA-FITC), an observation that has also been reported by Palchetti *et al*. In particular, PEGylated liposomes under shear stress conditions displayed a larger variety of proteins in the corona than when incubated in the absence of shear stress.[142]

All in all, these results indicate that although the PEGylation effect of the multicompartment carrier is rather limited, it is observed in all tested conditions.

The diminished binding of both IgG-FITC and BSA-FITC onto MG/L/PDA/PEG at $\tau_{0.5}$ was also verified by fluorescence microscopy images. The results show a lower fluorescence intensity signal for MG/L/PDA/PEG incubated with either IgG-FITC or BSA-FITC as compared to MG/L/PDA at all shear stress conditions, being more obvious for $\tau_{0.5}$ (Figure 4.1bi,ii). The fluorescence and DIC images revealed that the presence of both BSA and IgG, did not affect the colloidal stability in terms of aggregation for all

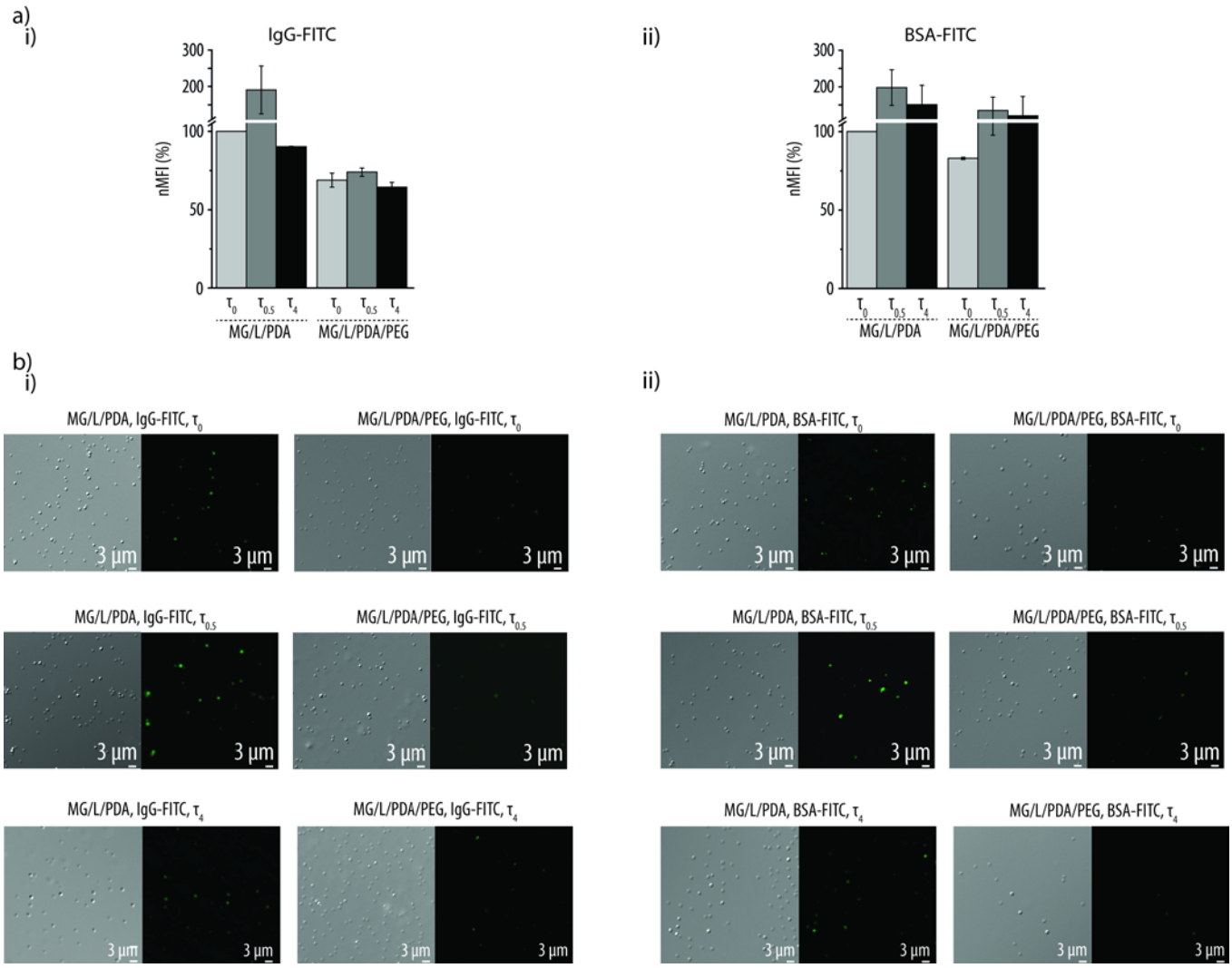

Figure 4.1 Protein adsorption onto the multicompartment carriers surface. a) Normalised mean fluorescence intensity (nMFI) non-PEGylated (MG/ L^F /PDA) and PEGylated (MG/L/PDA/PEG) carriers upon incubation with fluorescently labelled immunoglobulin G (IgG-FITC) (i) and bovine serum albumin (BSA-FITC) (ii) at $\tau = 0$ dyn cm^{-2} (τ_0, light grey bars), $\tau = 0.5$ dyn cm^{-2} ($\tau_{0.5}$, dark grey bars) and $\tau = 4.0$ dyn cm^{-2} (τ_4, black bars). b) Differential interference contrast and fluorescence microscopy images upon incubation with IgG-FITC (i) and BSA-FITC (ii). Adapted from reference [60] with permission. Copyright (2018) by Elsevier.

tested conditions.

4.3.2 Dual-cargo release kinetics

Although the building blocks of hydrogel-liposomes complexes, P(NIPAM-*co*-AAc) MGs[62–65] and liposomes,[2] have been largely investigated, the combination of both systems has been rarely reported in literature. Previous studies have been mainly focused on the control of the kinetic release of the liposomes by linking them to MGs through avidin-biotin conjugation[103] or by physically trapping them inside of a MG particle´s network.[104] However, the potential use of hydrogel-liposomes complexes as dual-drug delivery carriers has been only reported in one study.[26]

The main advantage of multicompartment systems is the possibility to co-encapsulate (incompatible) drugs in separated compartments, which can result in a potential synergistic effect.[2] The developed MG/L/PDA/PEG carrier consists of compartments of two different materials, liposomes and MGs, each of them capable of carrying different molecules in separated compartments. To demonstrate such compartmentalization, two distinguishable fluorophores were encapsulated. In particular, MB and Cal were entrapped in the MGs and the L core and their release profiles at 37 °C were assessed independently. Figure 4.2a and Figure 4.2b show the release of MB and Cal from the MGs and from the L, respectively, into the aqueous environment for both MG^{MB}/L/PDA, MG/L^{Cal}/PDA, MG^{MB}/L/PDA/PEG and MG/L^{Cal}/PDA/PEG multicompartment carriers. For MB, the results are normalised to the maximum amount of MB cumulative release in the tested time framework while, for Cal, the results are normalised to the Cal cumulative release upon addition of Triton X, which was added after 24 h incubation to rupture the liposomes and release the remaining entrapped Cal.

Regarding the MG^{MB}/L/PDA, for MB the kinetic curve shows a rapid release profile for the first 7-9 h where approximately 75-81% of the encapsulated MB gets released, followed by a slow increase of the release rate (Figure 4.2a, empty squares). The large pores of the MGs may be responsible for the fast release rate of the loaded cargo observed for the MGs.[26] In contrast, the Cal release profile reveals an initial burst release of approximately 20% after 1 h incubation, followed by a slower release rate, reaching 70% release after 24 h of incubation (Figure 4.2b, empty squares). For PEGylated carriers,

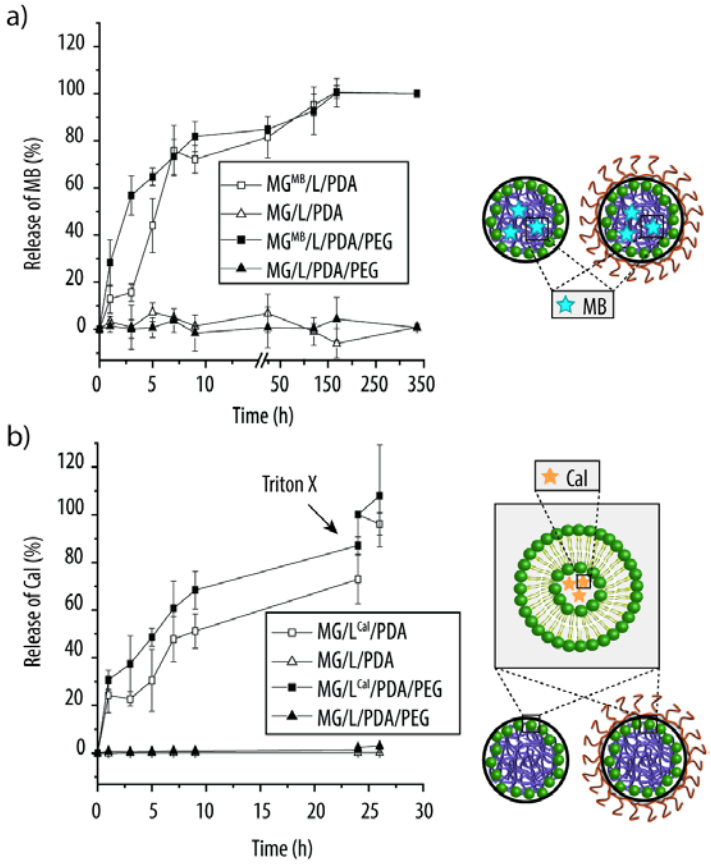

Figure 4.2 Dual-cargo release kinetics. a) Release of encapsulated methylene blue (MB) inside the microgels (MG^{MB}) core overtime from both non-PEGylated (MG^{MB}/L/PDA) and PEGylated (MG^{MB}/L/PDA/PEG) multicompartment carriers. b) Release of encapsulated Calcein (Cal) within the liposomes (L^{Cal}) overtime from both MG/L^{Cal}/PDA and MG/L^{Cal}/PDA/PEG. Adapted from reference [60] with permission. Copyright (2018) by Elsevier.

although the release profiles were similar to the non-PEGylated ones, a general increase in the release rate was observed for both cases (Figure 4.2a and 4.2b**,** black squares). Those results indicate that the PLL-*g*-PEG functionalisation slightly increases either the PDA or the underlying liposomes permeability.

In conclusion, Figure 4.2 demonstrates that for both non-functionalised and PEGylated carriers, in agreement with a previously reported study,[26] the release rate of MB encapsulated within MGs core is faster than the release rate of Cal encapsulated within the L^{Cal}.

4.3.3 Interaction of non-functionalised and PEGylated carriers with cells

The evaluation of the interaction of the multicompartment system with relevant cell lines (*i.e.*, HUVEC, RAW 264.7 and HeLa cells) is of outmost importance. In this chapter, the studies are brought to the next level by incorporating the dynamic human physiology factor.

It is well known that blood flow generates hemodynamic forces such as shear stress on the surface of endothelial cells, as well as to the circulating macrophages.[105] Several studies have reported the impact of physiological shear stress on the cell/carrier association,[109] illustrating the importance of considering shear stress in the *in vitro* characterisation in order to better mimic the physiological dynamics and improving the transition from *in vitro* to preclinical studies.[109] Despite the increasing evidence of its impact on the cell/carrier interaction, shear stress is often omitted in cell uptake studies. Hence, the impact of microvasculature physiological shear stress conditions (*i.e.*, $\tau_{0.5}$ and τ_4)[143] on the cellular uptake of MG/L^F/PDA and MG/L^F/PDA/PEG carrier was evaluated under by monitoring CMFI and CUE in the absence and presence of shear stress.

RAW 264.7 cells: As depicted in (Figure 4.3ai, light grey bars), at τ_0 there is a significant decrease of ~2.5 fold in CMFI and ~2 fold in CUE when RAW 264.7 cells are exposed to MG/L^F/PDA/PEG as compared to MG/L^F/PDA, which confirms the successful functionalisation of the carriers surface, in agreement with the ζ-potential and QCM-D results (Chapter 3, section 3.3.2.3). When exposed to $\tau_{0.5}$ (Figure 4.3ai, dark grey bars), there is an overall increase in both CMFI and CUE for both MG/L^F/PDA/PEG and MG/L^F/PDA carriers as compared to τ_0, indicating a higher uptake or cell association of the carriers with the cells. In particular, there is a ~1.9 and a ~2.7 fold higher CMFI for MG/L^F/PDA and MG/L^F/PDA/PEG carriers, respectively, as compared to τ_0. Additionally, there is also a ~31% and ~54% higher CUE upon applying $\tau_{0.5}$ as compared to τ_0 for MG/L^F/PDA and MG/L^F/PDA/PEG carriers, respectively (Figure 4.3ai-ii, light grey and dark grey bars). At $\tau_{0.5}$, the PEGylation effect is still preserved

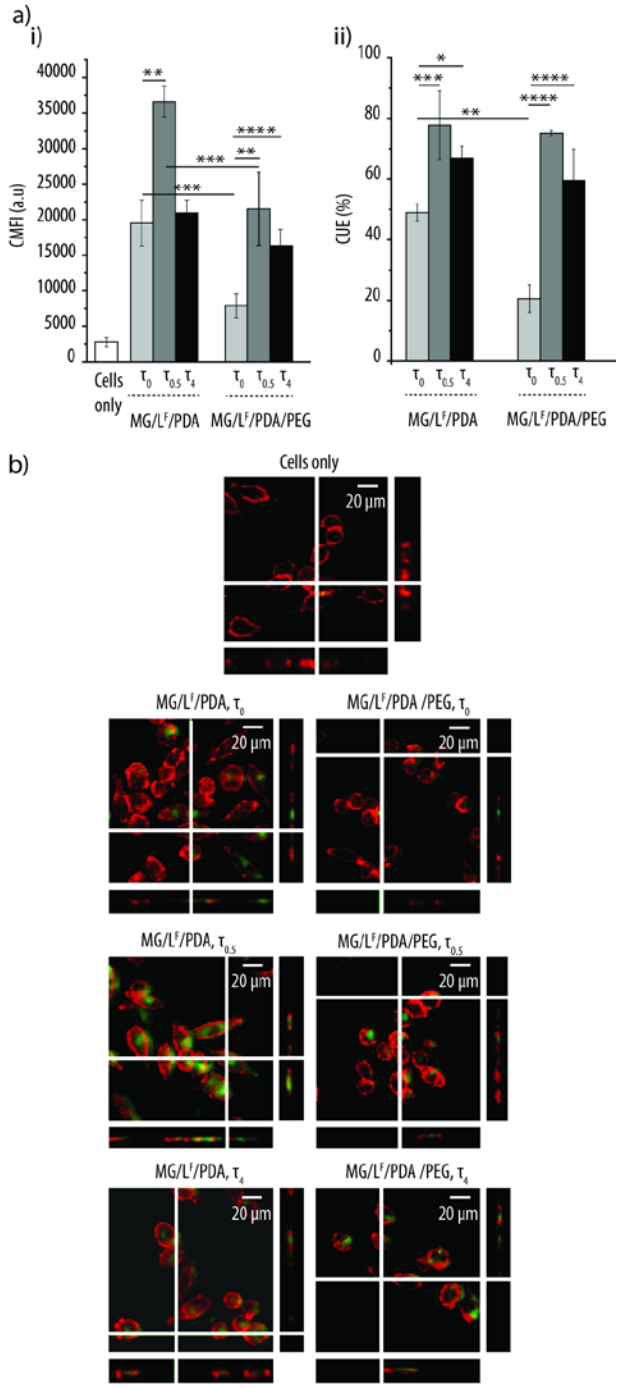

Figure 4.3 Interaction of non-PEGylated (MG/L^F/PDA) and PEGylated carriers (MG/L^F/PDA/PEG) with RAW 264.7 cells. a) i) Cell mean fluorescence intensity (CMFI) of RAW 264.7 cells upon exposure to the carriers at $\tau = 0$ dyn cm^{-2} (τ_0, light grey bars), $\tau = 0.5$ dyn cm^{-2} ($\tau_{0.5}$, dark grey bars) and $\tau = 4.0$ dyn cm^{-2} (τ_4, black bars). n = 3, *$p \leq 0.05$; **$p \leq 0.01$; ***$p \leq 0.001$; ****$p \leq 0.0001$. ii) Cell uptake efficiency (CUE) of the MG/L^F/PDA and MG/L^F/PDA/PEG carriers by RAW 264.7 cells at τ_0 (light grey bars), $\tau_{0.5}$ (dark grey bars) and τ_4 (black bars). b) Confocal laser scanning microscopy images showing the internalisation of MG/L^F/PDA and MG/L^F/PDA/PEG (green signal) by RAW 264.7 cells at different shear stress conditions.

with a significant decrease of ~1.7 fold in CMFI upon exposing MG/L^F/PDA/PEG carriers to RAW 264.7 as compared to their MG/L^F/PDA counterparts. In contrast, at τ_4 only the MG/L^F/PDA/PEG carriers generate a significant increase in the CMFI (~2 fold) as compared to τ_0 (Figure 4.3ai, light grey and black bars). However, at τ_4, an increase in CUE is observed for both MG/L^F/PDA and MG/L^F/PDA/PEG carriers (Figure 4.3aii, light grey and black bars). Unfortunately, at τ_4, the PEGylation effect was lost and there no significant differences in the CMFI or CUE when employing MG/L^F/PDA/PEG or MG/L^F/PDA carriers were observed (Figure 4.3ai and 4.3aii, black bars). Although these results show that the PEGylation effect of the system is quite limited, they are not surprising since similar results were obtained by Thingholm *et al*.,[21] when employing also a multicompartment carrier decorated with PLL-*g*-PEG.

To confirm that the multicompartment carriers had been internalised by the cells and were not only associated with them, the macrophages exposed to the multicompartment carriers were fixed, their membranes stained and visualised by CLSM. As controls, macrophages without the presence of multicompartment carriers were also fixed, stained and imaged.

Figure 4.3b shows representative images confirming the internalisation of the microreactors after 4 h of incubation in static conditions (τ_0, top images) and in the presence of the lowest ($\tau_{0.5}$, middle images) and highest shear stress (τ_4, bottom images). The insets depict the projection of the slides in the z-axis, which further corroborate the internalisation of the multicompartment carriers.

HUVEC cells: As shown in Figure 4.4ai and 4.4aii, applying shear stress results in an increase of both the CMFI and the CUE for both $\tau_{0.5}$ and τ_4. However, in contrast to RAW 264.7 cells where $\tau_{0.5}$ resulted in the higher CMFI, for HUVEC the higher the shear stress the higher the CMFI (Figure 4.4ai). An overall increase of CUE was also observed in the presence of shear stress although far less pronounced than for the RAW 264.7 cell line.

Additionally, there were no significant differences for the CUE independent on the shear stress applied and the presence or absence of a PEG coating (Figure 4.4aii). In the absence of shear stress (Figure 4.4, light grey bars), although the differences are not significant, there is a ~1.3 fold decrease in CMFI and a ~11% decrease in CUE when

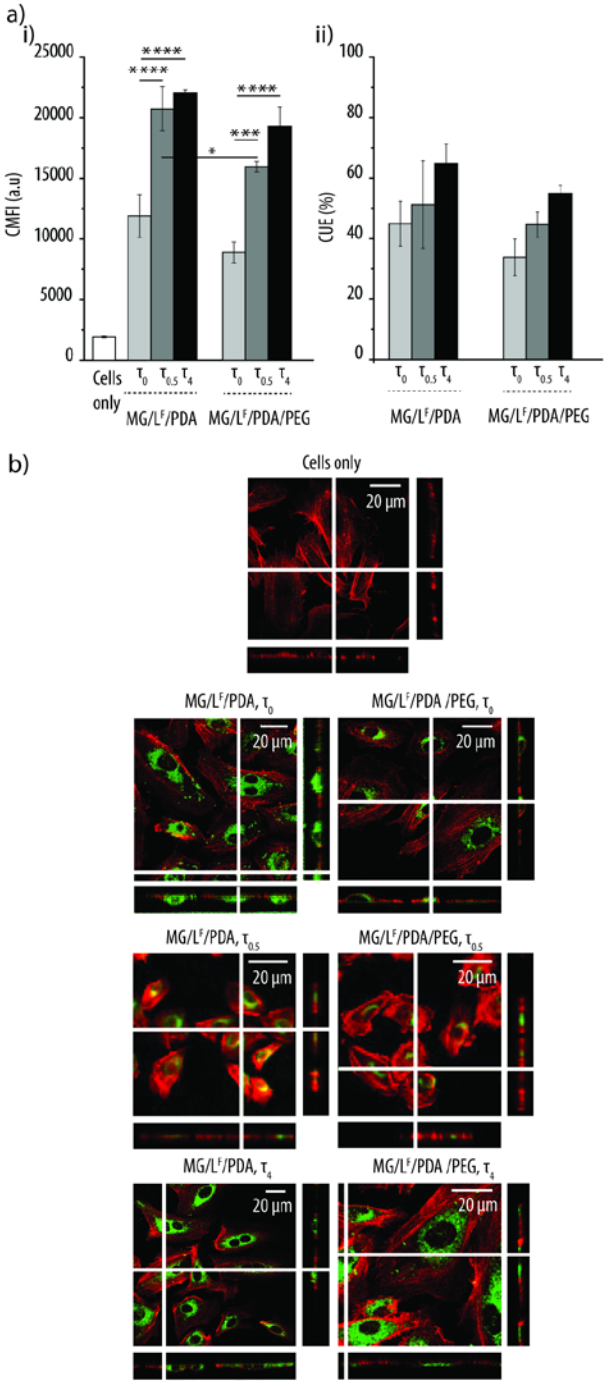

Figure 4.4 Interaction of non-PEGylated (MG/L^F/PDA) and PEGylated carriers (MG/L^F/PDA/PEG) with HUVEC cells. a) i) Cell mean fluorescence intensity (CMFI) of HUVEC cells upon exposure to the carriers at $\tau = 0$ dyn cm^{-2} (τ_0, light grey bars), $\tau = 0.5$ dyn cm^{-2} ($\tau_{0.5}$, dark grey bars) and $\tau = 4.0$ dyn cm^{-2} (τ_4, black bars). n = 3, *p ≤ 0.05; **p ≤ 0.01; ***p ≤ 0.001; ****p ≤ 0.0001. ii) Cell uptake efficiency (CUE) of the MG/L^F/PDA and MG/L^F/PDA/PEG carriers by HUVEC cells at τ_0 (light grey bars), $\tau_{0.5}$ (dark grey bars) and τ_4 (black bars). b) Confocal laser scanning microscopy images showing the internalisation of MG/L^F/PDA and MG/L^F/PDA/PEG (green signal) by HUVEC cells at different shear stress conditions. The actin filaments of the cells have been stained with phalloidin-TRITC (red signal). Adapted from reference [60] with permission. Copyright (2018) by Elsevier.

the HUVEC cells are exposed to MG/L^F/PDA/PEG as compared to MG/L^F/PDA. When exposing HUVEC cells to shear stress conditions, an increase of ~1.8 fold and ~1.9 fold in the CMFI was observed for MG/L^F/PDA when applying both $\tau_{0.5}$ and τ_4 (Figure 4.4ai, dark grey and black bars, respectively) as compared to τ_0 (Figure 4.4ai, light grey bars) and ~1.8 ($\tau_{0.5}$) and ~2.2 (τ_4) times higher for MG/L^F/PDA/PEG. However, although a decrease in CMFI was observed due to PEGylation at both $\tau_{0.5}$ and τ_4, this ~1.3 fold decrease in CMFI was only significant when applying $\tau_{0.5}$, and was far less pronounced than for the RAW 264.7 cell line.

Additionally, for HUVEC cells, the CUE values are relatively low as compared to the CUE values for macrophages, reaching a maximum of only ~65% for MG/L^F/PDA in the presence of τ_4. Similar to RAW 264.7 cells, although these results indicate a poor PEGylation effect of the PEG coating, they are in agreement with previously reported literature.[21] In particular, studies performed in HUVEC cells, reported a lack of PEGylation effect when applying a τ_4 shear stress and employing the copolymer PLL-*g*-PEG as a low-fouling coating.

With the aim of confirming internalisation by HUVEC cells, the cells were fixed after the 4 h incubation time, stained their membranes and visualised them by CLSM. The visualization confirmed the carrier's internalisation by the cells as shown by the green signal, due to the L^F of the multicompartment carriers, in the projection of the slides in the z-axis (Figure 4.4b).

HeLa cells: Great efforts have been invested on the study of the impact of shear stress on endothelial[144] and macrophages,[21] however when it comes to shear stress on tumour tissue the number of studies drops drastically.[145] Cancer cells are not only exposed to the vasculature shear stress (with values that range from 0.5 to 30.0 dyn cm^{-2}) but also to the shear stress produced by the interstitial flow with values as low as 0.1 dyn cm^{-2}.[145] Therefore, the interaction of the multicompartment carrier (MG/L^F/PDA/PEG and MG/L^F/PDA) with the model cancer cell line is evaluated under the effect of two physiologically relevant shear stresses ($\tau_{0.5}$ and τ_{20}).

The relevance of applying shear stress in the association/uptake of the microcarriers with tumour cells is highlighted in Figure 4.5. The results show that the exposure of HeLa cells to both MG/L^F/PDA and MG/L^F/PDA/PEG lead to a dramatic increase in CMFI upon applying shear stress (for both $\tau_{0.5}$ and τ_{20}) (Figure 4.5ai). In particular, an increase of ~3.2 fold and ~2.9 fold in CMFI for MG/L^F/PDA and MG/L^F/PDA/PEG was observed for $\tau_{0.5}$, while there was a ~4.6 fold and ~3.9 fold increase in CMFI for MG/L^F/PDA and MG/L^F/PDA/PEG carriers at τ_{20}. In contrast, no significant increase in CUE was observed upon applying shear stress (Figure 4.5aii).

The results also show that while no PEGylation effect was observed at τ_0, a slight decrease in CMFI was detected for MG/L^F/PDA/PEG at $\tau_{0.5}$. However, this decrease in CMFI was non-significant. Only τ_{20} resulted in a significant decrease in CMFI, and a reduction ~1.5 fold in CMFI upon incubation with MG/L^F/PDA/PEG as compared to the MG/L^F/PDA counter parts was measured, thus indicating a PEGylation effect. As depicted in Figure 4.5aii, no significant differences in the CUE of HeLa cells upon incubation of the multicompartment carriers at τ_0, $\tau_{0.5}$ or τ_{20} were observed, with values of ~90% for τ_0, ~94% for $\tau_{0.5}$ and ~95% for τ_{20}.

It is worth noticing that the CMFI of HeLa incubated with MG/L^F/PDA and MG/L^F/PDA/PEG, both at static and in the presence of shear stress, was much higher when compared to the CMFI of RAW 264.7 and HUVEC cells. In particular, for MG/L^F/PDA, at τ_0, the CMFI was ~1.6 and ~2.6 fold higher as compared to RAW 264.7 and HUVEC cells. For MG/L^F/PDA/PEG at τ_0, the CMFI was even higher, resulting in a ~3.2 and ~3 fold increase when compared to RAW 264.7 and HUVEC cells. In the presence of $\tau_{0.5}$ the CMFI increase resulted in ~2.7 and ~4.8 fold for HeLa cells upon exposure to MG/L^F/PDA as compared to RAW 264.7 and HUVEC cells. Incubation with MG/L^F/PDA/PEG at $\tau_{0.5}$ resulted in a ~3.5 and ~4.7 fold higher increase in CMFI as compared to RAW 264.7 and HUVEC cells. Those results suggest that HeLa cells preferentially internalised or associated with the carrier in comparison to RAW 264.7 or HUVEC cells independently of the intensity of shear stress and functionalisation of the carrier.

To confirm that the multicompartment carriers had been internalised by the cells, their

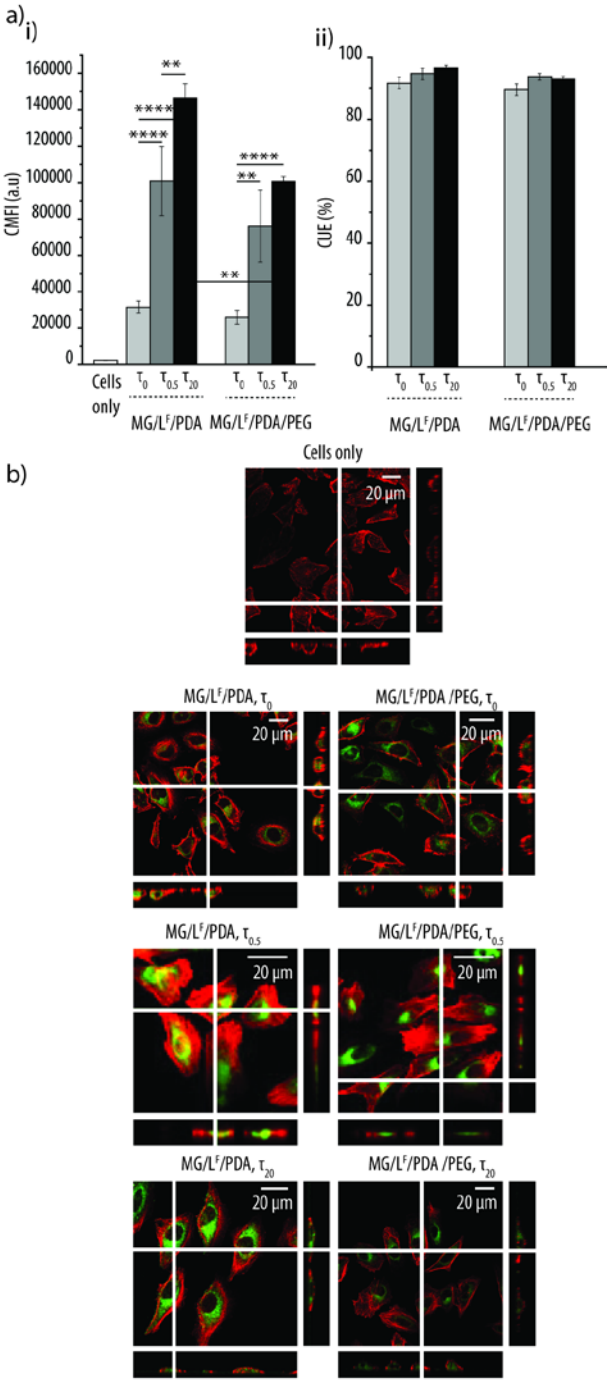

Figure 4.5 Interaction of non-PEGylated (MG/L^F/PDA) and PEGylated carriers (MG/L^F/PDA/PEG) with HeLa cells. a) i) Cell mean fluorescence intensity (CMFI) of HeLa cells upon exposure to the carriers at τ = 0 dyn cm^{-2} (τ_0, light grey bars), τ = 0.5 dyn cm^{-2} ($\tau_{0.5}$, dark grey bars) and τ = 20.0 dyn cm^{-2} (τ_{20}, black bars). n = 3, *p ≤ 0.05; **p ≤ 0.01; ***p ≤ 0.001; ****p ≤ 0.0001. ii) Cell uptake efficiency (CUE) of the MG/L^F/PDA and MG/L^F/PDA/PEG carriers by HeLa cells at τ_0 (light grey bars), $\tau_{0.5}$ (dark grey bars) and τ_{20} (black bars). b) Confocal laser scanning microscopy images showing the internalisation of MG/L^F/PDA and MG/L^F/PDA/PEG (green signal) by HeLa cells at different shear stress conditions. The actin filaments of the cells have been stained with phalloidin-TRITC (red signal). Adapted from reference [60] with permission. Copyright (2018) by Elsevier.

membranes were stained and imaged by CLSM (Figure 4.5b). The x-z and y-z projection panels confirmed the successful internalisation of the carrier.

After an extensive literature research, these results represent one of the first reports on the influence of shear stress on the PEGylation effect in a cancer cell line. Kang *et al.*,[112] also evaluated the cell uptake of a carrier by cancer cell lines in the presence of shear stress. In agreement with these findings, they demonstrated that the cellular uptake of polystyrene particles by three different cancer cell lines (*i.e.*, PANC-1, A540 and HT29) significantly increased in the presence of shear stress as compared to static conditions.[112] Although more in depth studies are required to understand the underlying mechanism, those results reveal the important role that shear stress plays on the cellular uptake of different carriers, in particular for cancer cell lines.

4.3.4 Cell viability

The lack of inherent cytotoxicity of MG/L/PDA and MG/L/PDA/PEG under the absence (τ_0) and presence of the highest shear stress tested (*i.e.*, τ_4 for RAW 264.7 and HUVEC, and τ_{20} for HeLa) was assessed in order to rule out any potential detrimental effect due to the experimental conditions. As shown in Figure 4.6, non-significant decrease in cell viability was observed for HUVEC and HeLa cells in any of the experimental conditions. However, a significant decrease of cell viability was observed for RAW 264.7 cells exposed to shear stress regardless of the carrier´s functionalisation. Those results can be explained by the semi-adherent nature of RAW 264.7 cell which, upon exposure to high levels of shear stress, can lead to the detachment of the cells, as previously reported by various studies.[146,147]

4.3.5 Cellular uptake pathway

Having established the impact of shear stress on the carrier´s interaction with different cell lines, the cell entry pathways employed by MG/L^F/PDA and MG/L^F/PDA/PEG for each cell line together with the effect of shear stress in such cell internalisation pathways were investigated.

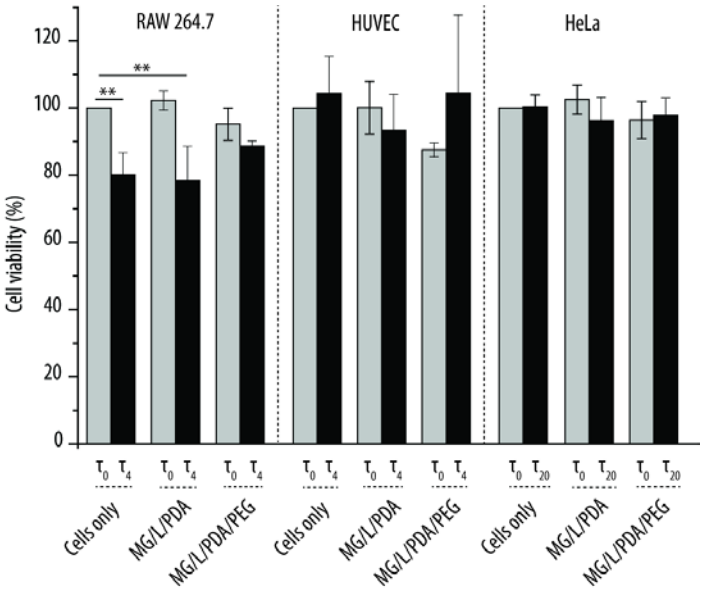

Figure 4.6 Cell viability of RAW 264.7, HUVEC and HeLa cells upon exposure to non-PEGylated (MG/L^F/PDA) and PEGylated (MG/L^F/PDA/PEG) carriers at $\tau = 0$ dyn cm^{-2} (τ_0), $\tau = 4$ dyn cm^{-2} (τ_4) and $\tau = 20$ dyn cm^{-2} (τ_{20}). n = 3, **p ≤ 0.01. Adapted from reference [60] with permission. Copyright (2018) by Elsevier.

Establishing the cell internalisation pathway is crucial for carriers, since it will determine the intracellular fate of the system[148] which could be varied depending on the desired target (*i.e.*, to avoid endosomal or lysosomal degradation, etc.). Therefore, the multicompartment carriers being uptake by the different cell lines in the presence of pathway inhibitors were studied.

Specifically, the cellular uptake of the carrier by RAW 264.7 macrophage cell line was evaluated in the presence of filipin, which inhibits caveolae-mediated endocytosis (CvME)[149] by binding to the cholesterol-rich membrane domains of the caveolae which leads to their distortion and subsequent loss of functionality;[150] amiloride, which inhibits macropinocytosis[151] by blocking the Na^+/H^+ exchange;[150] and latrunculin A, which inhibits phagocytosis[149] by binding to the monomeric actin and preventing the actin polymerisation which is required for phagocytosis to take place.[150]

In the case of HUVEC and HeLa cells the cellular uptake pathway was investigated in the presence of chlorpromazine, which is known to inhibit the clathrin-mediated endocytosis (CME)[151] by translocating both the clathrin and the adaptor complex 2, a major

component of clathrin pits, to intracellular endosomes;[150] filipin, since it is well known that caveolae is highly abundant at the surface of endothelial cells;[152] and amiloride. The internalisation pathway in HUVEC and HeLa was not evaluated in the presence of latrunculin A, due to the non-professional phagocytic nature of both cell lines. The shear stress condition with the largest effect on both the CMFI and the PEGylation effect on each cell line was the one chosen to elucidate the multicompartment carrier´s cell uptake pathway. In particular, $\tau_{0.5}$ was selected to study the cell internalisation mechanism for RAW 264.7 and HUVEC cells, while τ_{20} was selected to study the cell internalisation mechanism in HeLa cells.

It is worth noting that previous studies regarding the influence of shear stress on the target sites of the different inhibitors involved in the different cell uptake pathways (*i.e.*, CvME,[153] macropinocytosis[154] and phagocytosis)[155] have been conducted. In particular, latest reports indicate that the function of caveolae in endothelial cells is to act as mechanotransductor which sense or transduce hemodynamic changes of the blood flow into biochemical signals that regulate vascular function. As such, due to that intrinsic biological function of caveolae, they remain intact and functional in the presence of physiological shear stress.[153,156] Regarding the amiloride performance under shear stress, a previous study has reported that the amiloride binding kinetics to the ion channels of epithelial cells were not altered by the shear stress forces.[154] Finally, super-resolution optical microscopy studies have shown the complete disassembly of the actin filaments upon administering latrunculin A under physiological shear stress conditions, thus demonstrating the preservation of the inhibitor's functionality under dynamic conditions.[155]

Therefore, the results obtained in previous studies suggest that the functionality of the chemical inhibitors should not be affected by the shear stress. An exception is CME, where studies regarding the impact of shear stress on clathrin pit formation are lacking, thus making it difficult to elucidate the functionality of chlorpromazine under shear stress conditions. Nonetheless, previous reports have employed chlorpromazine to inhibit CME under the effect of shear stress.[112]

RAW 264.7 cells: The lack of inherent cytotoxicity of the inhibitor´s concentrations[11] was first confirmed (Figure 4.7a). Next, the cellular uptake pathway was evaluated in terms of CMFI normalised to the CMFI of MG/L^F/PDA or MG/L^F/PDA/PEG incubated with cells in the absence of inhibitors (Figure 4.7b, white bars). As shown in (Figure 4.7b, light grey bar), the internalisation of MG/L^F/PDA and MG/L^F/PDA/PEG multicompartment carriers was most efficiently inhibited by latrunculin A both in static as well as at $\tau_{0.5}$, being the only inhibitor that led to a significant decrease of the nCMFI regardless of the presence or absence of the shear stress. For MG/L^F/PDA, latrunculin A led to a significant decrease of the nCMFI (by 47 ± 11%) at τ_0, while neither filipin (Figure 4.7b, dark grey bar) and amiloride (Figure 4.7b, black bar) resulted in a non-significant effect on the nCMFI. Thus, suggesting that MG/L^F/PDA at τ_0 are preferentially internalised by a phagocytic pathway, as expected for a macrophage cell line.[11]

Interestingly, at $\tau_{0.5}$, the nCMFI of cells exposed to MG/L^F/PDA was significantly reduced by all tested inhibitors. While filipin inhibited cell internalisation by 19 ± 7%

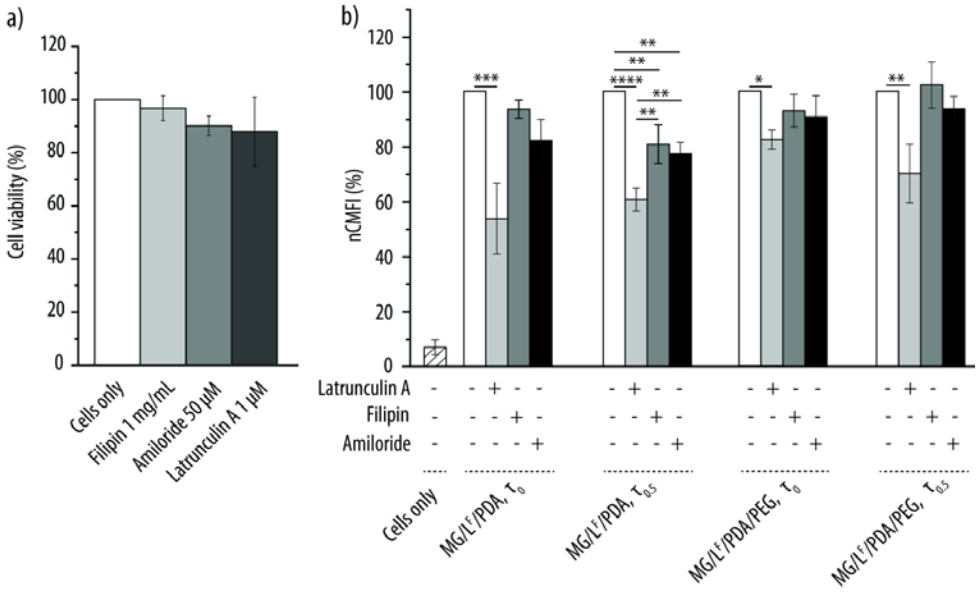

Figure 4.7 Cellular uptake pathways. a) Cell viability of RAW 264.7 cells upon exposure to chemical inhibitors (*i.e.*, filipin, amiloride or latrunculin A). b) Normalised cell mean fluorescence intensity (nCMFI) of RAW 264.7 cells upon exposure to non-functionalised (MG/L^F/PDA) or functionalised (MG/L^F/PDA/PEG) carriers in the presence of chemical inhibitor at τ = 0 dyn cm^{-2} (τ_0) and τ = 0.5 dyn cm^{-2} ($\tau_{0.5}$). n = 3, *p ≤ 0.05; **p ≤ 0.01; ***p ≤ 0.001; ****p ≤ 0.0001. Adapted from reference [60] with permission. Copyright (2018) by Elsevier.

(Figure 4.7b, dark grey bar), amiloride caused an inhibition of 23 ± 4% (Figure 4.7b, black bar) and latrunculin A originated the largest inhibition by a decrease of 39 ± 4% in nCMFI (Figure 4.7b, light grey bar). Thus, although phagocytosis remains to be the main pathway of internalisation, the presence of shear stress seems to prompt both CvME and macropinocytosis in this cell line. Those results are not surprising since both pathways have been previously reported to be the selected pathway by RAW 264.7 cells to internalize several drug delivery vehicles.[157,158]

When PEGylated, at τ_0, the multicompartment carrier is also mainly internalised by a phagocytic route. However, for the MG/L^F/PDA/PEG, latrunculin A treatment (Figure 4.7b, light grey bar) resulted in a significantly less effective inhibition of the phagocytic route as compared to MG/L^F/PDA. These results suggest that multiple pathways could be responsible for the internalisation of the MG/L^F/PDA/PEG carriers. Finally, when the cells are exposed MG/L^F/PDA/PEG at $\tau_{0.5}$, only the treatment with latrunculin A resulted in significant reduction of nCMFI (by 30 ± 11%, Figure 4.7b, light grey bar). Such reduction in cellular uptake was non-significantly different from the MG/L^F/PDA carrier at both τ_0 and $\tau_{0.5}$. All in all, these results demonstrate that phagocytosis is the main route of internalisation regardless the presence or absence of shear stress and the functionalisation of the carrier with PLL-*g*-PEG. However, the presence of shear stress seems to activate other routes of internalisation for MG/L^F/PDA/PEG carrier, although their role seems to be minor. After extensive literature research, these results represent the first study of an in depth characterisation of the influence of shear stress on the cellular uptake pathway in RAW 264.7 cells.

HUVEC cells: For this cell line, the maximum concentration of each inhibitor (*i.e.*, chlorpromazine, filipin and amiloride) that could be administered to the cells without causing a detrimental effect was first determined (Figure 4.8a).

Next, the effect of the different inhibitors on the cell uptake pathway was assessed for both MG/L^F/PDA and MG/L^F/PDA/PEG in the presence and absence of shear stress. As depicted in Figure 4.8b, the uptake of MG/L^F/PDA at τ_0 was highly inhibited by both

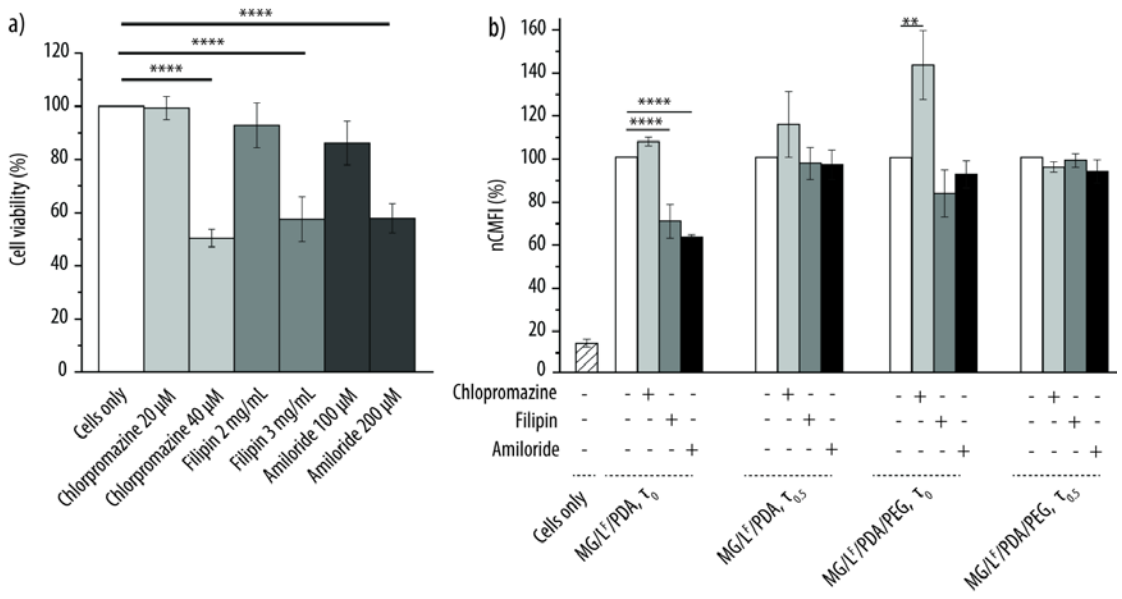

Figure 4.8 Cellular uptake pathways. a) Cell viability HUVEC cells upon exposure to chemical inhibitors (*i.e.*, filipin, amiloride or latrunculin A). b) Normalised cell mean fluorescence intensity (nCMFI) of HUVEC cells upon exposure to non-functionalised (MG/L^F/PDA) or functionalised (MG/L^F/PDA/PEG) carriers in the presence of chemical inhibitor at $\tau = 0$ dyn cm^{-2} (τ_0) and $\tau = 0.5$ dyn cm^{-2} ($\tau_{0.5}$). n = 3, **p ≤ 0.01; ****p ≤ 0.0001. Adapted from reference [60] with permission. Copyright (2018) by Elsevier.

filipin (Figure 4.8b, dark grey bar) and amiloride (Figure 4.8b , black bar) leading to a reduction of nCMFI of 30 ± 8% and 37 ± 1%, respectively. Therefore, the results suggest that MG/L^F/PDA are preferentially internalised trough CvME and macropinocytosis, which is in line with previous reports in which nanoparticles composed of silica[159] or gold[160] are internalised by endothelial cells through multiple endocytic pathways including CvME and macropinocytosis. In contrast, no decrease in the nCMFI was observed for any of the tested inhibitors when the cells were exposed to MG/L^F/PDA carriers at $\tau_{0.5}$ or the MG/L^F/PDA/PEG carriers at τ_0 and $\tau_{0.5}$. Similar results were reported in a previous study, in which in the presence of shear stress HUVEC cells use alternative uptake mechanisms such as CvME clathrin- and caveolae- independent endocytosis or a non- energy-dependent pathway.[113]

Interestingly, exposure of HUVEC cells to MG/L^F/PDA/PEG in the presence of chlorpromazine at τ_0 resulted in a significant increase of 43 ± 16% in nCMFI (Figure 4.8b, light grey bar). This result can be explained to the fact that the inhibition of a

specific route can lead to the activation of other uptake mechanisms. In summary, shear stress and surface functionalisation have a high impact on the cell entry mechanism in this cell line and, therefore, in the intracellular fate of the multicompartment carriers.

HeLa cells: Similar to HUVEC, the maximum working concentration for each inhibitor (*i.e.*, chlorpromazine, filipin and amiloride) without significant impact on cell viability was first determined (Figure 4.9a). Then, the cells were pre-exposed to each inhibitor followed by incubation with MG/L^F/PDA or MG/L^F/PDA/PEG at τ_0 and τ_{20}. As shown in Figure 4.9b, upon incubation with MG/L^F/PDA at τ_0 the treatment with chlorpromazine (Figure 4.9b, light grey bar) and amiloride (Figure 4.9b, black bar) resulted in a significant reduction by 42 ± 14% and 22 ± 2% of nCMFI, respectively. These results, in agreement with a previously reported study,[148] indicate that MG/L^F/PDA enter the cell preferentially trough CME while macropinocytosis plays a minor role. At τ_{20}, similarly to the previously studied cell lines (*i.e.*, RAW 264.7 and HUVEC), an effect of the shear stress in the cell internalisation pathway is observed. In particular, chlorpromazine

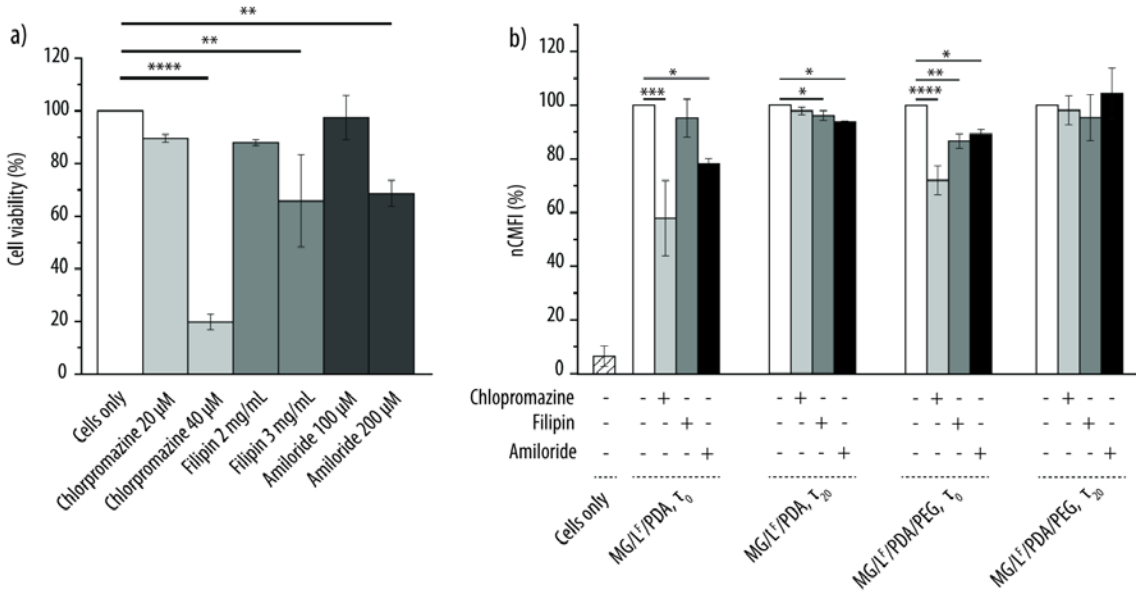

Figure 4.9 Cellular uptake pathways. a) Cell viability HeLa cells upon exposure to chemical inhibitors (*i.e.*, filipin, amiloride or latrunculin A). b) Normalised cell mean fluorescence intensity (nCMFI) of HeLa cells upon exposure to non-functionalised (MG/ L^F /PDA) or functionalised (MG/L^F/PDA/PEG) carriers in the presence of chemical inhibitor at τ = 0 dyn cm^{-2} (τ_0) and τ = 20 dyn cm^{-2} (τ_{20}). n = 3, *p ≤ 0.05; **p ≤ 0.01; ***p ≤ 0.001; ****p ≤ 0.0001. Adapted from reference [60] with permission. Copyright (2018) by Elsevier.

(Figure 4.9b, light grey bar) has a negligible effect on nCMFI, while filipin (Figure 4.9b, dark grey bar) and amiloride (Figure 4.9b, black bar) decrease the nCMFI in a lesser extent as compared to τ_0. Interestingly, when employing MG/L^F/PDA/PEG multicompartment carrier at τ_0, the three tested inhibitors resulted in a significant reduction of nCMFI. In particular, chlorpromazine (Figure 4.9b, light grey bar) caused a reduction of nCMFI by 28 ± 5%, filipin (Figure 4.9b, dark grey bar) by 13 ± 3% and amiloride (Figure 4.9b, black bar) by 11 ± 2%. Thus, similarly MG/L^F/PDA to at τ_0, the internalisation of MG/L^F/PDA/PEG seems to be mediated by multiple endocytic pathways including mainly CME and followed by macropinocytosis and CvME. In contrast, upon applying τ_{20} to MG/L^F/PDA/PEG carriers, none of the tested inhibitors had a significant effect on nCMFI, suggesting that the cell entry of MG/L^F/PDA and MG/L^F/PDA/PEG at τ_{20} is mediated by different mechanisms. Similar to these findings, Kang *et al*.,[114] demonstrated that shear stress activate alternative pathways on cancer cells.

In summary, similar to RAW 264.7 and HUVEC cells, the presence of shear stress has an influence on the cellular uptake pathway of both MG/L^F/PDA and MG/L^F/PDA/PEG in a model cancer cell line.

4.4 Conclusions

In this chapter, an in depth comparison between non-functionalised and functionalised carrier in terms of kinetic release profiles of the model cargo, protein adsorption, cellular uptake/association and cellular uptake pathway has been presented together with the influence of the shear stress on the cellular/carrier interaction and protein adsorption studies.

Based on the findings described and discussed above, although quite limited, the PEGylation of the surface provides protection against protein adsorption regardless of the presence of shear stress what is of outmost importance for a carrier administered intravenously.

What is more, the control over the release of model cargo is achievable by the combination of two inherently different building blocks (*i.e.*, P(NIPAM)-*co*-AAc MGs and liposomes), being the release profile of the MGs faster than the liposomes regardless of the functionalisation of the carrier. On the other hand, the influence of the shear stress was clearly demonstrated in various aspects: i) Cellular uptake, ii) cellular uptake efficiency, iii) PEGylation effect and iv) cellular uptake pathway. It was demonstrated that the multicompartment carrier is mainly internalised by the cancer cell line regardless of the PEGylation of the surface and the absence or presence of shear stress compared to the macrophages or endothelial cells. In all three tested cell lines the exposure to shear stress resulted in higher uptake of the carrier. However, the PEGylation effect seems to be shear stress and cell line dependent. Lastly, the cellular uptake pathway was also influenced by the presence of shear stress by activating alternative routes upon exposure to a dynamic environment.

All in all, the findings presented in this chapter evidence the importance of the careful consideration of relevant shear stress conditions on the evaluation of cell/carrier interactions in *in vitro* studies before moving forward to *in vivo* models.

Chapter V Multicompartment microreactor for ROS detoxification: the tandem antioxidant activity of poly(dopamine) and catalase-loaded liposomes

Summary

This chapter presents preliminary results regarding the evaluation of the non-PEGylated and PEGylated multicompartment carrier as microreactors. For this, the detoxification reaction of ROS (*i.e.*, $O_2^{\cdot -}$ and H_2O_2) was used as a proof-of-concept.

First, in a similar manner as in Chapter 3, the assembly of a multicompartment carrier entrapping positively charged liposomes within a PDA shell is presented (however, saturated liposomes are used for this application). Characterisation of the multicompartment carrier is performed by means of flow cytometry, DIC, fluorescence imaging, DLS and ξ-potential measurements.

Next, to achieve long-circulation time, the surface is coated with a low-fouling polymer (*i.e.*, PLL-*g*-PEG with different GRs). The low-fouling effect of PLL-*g*-PEG-coated multicompartment carriers depending on the GR was assessed by evaluating both the protein deposition (*i.e.*, upon incubation with BSA-FITC and IgG-FITC) and cellular uptake/association (*i.e.*, upon incubation with HUVEC and RAW 264.7 cells).

The potential of the multicompartment carrier as a microreactor is evaluated by entrapping the negatively charged CAT enzyme within the positively charged liposomes (L^{CAT}). The amount of entrapped CAT within L^{CAT} and the multicompartment carriers was quantified by micro-BCA assay. The functionality of the multicompartment working as a microreactor to remove ROS is evaluated in terms of CAT and SOD activity. While SOD catalyses the dismutation of the superoxide radical ($O_2^{\cdot -}$) into molecular oxygen (O_2) and hydrogen peroxide (H_2O_2), CAT catalyses the decomposition of the later into O_2 and H_2O. As such, first the ability of PDA to act as a SOD mimic is assessed by monitoring the conversion of $O_2^{\cdot -}$ into H_2O_2 by means of the cytochrome C assay. This was followed by evaluating the potential of the CAT-loaded microreactors to deplete H_2O_2. To do that the amplex red/HRP assays was used.

It is worth mentioning that upon further optimisation and *in vitro* validation of the multicompartment carrier as extracellular ROS scavenger (*i.e.*, in the presence of

endothelial cells and macrophages), the results presented in this chapter will be adapted for a scientific publication.

5.1 Introduction

ROS (*i.e.*, $O_2^{\cdot-}$, H_2O_2, $^{\cdot}OH$ and NOO^-) are highly reactive species that rapidly react with other molecules to stabilise their structure.[161] For radical species, this high reactivity is due to the unpaired electron in the outer orbital of $O_2^{\cdot-}$, and $^{\cdot}OH$ while, for compounds that do not contain an unpaired electron such as H_2O_2 it is due to their ability to exchange electrons with other molecules.[31] Within living organisms, physiological ROS levels are carefully maintained by their natural production by different biological pathways (*i.e.*, mitochondrial electron transport chain) and their removal by natural antioxidant mechanisms including SODs, CAT , glutathione peroxidases or peroxiredoxins.[32] However, when this balance is perturbed and the ROS production exceeds the antioxidant capacity of the body, oxidative stress is generated. At the intracellular level the ROS overproduction has been linked to an increased endothelial dysfunction (by increasing the vasoconstriction due to reaction with nitric oxide, which acts as a natural vasodilator), mitochondrial dysfunction, interferences in cell signalling, cell damage and DNA damage.[32] What is more, this oxidative stress is closely related to severe vascular diseases such as hypercholesterolemia, hypertension, diabetes, aging and sickle disease, among others.[31] Since some ROS (such as H_2O_2) are able to cross the membrane while others (such as $O_2^{\cdot-}$) are able to enter and exit the cell through chloride channels,[53] ROS originally generated at the intracellular level are capable of reaching the systemic circulation affecting other tissues.

At the extracellular level, it has been shown that once the ROS reach the systemic circulation distant organs can be affected, leading to severe pathologies. For example, patients with obstructive jaundice (which leads to the failure of the intestinal barrier resulting in increased levels of toxins in blood, known as endotoxemia) exhibit high levels of ROS in multiple organs such as liver, intestine, kidney, heard brain and blood.[54] Another example is the fulminant hepatic failure. It has been reported that this disease is partially produced by the release of ROS in the vicinity of Kupffer cells and endothelial cells leading to exacerbation of tissue damage by neutrophils.[162] Finally, patients with no proliferative diabetic retinopathy (leading cause of blindness) also exhibit

high levels of ROS in blood (leading to the breakdown of blood-retinal barrier altering the retinal blood flow and causing leakage of fluids that accumulate in the Müller cells, major type of glial cells in the retina).[163]

Therefore, the scavenging of ROS from the blood is of outmost importance. A solitary study presents a long circulating scavenger focused on the ROS detoxification at the systemic level.[162] The authors, designed a macromolecular reduced thiol (by employing PEG-conjugated BSA with multiple reduced thiols) in order to treat fulminant hepatic failure in mice. The idea lies on the neutralization of ROS by the reduced thiols present in the PEG-conjugated BSA. The authors demonstrated that upon intravenous administration, the PEG-conjugated BSA containing reduced thiols circulated for long time while reducing the levels of fulminant hepatic failure markers in plasma in contrast to three traditional reduced thiols (*i.e.*, L-cysteine, glutathione and dithiothreitol).

Although, a great number of reports focus on the ROS scavenging at an intracellular level,[27,164] few studies report the successful application of extracellular microreactors for ROS detoxification purposes at the extracellular level.[44,45,165] In particular, Armada-Moreira *et al*.,[165] assembled microreactors containing platinum nanoparticles (Pt-NP) using polystyrene microparticles (19.3 μm in diameter) as core. The authors showed the ability of the Pt-NP to successfully scavenge H_2O_2 and ammonia in the presence of human neuroblastoma cells resulting in improved proliferation of the cells. Regarding the usage of multicompartment systems, Städler´s group have expanded their application as extracellular microreactors.[44,45] In particular Städler´s group combined tissue engineering with ROS scavenging functionality. Zhang *et al*.,[44] demonstrated the H_2O_2 antioxidant capacity of a 10 μm microreactor (core-shell particles and capsosomes), made of a silica core containing L^{CAT} and further coated with a PDA layer, in the presence of hepatocytes in order to mimic liver functions. Finally, in a different study,[45] the authors used 40 μm alginate based-microreactors loaded with L^{CAT} to detoxify planar cultures and cell aggregates of hepatocytes resulting in improved cell viability.

Herein, a different approach towards ROS scavenging in the circulatory system is presented. For this, a multicompartment microreactor using P(NIPAM)-*co*-AAc MGs as

core coated with L^{CAT} and further covered with a PDA layer, which is easily functionalised with PLL-*g*-PEG (to avoid cellular internalisation), is assembled (Scheme 5.1). The proof of concept is based on the transformation of $O_2^{\cdot-}$ (the most dangerous ROS) into H_2O_2, and a mixture of products, by PDA followed by the transformation of H_2O_2 into H_2O and O_2 by CAT. Although the cascade reaction described above is used as

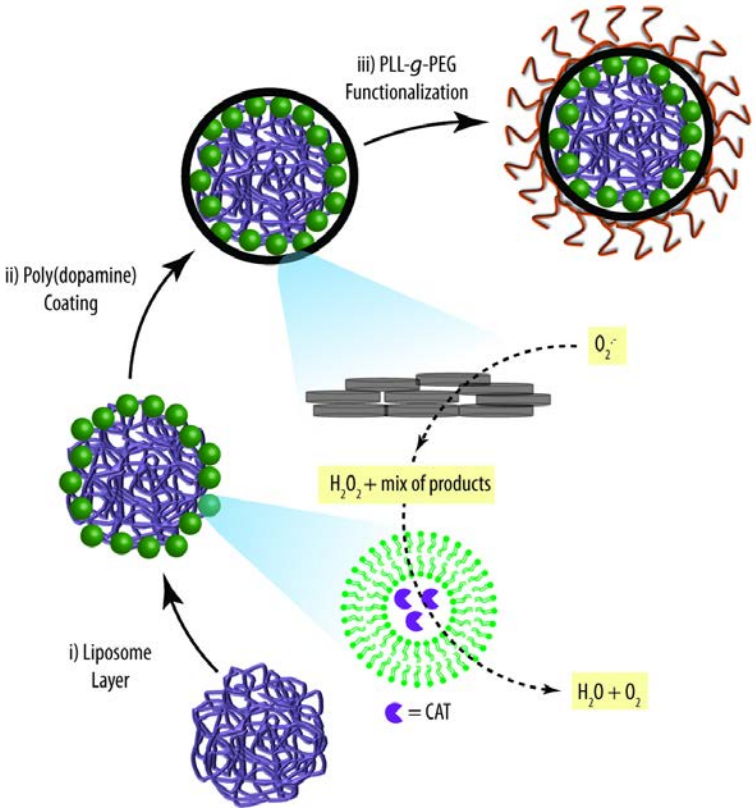

Scheme 5.1 Schematic representation of the multicompartment microreactor and ROS detoxification cascade. The microreactor is assembled using a P(NIPAM)-*co*-AAc MGs as core decorated with a catalase (CAT)-loaded liposome layer (i), next a poly(dopamine) (PDA) layer coats the MG/L assembly (ii) which is easily functionalised with poly(*L*-lysine)-*grafted*-poly(ethylene glycol) (PLL-*g*-PEG). The insets represent the cascade reaction in which the superoxide radical anion ($O_2^{\cdot-}$) is transformed into H_2O_2 (and a mixture of products) by the catechol groups present in the PDA layer, H_2O_2 then acts as substrate for the catalase (CAT) loaded within the liposome core to yield H_2O and O_2.

a simple proof-of-concept for this PhD thesis, the compartmentalized structure of the reactor offers the possibility to co-encapsulate other antioxidant molecules. For example, the co-encapsulation of resveratrol (which neutralizes $^{\cdot}OH$)[166] in a separate liposome compartment could expand the antioxidant capacity of the microreactor.

Although the antioxidant properties of PDA are well known, the information regarding the SOD-like activity of PDA (reaction with $O_2^{\cdot -}$ to yield H_2O_2) remains scarce. It has been reported that despite the exact mechanism being unknown, the reaction of catechol groups with $O_2^{\cdot -}$ yields H_2O_2 and catechol radical anion.[55] Considering that PDA is rich in catechol groups, a SOD-like activity could be expected. In a very recent study, Huang *et al*.,[59] demonstrated the synergistic effect of selenium particles coated with PDA in the detoxification of $O_2^{\cdot -}$, $^{\cdot}OH$ and H_2O_2. In particular, the authors demonstrated the antioxidant activity of PDA towards $O_2^{\cdot -}$ and $^{\cdot}OH$ and selenium particles towards H_2O_2 in test tubes, *in vitro* and *in vivo* studies using a lung inflammation model.

In this chapter, preliminary results regarding the performance of the multicompartment carrier as microreactor (*i.e*., to perform the cascade reaction towards ROS detoxification) in test tubes is presented.

5.2 Materials and Methods

5.2.1 Materials

Tris, NaCl, DA, CAT from bovine liver (EC1.11.1.6, 10000 U mg^{-1}) , FITC, IgG-FITC, BSA, PBS, DMEM D5796, sodium pyruvate, penicillin/streptomycin, FBS, trypsin, endothelial cell line HUVEC, DMSO, $NaHCO_3$, PLL (Mw 15 000-30 000 Da), HRP (EC1.11.1., 250 U mg^{-1}), cytochrome C from equine heart, ethylenediaminetetraacetic acid solution (EDTA), xanthine, xanthine oxidase from bovine milk, SOD from bovine erythrocytes (EC1.15.1.1, 3000 U mg^{-1}) and Triton-X 100 were purchased from Sigma-

Aldrich (Saint Louis, MO, USA). 1,2-Dimyristoyl-*sn*-glycero-3-phosphocholine (DMPC), DPPC, 1,2-stearoyl-3-trimethylammonium-propane (chloride salt) (DSTAP) and NBD-PC were obtained from Avanti Polar Lipids (Alabaster, AL, USA). EGM-2 was purchased from Lonza (Basel, Switzerland). The EGM-2 is composed of EBM, hEGF, VEGF, R3-IGF-1, ascorbic acid, hydrocortisone, FBS, human hFGF-β, heparin and GA. The macrophage cell line RAW 264.7 was obtained from ECACC, Wiltshire, UK. Me-PEG-NHS (Mw_{PEG} = 2000 Da) was purchased from Iris Biotech GmbH (Marktredwitz, Germany). Micro BCA assay kit and amplex red were purchased from Thermo Fisher Scientific (Waltham, MA, USA). Tris 1 buffer is composed of 10 mM Tris (pH 8.5); Tris 2 is composed of 10 mM Tris and 150 mM NaCl (pH 7.4). All buffers were made with ultrapure water (Milli-*Q*, gradient A 10 system, TOC < 4 ppb, resistance 18 MV cm, EMD Millipore, USA).

5.2.2 Methods

5.2.2.1 Liposomes assembly

The liposomes were assembled by the lipid film hydration method.[72] Specifically, 1.63 mg DMPC, 0.63 mg DPPC and 0.25 mg DSTAP were dissolved in chloroform followed by the formation of a lipid film using a nitrogen flow. Next, the lipid film was exposed to vacuum for at least 1 h in order to completely evaporate the organic solvent. Upon rehydration in Tris 2 buffer (1 mL), the 3.2 mM liposome solution was extruded through 100 nm nucleopore polycarbonate filters (drain disc 10 mm PE, Whatman, Maidstone, UK) 11 times at 45 °C in order to yield unilamellar empty liposomes. In order to prepare fluorescently labelled liposomes (L^F), 2 wt% of NBD-PC was added to the lipid mixture prior to the lipid film formation. Only L, L^F with a PDI below 0.14 were used for the following experiments.

5.2.2.2 Assembly and characterisation of empty microreactor

The assembly of the empty microreactor (which does not contain L^{CAT}) follows the same procedure explained for the multicompartment carrier in previous chapters. However,

since in this chapter its application as microreactor is studied the multicompartment carrier will be called microreactor from now on.

Optimisation of liposome deposition: In order to optimise the amount of liposomes per MG, a suspension of 479 µg of MGs was washed 2 × in Tris 1 buffer for 15 min at 13 500 rpm, using a bench top centrifuge (MiniSpin, Eppendorff, AG, Germany). Next, the MGs were incubated with increasing amounts of L^F keeping the total volume constant for 1.5 h at room temperature in a tube rotator. After the incubation time, the MGs suspension was washed 2 × in Tris 1 buffer for 6 min at 10 000 rpm. Finally, the amount of L^F needed to saturate the MGs surface was assessed by monitoring the fluorescence intensity of L^F-coated MGs by flow cytometry. A BD Accuri C6 flow cytometer (BD Biosciences, Sparks, MD, USA) equipped with a 488 nm laser and an emission detection of 530 nm. At least 20 000 events were recorded and two independent experiments were carried out.

Assembly of the empty microreactor: Once the maximum amount of L^F that could be adsorbed onto the MGs without causing aggregation of the assembly was assessed, the empty microreactors were assembled. Microreactors containing empty L (MG/L/PDA) and fluorescently labelled L^F (MG/L^F/PDA), were prepared. First, a suspension containing 958 µg MGs was washed in Tris 1 buffer for 14 min at 8500 rpm followed by incubation with liposomes (L and L^F) (0.25 mg lipids) for 1.5 h at room temperature in a tube rotator. Next, in order to assemble a PDA-coating shell, the suspension was concentrated to a volume of 100 µL followed by exposure to a DA solution (1 mg mL^{-1} in Tris 1 buffer) for 16 h at room temperature in a tube rotator. Finally, the unreacted DA and PDA were washed away by conducting 2 × washing cycles in Tris 2 for 7 min at 10 000 rpm. In order to minimize the loss of sample during the assembly process, all the steps prior PDA deposition were performed employing amicon ultra centrifugal filters (100 kDa).

DIC and fluorescence imaging: The DIC and fluorescence images of the multicompartment carriers were taken with an Olympus Inverted IX83 microscope equipped with a 60x oil-immersion objective.

5.2.2.3 PEGylation effect on protein adsorption

Synthesis of PLL-*g*-PEG: PLL-*g*-PEG polymers at three different PEG-grafting ratios (number of lysine monomer units per grafted PEG chain) were synthetized according to a previously published protocol.[140] Me-PEG-NHS (different amounts, namely 144 mg, 76 mg and 58 mg for theoretical GR of 2, 3.5 and 5, respectively) was dissolved in cold HEPES buffer and added to a solution of PLL (30 mg in 0.5 mL) in cold HEPES buffer (see Table 5.1) followed by 4 h incubation at 4 °C under constant shaking. Next, the reaction mixture was purified by two days dialysis using a cellulose dialysis membrane with a cut-off of 14 kDa. Nuclear magnetic resonance (^{1}H NMR) analysis was used in order to assess the GR. ^{1}H NMR (D_2O, ppm) spectrum: 1.41, 1.65, 1.72 (-CH_2-); 2.95 (-CH_2-N-); 3.34 (PEG); 4.28 (-N-CHR-COO-). In order to estimate the GR, the areas of the lysine side-chain peaks were compared with the area of the PEG peak.[140]

Theoretical grafting ratio	Experimental grafting ratio [a]	PLL (mmol)	Me-PEG-NHS (mmol)
2	1.6	0.143	0.072
3.5	3.2	0.143	0.038
5	2.5	0.143	0.029

Table 5.1 Overview of the synthesised Poly(*L*-lysine)-graft-poly(ethylene glycol) (PLL-g-PEG) varying the grafting ratios. [a]Grafting ratio calculated from nuclear magnetic resonance analysis

Functionalisation of the empty microreactors with PLL-*g*-PEG: The MG/L/PDA microreactors were PEGylated (MG/L/PDA/PEG) by incubating 958 µg of suspensions with PLL-*g*-PEG 1 mg mL^{-1} (at different GR, namely 1.6, 2.5 and 3.5) in Tris 1 for 1 h at room temperature in a tube rotator, followed by washing the PLL-*g*-PEG excess by conducting 2 × washing cycles in Tris 2 (7 min, 10 000 rpm).

ξ-potential measurements: The assembly of the microreactor was monitored by measuring the ξ-potential after each deposition step using a Zetasizer nanoseries nano-ZS

(Malvern Panalytical, UK) . To do that, 100 µL of sample was added to 700 µL of Milli-*Q* water. At least two independent experiments were carried out.

Protein labelling: BSA and IgG were fluorescently labelled to render BSA-FITC and IgG-FITC following a previously published protocol.[139] In particular, a FITC solution (3.7 mg of FITC in 300 µL DMSO) was added dropwise to a BSA or IgG solution containing 30 mg of protein in 6 mL of $NaHCO_3$ 0.05 M at pH 10. The reaction mixture was allowed to proceed overnight at room temperature under vigorous shaking in a tube rotator. Upon incubation, the excess of FITC was removed by two days dialysis against Milli-Q water (with a cellulose dialysis membrane with a cut-off of 12.4 kDa).

Protein adsorption: A suspension containing 0.47 mg MG/L/PDA or MG/L/PDA/PEG in 0.2 mL PBS was incubated with BSA-FITC or IgG-FITC at two different concentrations (*i.e.*, 0.075 mg mL^{-1} or 0.5 mg mL^{-1} final concentration) at 37°C for 4 h. After the incubation time unbound proteins were removed by extensive washing in PBS. Next, in order to assess the extent of protein adsorption on the multicompartment microreactors surface the fluorescence intensity of the microreactors due to the adsorbed fluorescent proteins was measured by flow cytometry. At least three independent experiments were carried out (analysing at least 20 000 events) and the data was analysed using one-way ANOVA with a confidence level of 95% ($\alpha = 0.05$) followed by Tukey´s multiple comparison posthoc test (*$p \leq 0.05$; **$p \leq 0.01$; ***$p \leq 0.001$; ****$p \leq 0.0001$) in a GraphPad Prism 7 software.

5.2.2.4 PEGylation effect on cell uptake/association

Functionalisation of the empty microreactor with PLL-*g*-PEG: The MG/L^F/PDA microreactors were PEGylated (MG/L^F/PDA/PEG) by incubating 958 µg of suspensions with PLL-*g*-PEG 1 mg mL^{-1} (at different GRs, namely 1.6, 2.5 and 3.2) in Tris 1 for 1 h at room temperature in a tube rotator, followed by washing the PLL-*g*-PEG excess by conducting 2 × washing cycles in Tris 2 (7 min, 10 000 rpm).

Cell culture conditions: The mouse macrophage RAW 264.7 cell line was cultured in DMEM supplemented with 2% (v/v) HEPES, 1% sodium pyruvate, 10% (v/v) FBS and

1% (v/v) penicillin/streptomycin (10 000 U/mL and 10 µg/mL, respectively) at 37°C in a humidified incubator with 5% CO_2 level. The endothelial HUVEC cell line was cultured in EBM-2 supplemented with 0.1% (v/v) hEGF, 0.1% (v/v) VEGF, 0.1% (v/v) R3-IGF-1, 0.1% (v/v) ascorbic acid, 0.04% (v/v) hydrocortisone, 0.4% (v/v) hFGF-β, 0.1% (v/v) heparin, 2% (v/v) FBS and 0.1% (v/v) GA. The cell media was renewed every 2-3 days and only passages between 3-9 and 1-4 of RAW 264.7 cells and HUVEC cells, respectively, were used in all the experiments. The cells were allowed to grow up to ~80% confluence before being detached from the culture flask using trypsin (3 mL, 0.5 mg mL^{-1}) in the case of HUVEC and a cell scraper for RAW 264.7 cells. Next, the trypsin was removed by centrifugation (1000 rpm, 5 min) and the cells were re-suspended in new cell culture media.

Cellular uptake/association experiments: 30 000 cells (RAW 264.7) or 15 000 cells (HUVEC) per well were seeded into 96-well plates in 200 µL cell culture media and allowed to attach to the surface for 24 h at 37°C and 5% CO_2. Next, the cells were incubated with 3.7 ng microreactor per cell (MG/L^F/PDA or MG/L^F/PDA/PEG) in 200 µL cell culture media for 4 h at 37°C, 5% CO_2 followed by washing 2 × in 200 µL of pre-warmed PBS in order to remove non-internalised/non-associated microreactors. Then, the cells were detached from the wells by scrapping (RAW 264.7 cells) or by trypsinization with 60 µL trypsin (0.5 mg mL^{-1}) (HUVEC). Finally, the cell association/uptake of the microreactors was evaluated by measuring the CMFI and CUE of at least 2000 cells by flow cytometry. The concentration of the microreactor solution was determined by fluorescence measurements of MG/L^F/PDA or MG/L^F/PDA/PEG followed by serial dilutions to achieve the desired concentration. At least three independent experiments were carried out and the data was analysed using one-way ANOVA with a confidence level of 95% ($\alpha = 0.05$) followed by Tukey´s multiple comparison posthoc test (*$p \leq 0.05$; **$p \leq 0.01$; ***$p \leq 0.001$; ****$p \leq 0.0001$) in a GraphPad Prism 7 software.

5.2.2.5 Assembly and characterisation of CAT loaded microreactor

CAT labelling: CAT was fluorescently labelled to render CAT-FITC following the same procedure as for BSA-FITC and IgG-FITC (Chapter 5, section 5.2.2.3). However, the excess of FITC was removed by SEC using an Illustra Nap-10 column (GE Healthcare Life Science, Brondby, Denmark).

CAT encapsulation and quantification within liposomes: The lipid film was created as described before (Chapter 5, section 5.2.2.1). In order to optimise the maximum amount of CAT that can be encapsulated within the liposomes, the lipid film was rehydrated with different amounts of CAT in Tris 2 followed by vortexing and incubation at 45 °C for 20 min. Next, the solution was extruded through 800, 400, 200 and 100 nm filters 11 times at 45°C. To remove the non-encapsulated enzyme, the liposome solution was purified by SEC using a Sepharose CL-4B column (collecting the fractions from 5 to 15, appendix A Figure A1). Finally, the liposome solution was up-concentrated by centrifugation at 2500 g for 30 min (Thermo Scientific SL16R high speed centrifuge) using amicon ultra-15 100 kDa filters. The amount of CAT encapsulated within the liposomes was quantified by breaking the liposomes with 0.1% Triton X-100 for 30 min followed by micro BCA analysis (as instructed by the supplier's protocol) using empty liposomes as control. The size and PDI of the liposomes (L, L^{F}, L^{CAT}) was determined by DLS and ʒ-potential measurements. At least two independent experiments were carried out.

Assembly of CAT loaded microreactor: Once the maximum amount of CAT that can be encapsulated within the liposomes was determined, the CAT loaded microreactors were assembly. For this, the lipid film was rehydrate with 500 µg mL^{-1} of CAT or CAT-FITC ($L^{F,CAT}$, L^{CAT}, $L^{CAT\text{-}FITC}$) in Tris 2 followed by extrusion, purification and up-concentration. Next, the CAT loaded microreactor was assembled following the same procedure as for the empty microreactor (Chapter 5, section 5.2.2.1), but using $L^{F,CAT}$, L^{CAT} or $L^{CAT\text{-}FITC}$ followed by PDA coating yielding MG/$L^{F,CAT}$/PDA, MG/L^{CAT}/PDA or MG/ $L^{CAT\text{-}FITC}$/PDA. Finally, the MG/$L^{F,CAT}$/PDA and MG/L^{CAT}/PDA were PEGylated using PLL-*g*-PEG GR = 3.2.

ξ-potential measurements: The assembly of the microreactor was monitored by measuring the ξ-potential after each deposition step (being the PLL-*g*-PEG layer GR = 3.2). To do that, 100 µL of sample was added to 700 µL of Milli-*Q* water. At least two independent experiments were carried out.

Quantification of CAT loaded within microreactors: The quantification of the CAT in the microreactors was performed by incubating 9600 µg of MG/L and MG/L^{CAT} with 0.1% Triton-X 100 for 30 min at room temperature. Next, the samples were centrifuge for 30 min at 20 000 x g in order to separate the particles from the free CAT. Finally 150 µL of the supernatant of MG/L and MG/L^{CAT} was analysed by micro BCA following the supplier protocol. At least two independent experiments were carried out.

5.2.2.6 SOD-like activity of PDA

Functionalisation of the empty microreactor with PLL-*g*-PEG: The MG/L^{F}/PDA microreactors were PEGylated (MG/L^{F}/PDA/PEG) by incubating 958 µg of suspensions with PLL-*g*-PEG 1 mg mL^{-1} (GR = 3.2) in Tris 1 for 1 h at room temperature in a tube rotator, followed by washing the PLL-*g*-PEG excess by conducting 2 × washing cycles in Tris 2 (7 min, 10 000 rpm).

SOD-like activity of PDA-coated empty microreactors: The SOD-like activity of both MG/L^{F}/PDA and MG/L^{F}/PDA/PEG was evaluated and compared to different concentrations of the natural SOD enzyme (expressed in units) (Figure A.2, appendix A). For this the cytochrome C assay was used (Figure 5.6) following a previously published protocol.[52] In particular, different amounts of SOD (in units) or 800 µg of MG/L^{F}/PDA or MG/L^{F}/PDA/PEG were added to a reaction mixture consisting of 10^{-4} M EDTA, 10^{-5} M cytochrome C and 5×10^{-5} M xanthine in Tris 2 buffer (500 µL). The reaction was initiated by the addition of 10 µL of xanthine oxidase (0.58 U mL^{-1} in Tris 2 buffer) and allowed to proceed for 30 min at 37°C. As a control, the reaction between reaction mixture containing Tris 2, instead of SOD or microreactors, and xanthine oxidase was considered. Finally, the absorbance of the reduced cytochrome C was measured at 550 nm. At least two independent experiments were carried out.

Reaction kinetics: The kinetics of the SOD-like activity of the microreactors due to the PDA coating, was investigated using the cytochrome C assay based on a previously published protocol.[52] In particular, 800 μg of MG/L^F/PDA, MG/L^F/PDA/PEG or 2.8 U of SOD were added to the reaction mixture (500 μL: 10^{-4} M EDTA, 10^{-5} M cytochrome C and 5×10^{-5} M xanthine in Tris 2). The reaction was initiated by the addition of 10 μL of xanthine oxidase (0.58 U mL^{-1} in Tris 2 buffer) and allowed to proceed for up to 72 h at 37°C under constant shaking. Next, at different time points, the microreactors were spun down for 7 min at 8500 rpm and 200 μL of the supernatant were transferred to a 96-well plate. The absorbance of the reduced cytochrome C was measured at 550 nm using reaction mixture with Tris 2 buffer (without microreactors) and xanthine oxidase as control (blank). The results were normalised to the absorbance peak height at 550 nm of the blank solution at the different time points. At least two independent experiments were carried out.

Empty microreactor recyclability: Next, the recyclability of the microreactors (whether they could sustain multiple rounds of catalysis) as an SOD-mimic was evaluated using the cytochrome C assay. Thus, 800 μg of MG/L^F, MG/L^F/PDA or MG/L^F/PDA/PEG were suspended in a reaction mixture (500 μL: 10^{-4} M EDTA, 10^{-5} M cytochrome C and 5×10^{-5} M xanthine in Tris 2) and incubated for 30 min at 37°C with 10 μL of xanthine oxidase (0.58 U mL^{-1} in Tris 2 buffer). After the incubation time, the samples were spin down and the supernatants collected and the absorbance peak measured at 550 nm. Next, the microreactors were washed 1 × in Tris 2 buffer to remove the reduced cytochrome C and new reaction mixture (500 μL: 10^{-4} M EDTA, 10^{-5} M cytochrome C and 5×10^{-5} M xanthine in Tris 2) and xanthine oxidase was feed to the microreactors followed by incubation at 37°C for 30 min. This procedure was repeated 5 times. As a control, reaction mixture (500 μL: 10^{-4} M EDTA, 10^{-5} M cytochrome C and 5×10^{-5} M xanthine in Tris 2) containing Tris 2 buffer, instead of multicompartment carriers, was incubated with xanthine oxidase (blank). The data was analysed by normalizing the height of the peak at 550 nm of the sample to the height of the peak at 550 nm of the blank At least two independent experiments were carried out.

5.2.2.6 Cascade enzymatic reaction: CAT loaded microreactors

Cascade enzymatic reaction: Then, potential of the microreactors to conduct an enzymatic reaction where $O_2^{\cdot-}$ is first converted into H_2O_2 by the PDA-coated microreactors (due to the SOD-like activity) was evaluated. Next, H_2O_2 is converted into H_2O and O_2 by the CAT enzyme loaded within the microreactors (MG/L^{CAT}/PDA). The tandem reaction was monitored by following the conversion of H_2O_2 which, in the presence of HRP, is able to convert the substrate amplex red into the resorufin fluorescent probe. For this, a previously published protocol was followed,[52] and, specifically, a solution containing 800 µg of MG/L^F, MG/L^F/PDA, MG/L^F/PDA/PEG, MG/$L^{F,CAT}$/PDA or MG/$L^{F,CAT}$/PDA/PEG in Tris 2 buffer (500 µL) was incubated with 10 µL of KO_2 (which spontaneously generates $O_2^{\cdot-}$, 10 µg mL^{-1} in Tris 2 buffer) for 30 min at 37°C under constant shaking. Next, the samples were centrifuged for 7 min at 8500 rpm and 200 µL of the supernatant were incubated for 5 min at 37 °C with 100 µL HRP (2 U mL^{-1} in Tris 2 buffer) and 10 µL amplex red (0.1 mM in Tris 2 buffer). Finally, the resorufin signal was measured at λ_{ex}= 530 nm and λ_{em}= 586 nm by transferring 200 µL to a black 96-well plate. As control, Tris 2 buffer without microreactors was incubated with KO_2. At least two independent experiments were carried out.

Microreactor recyclability: To assess whether the microreactors were able to conduct several rounds of enzymatic reaction in tandem, a solution containing 800 µg MG/L^F, MG/L^F/PDA, MG/L^F/PDA/PEG, MG/$L^{F,CAT}$/PDA or MG/$L^{F,CAT}$/PDA/PEG in Tris 2 buffer (500 µL) was incubated with 10 µL of KO_2 (which spontaneously generates $O_2^{\cdot-}$, 10 µg mL^{-1} in Tris 2 buffer) for 30 min at 37°C under constant shaking. Next, the samples were centrifuged and 200 µL of the supernatant was incubated for 5 min at 37°C with 100 µL HRP (2 U mL^{-1} in Tris 2 buffer) and 10 µL amplex red (0.1 mM in Tris 2 buffer). The resorufin signal was measured at λ_{ex}= 530 nm and λ_{em}= 586 nm by transferring 200 µL to a black 96-well plate. Next, the microreactors were washed 1× in Tris 2 buffer in order to remove the resorufin followed by resuspension in Tris 2 buffer and incubation with fresh KO_2. This procedure was repeated 5 times. As control, Tris 2 buffer without microreactors was incubated with KO_2. At least two independent experiments were carried out.

5.3 Results and discussion

5.3.1 Microreactor assembly and characterisation

5.3.1.1 Liposome deposition and PDA coating

In order to assemble multicompartment carriers entrapping the highest amount of liposomes, the maximum amount of L^F (expressed as mg of lipid) that could be adsorbed onto the MGs surface avoiding particle aggregation was evaluated. For this, a suspension of negatively charged MGs was incubated with increasing amounts of positively charged and L^F for 1.5 h. The fluorescence intensity of the MG/L^F particles depending on the amount of added L^F was monitored by flow cytometry.

The saturated DMPC: DPPC: DSTAP formulation was chosen based on the T_m of each lipid (~24°C,[12] ~41°C,[12] and ~50-60°C,[167] respectively). Taking into consideration the ratio (6.5:2.5:1.0, DMPC: DPPC: DSTAP) used to assemble the liposomes, a T_m close to 32°C is expected for this formulation. This means that at 37°C the lipid bilayer will be permeable enough to allow the diffusion of substrates and products. However, proper differential scanning calorimetry studies are need to accurately measure the T_m of the formulation.[168]

As depicted in Figure 5.1a, the results, which have been normalised to the mean MFI readings upon adsorption of 0.5 mg of lipids onto the MGs, show saturation of the MGs surface upon incubation with 0.225 mg of lipids. Nonetheless since particle aggregation was observed when the MGs were incubated with 0.175 mg L^F (according to the DIC images, Figure 5.1a, inset), to ensure the assembly of a non-aggregated the multicompartment carriers, the assembly was conducted employing 0.125 mg L^F for 0.48 mg MGs.

Figure 5.1b shows good colloidal stability for 0.48 mg MGs incubated with 0.125 mg of lipids as evidenced by the DIC imaging (Figure 5.1b). Importantly, such stability was not compromised once the PDA layer was deposited on the surface of the MG/L^F/PDA according to the DIC images (Figure 5.1b). Finally, the first evidence of PDA deposition

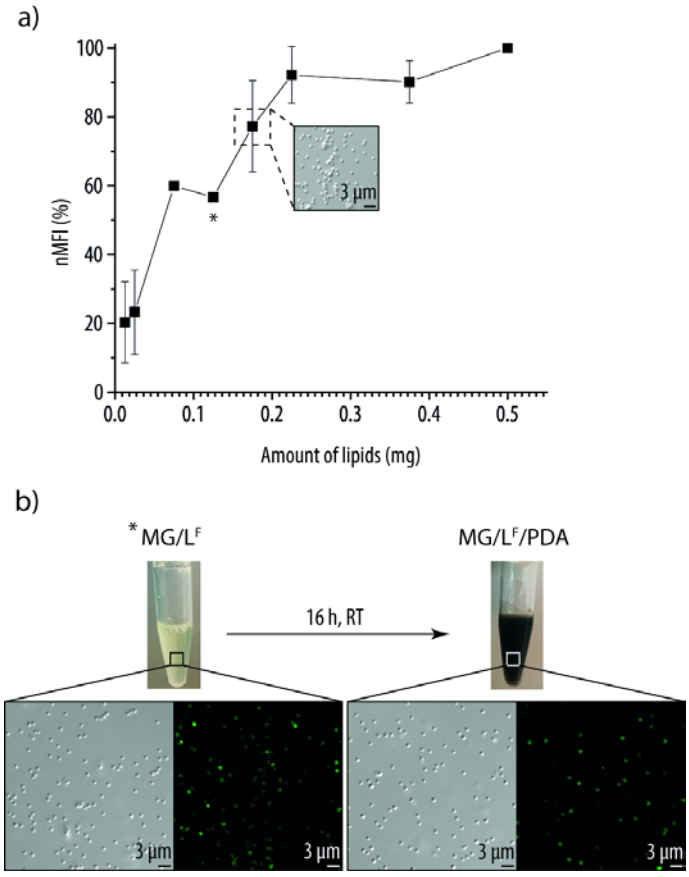

Figure 5.1 Liposomes deposition and poly(dopamine) coating. a) Normalised mean fluorescence intensity (nMFI) of MGs upon incubation in increasing amount of lipids, the inset shows a Differential interference contrast (DIC) image of the aggregated sample. b) DIC and fluorescent images showing good colloidal stability of MGs decorated with fluorescent liposomes (L^F) (MG/L^F) and further coated with a polydopamine layer (PDA) (MG/ L^F /PDA). The Eppendorf tube pictures show the change in colour of the solution upon incubation of MG/L^F with DA for 16 h at RT yielding MG/ L^F /PDA.

was confirmed by the change of colour (from pale yellow, due to L^F, in MG/L^F to black in MG/L^F/PDA, Figure 5.1b) upon incubation of MG/L^F with a DA solution for 16 h at room temperature.

5.3.1.2 PEGylation effect on protein deposition

For the envisioned application, which is acting as a microreactor to remove ROS in the bloodstream, assembling a long-circulating carrier is essential. It is well known that the

adsorption of proteins with an opsonic effect on the surface of the particles will increase its chances to be cleared from the body by the MPS.[100] As such, to diminish the protein deposition, PEGylation of the particle surface has been emerged as a golden strategy.[101]

Next, in order to investigate the low-fouling properties of a PEG coating on the microreactors surface, MG/L/PDA was coated with three different PLL-*g*-PEG exhibiting different GRs (*i.e.*, 1.6, 2.5 and 3.2. Having GR =1.6 the highest PEG content and GR = 3.2 the least) (Figure 5.2). Different GRs, which is defined as the ratio of the number of lysine monomers to the number of PEG side chains, were evaluated since is the density of the PEG chains on the particle surface greatly influences the PEGylation effect. It has been shown that the more the PEG chains overlap the less protein deposition is observed.[169] This effect is explained by the lower chances of small proteins to diffuse through the PEG chains, and therefore reach the particle surface, when the PEG chains are overlapping.[169] The GRs studied in this PhD thesis are close to 3.5 since it has been previously reported that this GR is the optimal in terms of protein deposition in planar surfaces[170] and adhesion to macrophages and dendritic cells to glass.[171] However, it is worth mentioning that GR = 3.5 did not outperform as compared to others GR when micro particles coated with PLL-*g*-PEG were exposed to phagocytosis (using GR = 2.2, 3.5 and 5.7) or protein deposition.[171]

The coating of the microreactors surface by PLL-*g*-PEG was first assessed by ξ- potential measurements (Figure 5.2a). The bare MGs, as expected, displayed an overall negative charge (-32.1 ± 1.5 mV). Next, the liposomes deposition was confirmed by an increase in ξ-potential (from -32.1 ± 1.5 mV to -24.1 ± 1.9 mV) due to the positive charge of the liposomes. A further increase in ξ-potential (up to -17.9 ± 0.6 mV) was observed upon PDA deposition. This increase could be explained by the large polymerisation time since non alterations or slightly decrease in ξ-potential values upon PDA deposition has been previously reported for shorter polymerisation times.[21,95,96,131,132] The results are in agreement with the ones reported in Chapter 3, section 3.3.2.3. Finally, the PDA-coated assemblies were further functionalised with PLL-*g*-PEG of three different GRs. Only a

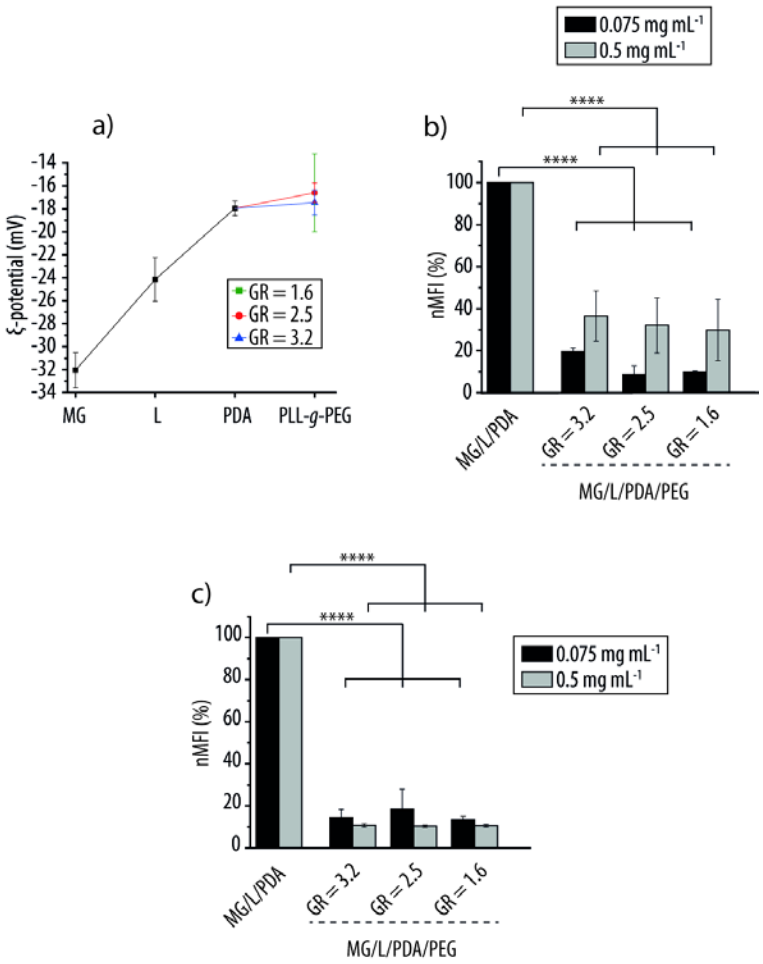

Figure 5.2 PEGylation effect towards protein adsorption. a) ξ-potential measurements of each assembly step. Normalised mean fluorescence intensity (nMFI) of non-PEGylated (MG/L/PDA) and PEGylated (MG/L/PDA/PEG) microreactors with different grafting ratios (GR) upon incubation with two concentrations (0.075 mg mL^{-1} and 0.5 mg mL^{-1}) of a) BSA-FITC and b) IgG-FITC. n=3; ****$p \leq 0.0001$.

slight variation on the ξ-potential values respect to the PDA layer could be observed and no differences depending on the GR are noted (-20.5 ± 3.3 mV for GR = 1.6; -16.6 ± 0.8 mV for GR = 2.5 and -17.5 ± 1 mV for GR =3.2). It is worth mentioning that to draw a stronger conclusion about the successful coating of the assembly with PLL-*g*-PEG further characterisation needs to be conducted (*i.e.*, by QCM-D).

As an indirect way to assess the PEGylation of the assembly, the PEG effect on protein deposition was evaluated. Specifically, MG/L/PDA and three different MG/L/PDA/PEG differing in the GR of the PLL-PEG coating (namely, GR= 1.6, 2.5 and 3.2) were

incubated at 37°C for 4 h with two different protein concentrations of BSA-FITC and IgG-FITC commonly used in literature (*i.e.*, 0.075 mg mL^{-1}[169] and 0.5 mg mL^{-1}[170]). The results were normalised to the MFI readings of MG/L/PDA exposed to either 0.075 mg mL^{-1} or 0.5 mg mL^{-1} protein (Figure 5.2b and Figure 5.2c).

As shown Figure 5.2b, the exposure of MG/L/PEG to BSA-FITC resulted in a significant decrease in nMFI as compared to MG/L/PDA independent of the GRs and protein concentration. In particular, the functionalisation of the microreactors with a PLL-*g*-PEG of a GR =1.6, 2.5 and 3.2 resulted in a reduction in nMFI by 90 ± 1%, 91 ± 4% and 80 ± 2%, respectively, as compared to MG/L/PDA upon incubation with 0.075 mg mL^{-1} of protein (Figure 5.2b, black bars). Interestingly, upon exposure to 0.5 mg mL^{-1}, the reduction in nMFI obtained for the PEGylated carriers (by ~83% for GR= 1.6, 2.5 and 3.2 as compared to MG/L/PDA) is smaller than the reduction observed for lower protein concentration (0.075 mg mL^{-1}). Looking more closely, non-significant differences were found between the different GRs for any of the concentrations.

Regarding the PEGylation effect on IgG-FITC deposition (Figure 5.2c), the PEGylation of the surface resulted in a significant decrease in nMFI as compared to MG/L/PDA independent of the GR and the protein concentration. In particular, the incubation of the functionalised microreactor with a PLL-*g*-PEG of a GR = 1.6, 2.5 and 3.2 resulted in a similar reduction in nMFI (by ~85%, Figure 5.2c, black and grey bars) as compared to MG/L/PDA regardless of the protein concentration as compared to MG/L/PDA. Similar to BSA-FITC, non-significant differences between the different GRs were found for any of the concentrations. The results obtained for GR = 1.6, 2.5 and 3.2 upon incubation with IgG-FITC are in agreement with literature.[171]

It is worth mentioning that these results indicate a more optimal PEGylation effect towards protein deposition as compared to GR = 3.5 which is the one used in chapter 4, section 4.3.1 (resulting in a decrease in nMFI by 44 ± 2% upon incubation with BSA-FITC and by 37 ± 5% upon incubation with IgG-FITC as compared to MG/L/PDA). Interestingly, this less optimal PEGylation effect observed for GR = 3.5 compared to the other GRs is not in agreement with literature.[171] It is important to note that different liposome formulations were used to assemble both systems (unsaturated lipids in chapter

4 for GR =3.5 and saturated lipids in chapter 5 for GR = 1.6, 2.5 and 3.2). This difference in liposome formulation could potentially affect the PDA layer, which is deposited onto the liposomes, and therefore the subsequent PLL-*g*-PEG layer. It is therefore difficult to speculate about the improved PEGylation effect, since both systems cannot be compared directly.

5.3.1.3 PEGylation effect on cell uptake/association

The PEGylation effect of the microreactors coated with PLL-*g*-PEG at the three different GRs was further investigated *in vitro*, using relevant cell populations such as macrophages (RAW 264.7) and endothelial cells (HUVEC). The results have been normalised to the CMFI readings of the cells exposed to MG/L^F/PDA (Figure 5.3)

RAW 264.7 cells: Upon incubation of the cells with the three PEGylated microreactors, a significant decrease as compared to the uncoated counterparts was observed for the three microreactors independent of the GR. As such, a decrease of 29 ± 12% in nCMFI was observed for a GR = 1.6 while a decrease of 46 ± 13% and 43 ± 10% in nCMFI was observed for a GR = 2.5 and 3.2, respectively, as compared to cells incubated with MG/L^F/PDA (Figure 5.3ai). In agreement with the protein adsorption results, non-significant differences were found amongst the different GR. Figure 5.3aii shows the CUE, which corresponds to the percentage of cells with a CMFI higher than the auto fluorescence level of untreated cells. Although no significant, Figure 5.3aii shows a reduction of CUE by 18 ± 12% for cells incubated with PEGylated microreactors functionalised with a PLL-*g*-PEG of a GR = 1.6 as compared to MG/L^F/PDA. However, a significant reduction in CUE is observed when the cells are exposed to PEGylated microreactors functionalised with a PLL-*g*-PEG of a GR = 2.5 and 3.2 (by 26 ± 9% for 2.5 and 26 ± 11%) as compared to MG/L^F/PDA.

HUVEC cells: A similar trend as observed for the protein adsorption was found when HUVEC cells were exposed to either MG/L^F/PDA or MG/L^F/PDA/PEG with the different GR. All the GRs resulted in a significant reduction in CMFI (by 51 ± 9% for 1.6, 57 ± 5% for 2.5 and 56 ± 5% for 3.2) as compared to the cells exposed to MG/L^F/PDA (Figure

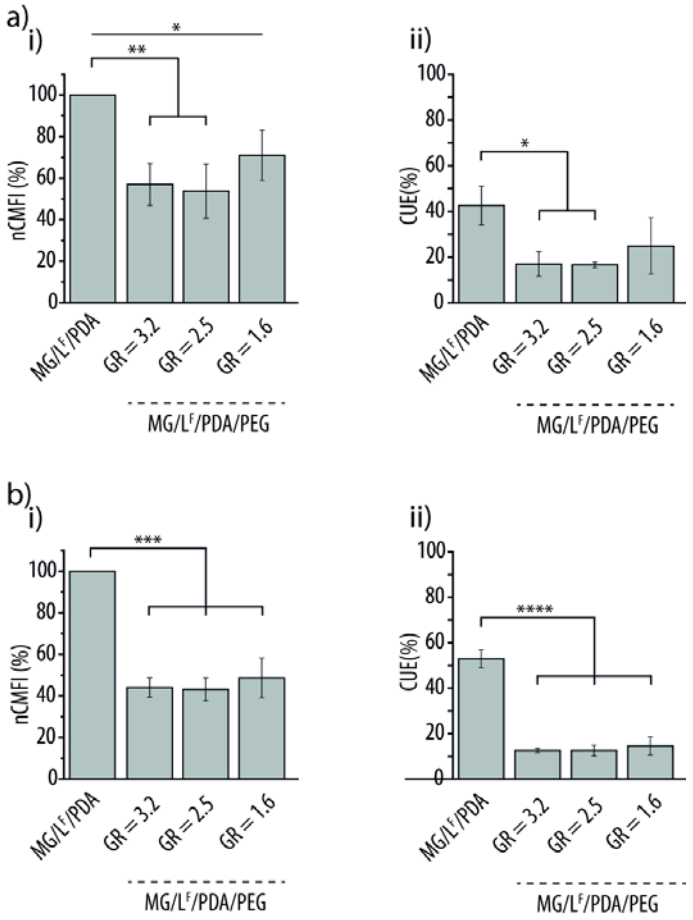

Figure 5.3 PEGylation effect towards cell uptake/association. i) Normalised cell mean fluorescence intensity (nCMFI) and ii) Cellular uptake efficiency (CUE) of a) RAW 264.7 and b) HUVEC cells upon incubation with MG/L^F/PDA or MG/L^F/PDA/PEG with different grafting ratios (GR). n=3, *$p \leq 0.05$; **$p \leq 0.01$; ***$p \leq 0.001$; **** $p \leq 0.0001$.

5.3bi). In the case of CUE (Figure 5.3bii), all the GRs resulted in a similar significant reduction of the CUE (~39%) as compared to the cells incubated with MG/L^F/PDA. All in all, although there are slight differences between the two proteins and the two cell lines studied, there is an overall successful PEGylation effect for the carriers functionalised with GR = 1.6, 2.5 and 3.2. Therefore, the GR = 3.2 is the one selected for the further experiments of the thesis.

5.3.1.4 CAT encapsulation

Once the assembly of the empty microreactor (without CAT) had been optimised, its potential as a microreactor for ROS depletion was evaluated. As a first step the encapsulation of the CAT enzyme within liposomes was optimised in order to incorporate them into the microreactor.

To assess the maximum amount of CAT that could be incorporated into the liposomes, the lipid film was rehydrated with increasing amounts of CAT followed by vortexing and incubation at 45°C for 20 min which were subsequently extruded in order to yield unilamellar liposomes. Upon purification by SEC (Appendix A, Figure A.1) and up-concentration, the CAT-loaded liposomes were characterised in terms of CAT entrapment, size and ξ-potential (Figure 5.4).

The amount of CAT entrapped within the different liposomes was evaluated by disassembling the liposomes (employing 0.1% Triton X-100) and making use of a micro BCA assay to establish the enzyme concentration. Figure 5.4a, shows the CAT concentration as obtained by means of the micro BCA assay (y axis, Experimental CAT concentration) compared to the concentration of CAT employed for the lipid film hydration (x axis, Theoretical CAT concentration). The results shows that when employing CAT concentrations higher than 500 μg mL^{-1} to rehydrate the lipid film no increase in the experimental CAT concentration is observed, thus indicating saturation of the system (rehydration with 500 μg mL^{-1} CAT yields liposomes entrapping/associated with 17.1 ± 2.9 μg mL^{-1} CAT). It is worth noticing that this experiment only provides information regarding the association of the CAT enzyme with the liposomes that is it cannot be claimed whether the CAT enzyme is encapsulated within the liposomes or just associated with their membrane. The encapsulation efficiency (EE) was determined to be 3.0 ± 0.8%. While this EE is low, it is in agreement with literature.[39,172] In particular, Zhu *et al*.,[172] obtained a 3 ± 1% EE (as determined by BCA assay) upon rehydration and purification of 1,2-Dioleoyl-*sn*-glycero-3-phosphocholine (DOPC) liposomes with a 1 mg mL^{-1} CAT solution. In another study, Armada-Moreira *et al*.,[39] reported a total 11.3 ± 0.6% EE (CAT + GOx, determined by BCA assay) upon rehydration and

purification of DOPC liposomes with a 724.4 μg mL^{-1} CAT + GOx solution (1:1 enzyme ratio). This low EE observed for CAT-loaded liposomes could be explained due to the large size of the protein which is ~ 250 KDa.

The different liposomes fabricated with various CAT concentrations were further characterised by DLS to assess their size and PDI. As shown in Figure 5.4b, the diameters of the different CAT-loaded liposomes were ~100-120 nm in diameter independent of the theoretical CAT concentration. Also, similar low values in PDI (~0.07-0.12) were obtained for the different theoretical CAT concentrations. An exception are obviously the empty liposomes (a theoretical CAT concentration of 0 μg mL^{-1}) which displayed a PDI of 0.05 ± 0.02.

Finally, the ξ-potential of the different liposomes was also evaluated (Figure 5.4c). While empty liposomes showed a positively ξ-potential of 46.1 ± 3.2 mV, a decrease in ξ-potential was observed for liposomes loaded with CAT. The higher the theoretical CAT concentration the lower the ξ-potential measurements. As such, a ξ-potential of 44 ± 4 mV was observed for liposomes assembled with a 100 μg mL^{-1} theoretical CAT concentration as opposed to liposomes fabricated with a 500 μg mL^{-1} theoretical CAT concentration which displayed a decreased ξ-potential of 42 ± 7 mV. Such decrease in ξ-potential could be explained by the partial deposition of the negatively charged CAT on the liposomes surface. This result is not surprising since it has been previously reported that enzyme encapsulation renders liposomes with enzyme entrapped within the liposomes core as well as enzyme associated with the liposomes surface.[11] Additionally, no decrease in ξ-potential was observed for theoretical CAT concentrations above 500 μg mL^{-1}, thus indicating saturation of the system.

Therefore, 500 μg mL^{-1} CAT solution was chosen to assemble the CAT-containing liposomes (L^{CAT}) employed for the microreactors fabrication.

5.3.1.5 CAT-loaded microreactor characterisation

Next, the microreactor assembly was characterised by monitoring the ξ-potential of each building step followed by the quantification of μg of CAT per μg of MG by micro BCA

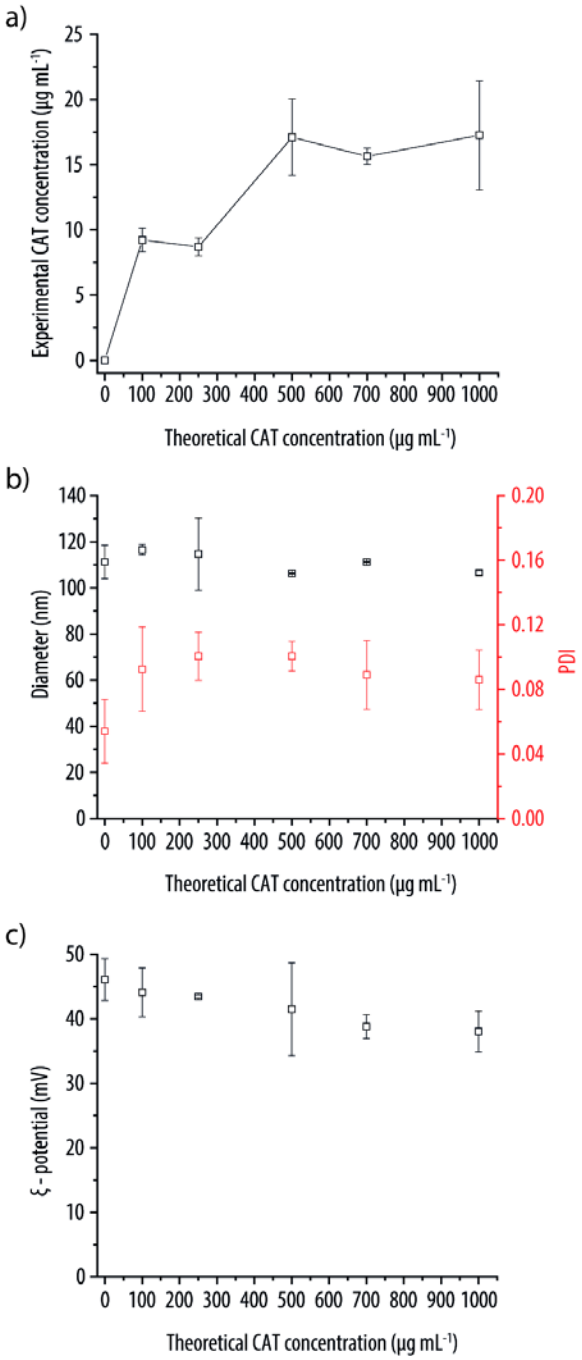

Figure 5.4 Catalase (CAT) encapsulation. a) Liposome saturation upon incubation with increasing CAT concentration measured by micro BCA assay yielding L^{CAT}. b) Diameter and polydispersity (PDI) of empty L and L^{CAT}. c) ξ-potential of empty L and L^{CAT}.

assay (Figure 5.5).

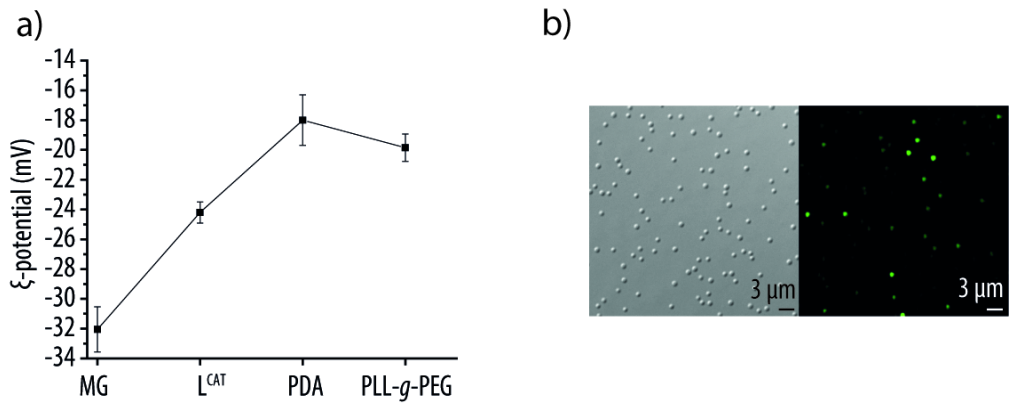

Figure 5.5 Microreactor characterisation. a) ξ- potential measurements after each deposition step: First bare MGs are decorated with catalase-loaded liposomes (L^{CAT}) followed by the poly(dopamine) (PDA) coating and functionalised with poly(*L*-lysine)-*grafted*-poly(ethylene glycol) (PLL-*g*-PEG). b) Differential interference contrast and fluorescent image of MG/$L^{CAT\text{-}FITC}$/PDA.

The L^{CAT} deposition was confirmed by an increase in ξ-potential from 32 ± 2 mV for bare MGs to -24.2 ± 0.7 mV for MG/L^{CAT} upon incubation of bare MGs with the positively charged L^{CAT} (Figure 5.5a). Finally, upon deposition of PDA a further increase in ξ-potential up to -18.0 ± 1.7 mV was observed in agreement with the results obtained in Chapter 3, section 3.3.2.3. Since non-significant differences were found for the different GRs and GR = 3.2 requires less material to conduct its synthesis, it was decided to assemble the microreactor with PLL-*g*-PEG of a GR = 3.2. The functionalisation of the PDA surface with PLL-*g*-PEG (GR = 3.2) resulted in similar ξ-potential (-19.8 ± 0.9 mV) as obtained in Figure 5.2a. The assembly of monodisperse and non-aggregated microreactors was confirmed by DIC and fluorescence microscopy. To do so, the microreactors were assembled with liposomes loaded with fluorescently labelled CAT (CAT-FITC). Figure 5.5b shows DIC images confirming the good colloidal stability of the microreactors in terms of aggregation. Fluorescence microscopy images show a homogeneous distribution of $L^{CAT\text{-}FITC}$ as shown by the regular fluorescence signal.

Finally, the µg of CAT per µg of MG was quantified by micro BCA. For this, the MG/L^{CAT} and MG/L were first exposed to 0.1% Triton X-100 for 30 min at room temperature followed by centrifugation, then the supernatant was analysed by micro BCA assay. The micro BCA assay resulted in 0.83 ± 0.12 µg of CAT per µg of MG for

MG/L^{CAT} and 0.01 ± 0.00 µg of CAT per µg of MG for the control (MG/L). It is worth to note that the µg of CAT per µg of MG was measured without the PDA coating to avoid interferences with the quantification method.

5.3.1.6 SOD-like activity of MG/L^F/PDA/PEG

In order to evaluate the performance of the multicompartment system as a microreactor, to demonstrate the proof-of-concept, a common bi-enzymatic reaction used to deplete ROS was chosen. In this reaction, the SOD enzyme catalyses the dismutation of $O_2^{\cdot-}$. into O_2 and H_2O_2. H_2O_2 then acts as a substrate for the CAT enzyme which catalyses the decomposition of H_2O_2 into H_2O and O_2.

ROS removal from blood was chosen due to their severe detrimental effects on the body.[31] Being able to enter and exit the cells,[53] ROS are able to reach distant organs leading to important pathologies.[54]

As a first step, the SOD-like activity of PDA is employed to perform the first step of the bi-enzymatic cascade reaction. It is well-known that melanin has antioxidant properties, in particular it exhibits SOD-like activity towards $O_2^{\cdot-}$ due to the catechol groups present in its structure.[173] Considering that PDA has a structure similar to that of melanin it is reasonable to expect a SOD-like activity of PDA.[56] This SOD-like activity was recently reported by Huang *et al*.[59] For this, coated selenium particles with PDA in order to scavenge $O_2^{\cdot-}$, $^{\cdot}OH$ and H_2O_2 in a synergistic way. The authors demonstrated the scavenging activity of PDA towards $O_2^{\cdot-}$ and $^{\cdot}OH$ and the antioxidant activity of selenium particles towards H_2O_2 in test tubes, *in vitro* (resulting in the inhibition of the detrimental effects caused by ROS such as DNA damage and lipid peroxidation upon treatment with the PDA-coated selenium particles), and *in vivo* using a pneumonia model (resulting in the alleviation of the inflammation reaction due to ROS scavenging upon treatment with the PDA-coated selenium particles).

Next, H_2O_2 is enzymatically transformed into H_2O and O_2 by the CAT encapsulated within the L^{CAT} used to assemble the microreactor (Scheme 5.1).

Although the following assays require further optimisation, the preliminary results presented in this section are useful to have an initial idea of the performance of the microreactor.

First, the SOD-like activity, that is, the ability to catalyse the dismutation of $O_2^{\cdot -}$ of both PEGylated and non-PEGylated MG/L^F/PDA and MG/L^F/PDA/PEG microreactors was assessed by the cytochrome C method (Figure 5.6). This method relies on the ability of xanthine and xanthine oxidase to generate $O_2^{\cdot -}$ from O_2. Next, the cytochrome^{3+} C substrate is reduced by $O_2^{\cdot -}$ to cytochrome^{2+} C which can be detected by its characteristic absorbance peak at 550 nm. As such, upon incubation of MG/L^F/PDA and MG/L^F/PDA/PEG microreactors with xanthine, xanthine oxidase and cytochrome^{3+} C, a decrease on the absorbance peak height is expected due to the catalysed dismutation of $O_2^{\cdot -}$ by the microreactors.

First, the amount of SOD units that MG/L^F/PDA and MG/L^F/PDA/PEG activity is equivalent to was determined by incubating the microreactors or increasing amount of SOD units with xanthine, xanthine oxidase and cytochrome^{3+} C for 0.5 h at 37°C. MG/L^F was used as control (Appendix A, Figure A.2a). According to the calibration curve (Appendix A, Figure A.2b), the MG/L^F/PDA and MG/L^F/PDA/PEG activity is equivalent to 2.8 ± 0.3 and 1.3 ± 0.1 SOD units, respectively.

Next, the reaction kinetics was evaluated over time as shown in Figure 5.6a. The results were normalised to the absorbance peak height at 550 nm of the blank solution at the different time points. The results show already a 55 ± 2% decrease in the normalised peak height as compared to the blank for samples incubated in the presence of the non-PEGylated (MG/L^F/PDA) microreactors after 0.5 h of reaction. A further decrease (74 ± 21% decrease as compared to the blank) is observed after 4 h of reaction. This decrease in normalised peak height is maintained through the whole time-frame (up to 72 h). However, the results for the PEGylated (MG/L^F/PDA/PEG) microreactors were different. While a 27 ± 7% decrease in normalised peak height as compared to the blank, is observed after 0.5 h of reaction, only a decrease of 10 ± 4% is observed after 2 h of reaction and no decrease in normalised peak height was observed after 4 h of incubation.

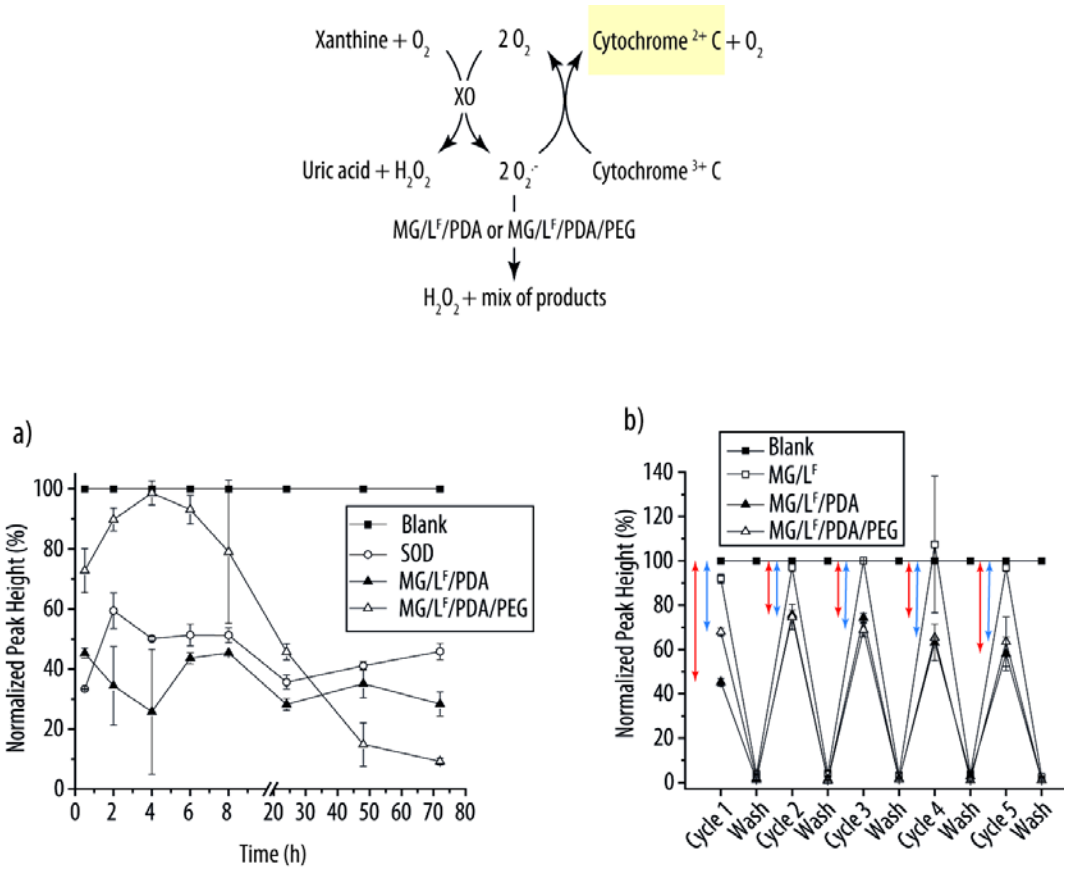

Figure 5.6 Superoxide dismutase like-activity of poly(dopamine) (PDA). The detection method is based on the production of $O_2^{\cdot-}$ by the xanthine/xanthine oxidase system which reduces cytochrome C that can be detected measuring absorbance at 550 nm. When the superoxide dismutase (SOD), MG/L^F/PDA or MG/L^F/PDA/PEG microreactors are present they inhibit the reduction of cytochrome C by transforming $O_2^{\cdot-}$ into H_2O_2 and a mix of products. a) Reaction kinetics. b) Recyclability of the microreactors.

A decrease in normalised peak height is again observed after 6 h of incubation (7 ± 5%) being it more pronounced after 8 and 24 h (of 21 ± 23% and 54 ± 3% after 8 and 24 h of incubation, respectively). While the differences in the reaction kinetics profile of non-PEGylated and PEGylated microreactors cannot be fully explained, it is worth mentioning that both systems showed a pronounced SOD-like activity reaching stability after 48 h of reaction, probably due to full consumption of the $O_2^{\cdot-}$.

It is hypothesised that the differences in catalytic activity of the two microreactors, that is non-PEGylated (MG/L^F/PDA) and PEGylated (MG/L^F/PDA/PEG), may be due to the modification of the PDA by PLL-*g*-PEG. Although the exact structure of PDA is still

being highly debated, it has been reported that PDA structure possess a mixture of catechols and *o*-quinones (Figure 1.7, Chapter 1).[42] Aliphatic amines (such as the side chains of the lysine moieties of PLL-*g*-PEG) react with *o*-quinones trough Schiff base reaction yielding the corresponding imine (Scheme 5.2).[133] Therefore affecting the number of *o*-quinones available to react with $O_2^{\cdot-}$. The dismutation of the $O_2^{\cdot-}$ radical by

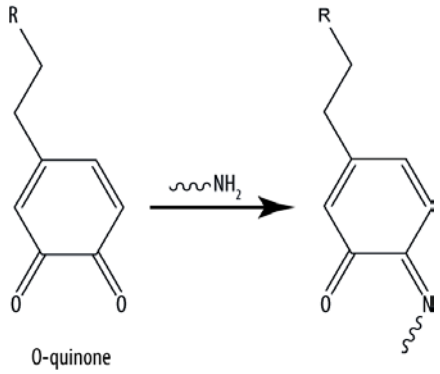

Scheme 5.2 Reaction of aliphatic amines with *o*-quinones

the PDA coating is due to the reaction of $O_2^{\cdot-}$ with both the catechols and *o*-quinones of the PDA. When $O_2^{\cdot-}$ reacts with the catechol moieties, it yields H_2O_2 and a catechol anion radical which is rapidly transformed into the starting catechol and the equivalent *o*-quinone.[133] In contrast, when $O_2^{\cdot-}$ reacts with the *o*-quinones it yields radical semiquinones (radical form of a quinone) that dismutates into the starting *o*-quinone.[174] As such, the fact that PLL-*g*-PEG reacts with the *o*-quinones of the PDA coating, thus diminishing the number of available *o*-quinones to react with $O_2^{\cdot-}$, could partially explain the differences in the reaction kinetics between the two types of microreactors. An in depth discussion of the reaction mechanism is beyond the scope of this study.

Next, it was investigated whether the microreactors could sustain multiple rounds of catalytic activity. Several multicompartment microreactors have been reported to successfully perform the enzymatic reaction for at least four cycles.[11,12,20,37] For the envisioned application, is desirable that the microreactors are able to conduct the ROS depletion in a sustained manner for an extended period of time. This will allow to reduce the dosage frequency and therefore improve the patient compliance.[20]

The recyclability of MG/L^F/PDA and MG/L^F/PDA/PEG was evaluated by conducting the reaction cycles for 0.5 h at 37 °C followed by absorbance measurement of the reduced cytochrome^{2+} C at 550 nm. After each reaction cycle, the microreactors were washed and the absorbance of the supernatants after the wash was measured at 550 nm to confirm complete removal of the of the cytochrome^{2+} C product. Following addition of fresh xanthine/xanthine oxidase and cytochrome^{3+} C, the reaction was allowed to proceed for another cycle. The results, which have been normalised to the absorbance peak height of the blank at any given cycle, show a reduction of the normalised absorbance peak height of 32 ± 2% and 55 ± 2% as compared to the control for PEGylated and non-PEGylated microreactors respectively (Figure 5.6b). Importantly, the catalytic activity for the PEGylated microreactor was not affected after the 5 cycles since a reduction of 41 ± 12% (empty triangles) as compared to the control was observed for the fifth cycle. The results for the non-PEGylated microreactor were different and the reduction after the fifth cycle (black triangles, 47 ± 5%) was lower as compared to the first one (black triangles, 55 ± 2%). All in all, the results indicate that the microreactors can be successfully reused for at least five cycles regardless of the PEGylation. As controls, carriers without the PDA-coating (MG/L^F) were also considered and, as expected, no decrease in the absorbance peak height as compared to the blank was observed for the different cycles.

5.3.1.7 Enzymatic cascade reaction

On a next step, the ability of MG/L^F/PDA, MG/L^F/PDA/PEG, MG/$L^{F,CAT}$/PDA and MG/$L^{F,CAT}$/PDA/PEG to deplete ROS through a cascade reaction was investigated. KO_2 spontaneously dissociates into $O_2^{\cdot-}$ which will be transformed by MG/$L^{F,CAT}$/PDA or MG/$L^{F,CAT}$/PDA/PEG into H_2O_2 (and a mix of products) due to the SOD-like activity of the carriers. Next, H_2O_2 product acts as a substrate for the CAT enzyme entrapped within the liposomal compartments of the microreactor yielding H_2O and O_2 (Figure 5.7). The depletion of H_2O_2 was monitored by making use of the amplex red/HRP assay. H_2O_2 acts as a co substrate for the oxidation of amplex red by HRP, generating a fluorescent product named resorufin.

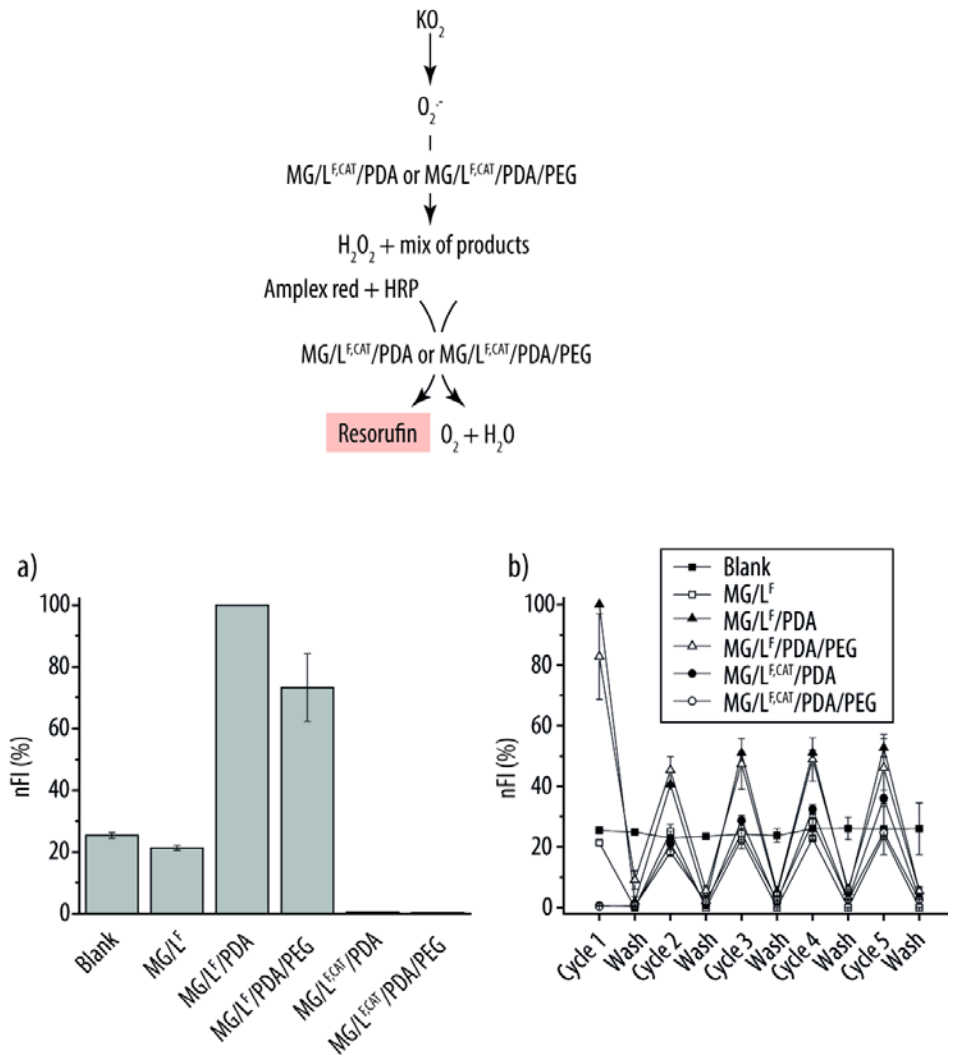

Figure 5.7 Cascade reaction using amplex red/horseradish peroxidase (HRP) assay. The detection method is based on the production of $O_2^{\cdot-}$ by KO_2 which in the presence of MG/L^{F,CAT}/PDA or MG/L^{F,CAT}/PDA/PEG is transformed into H_2O_2. The generated H_2O_2 acts as substrate for the CAT contained in MG/L^{F,CAT}/PDA and MG/L^{F,CAT}/PDA/PEG being transformed into H_2O and O_2. The reaction is evaluated by the detection of the fluorescent product named resorufin which is produced by the amplex red oxidation by HRP and H_2O_2. a) Normalised fluorescence intensity (nFI) of buffer (blank), MG/L^{F}, MG/L^{F}/PDA, MG/L^{F}/PDA/PEG, MG/L^{F,CAT}/PDA and MG/L^{F,CAT}/PDA/PEG upon incubation with KO_2 for 0.5 h at 37°C and detected with the amplex red/HRP assay. b) Recyclability of the microreactors.

To assess the potential of the microreactors (MG/L^{F,CAT}/PDA and MG/L ^{F,CAT}/PDA/PEG) to conduct a bi-enzymatic cascade reaction towards ROS depletion, the production of resorufin was monitored by its characteristic FI peak after 0.5 h of incubation (Figure 5.7a). As controls, MG/L^{F}/PDA, MG/L^{F}/PDA/PEG, MG/L^{F} and buffer only (blank) were

considered.

The results (Figure 5.7a), which have been normalised to the FI readings after incubating MG/L^{F}/PDA microreactors (SOD-like activity only) with KO_2 for 0.5 h, show an increase of 75 ± 1% and 48 ± 12% in nFI for MG/L^{F}/PDA and MG/L^{F}/PDA/PEG, respectively as compared to the blank. These results again show the SOD-like activity of the PDA-based carriers but with a different detection method. The ability of the CAT-loaded microreactors in depleting H_2O_2 is also demonstrated by the 99 ± 0% and 94 ± 7% decrease in nFI, for MG/$L^{F,CAT}$/PDA and MG/$L^{F,CAT}$/PDA/PEG, respectively as compared to the MG/L^{F}/PDA and MG/L^{F}/PDA/PEG. It is also worth pointing out that upon incubation of KO_2 in the absence (blank) or presence of MG/L^{F} a nFI signal of 25 ± 1% and 21 ± 1%, respectively, is observed. This fact is attributed to the spontaneously dismutation of $O_2^{\cdot-}$ spontaneously into H_2O_2.[52] The finding that the nFI signal measured after incubating both MG/$L^{F,CAT}$/PDA and MG/$L^{F,CAT}$/PDA/PEG is lower than the nFI signal of both controls (blank and MG/L^{F}) indicates that both CAT-loaded microreactors are not only able to scavenge the H_2O_2 produced by MG/L^{F}/PDA and MG/L^{F}/PDA/PEG but also the H_2O_2 obtained by the spontaneous dismutation of $O_2^{\cdot-}$.

For a successful microreactor able to deplete ROS for an extended period of time, it is desirable that the microreactors are able to conduct repeated enzymatic conversions. Thus, the ability of MG/$L^{F,CAT}$/PDA and MG/$L^{F,CAT}$/PDA/PEG to conduct multiple rounds of enzymatic reactions was evaluated. First, the microreactors were incubated with KO_2 for 0.5 h at 37°C and the H_2O_2 reaction product was detected by the amplex red/HRP assay. A blank and MG/L^{F} were considered as controls. The results were normalised to the FI signal measured after incubating MG/L^{F}/PDA for 0.5 h. The complete removal of the fluorescent resorufin product after washing was assessed by measuring the FI signal of the supernatant of the wash. Next, the microreactors were again incubated with KO_2 for 30 min and the FI signal of the resorufin product was measured after 0.5 h. This procedure was repeated for five cycles.

The results show that, similar to the results obtained for the cytochrome^{3+} c assay, the catalytic activity of the non-PEGylated MG/L^{F}/PDA microreactors (Figure 5.7b ,black triangles) is higher after the first cycle as compared to the fifth cycle (with a nFI increase

of 75 ± 1% after the first cycle versus 22 ± 6% after the fifth cycle, compared to the black). However, a successful increase in nFI of 22 ± 6% is still observed after the last catalytic cycle. A similar trend was obtained for the catalytic activity of the PEGylated microreactor MG/L^{F}/PDA/PEG (Figure 5.7b, empty triangles) with a successful increase of nFI of 13 ± 2% after the fifth cycle as compared to the blank.

Finally, both MG/$L^{F,CAT}$/PDA (Figure 5.7b, black circles) and MG/$L^{F,CAT}$/PDA/PEG (Figure 5.7b, empty circles) microreactors also showed their ability to be recycled for at least five cycles with a successful reduction in nFI of 11 ± 2% and 14 ± 0% after the fifth cycle upon incubation of KO_2 with MG/$L^{F,CAT}$/PDA and MG/$L^{F,CAT}$/PDA/PEG respectively, as compared to MG/L^{F}/PDA and MG/L^{F} /PDA/PEG . Although a decrease of enzymatic activity for both MG/$L^{F,CAT}$/PDA and MG/$L^{F,CAT}$/PDA/PEG was observed over the subsequent cycles this has been previously reported in other multicompartment microreactors,[11,12,20] and for CAT using a different system.[175] In particular, Cui *et al*.,[175] reported that the CAT encapsulated within a metal-organic framework contained in large mesoporous silica structure, could be recycle up to ten cycles maintaining ~50% of the initial activity.

5.4 Conclusions

In this chapter, results regarding the evaluation of the multicompartment carrier performance as a microreactor towards ROS detoxification in test tubes is described and discussed. However, *in vitro* validation of the results is necessary.

The empty and the CAT-loaded microreactor was successfully assembled and characterised by various techniques. The different GRs of PLL-*g*-PEG were evaluated in terms of PEGylation effect towards protein deposition and cellular uptake/association. Based on the results presented above, all GRs exhibited a large PEGylation effect when incubated with proteins and cells.

Regarding the SOD-like activity of PDA, it was confirmed through two different assays (*i.e.*, cytochrome^{3+} C and amplex red/HRP assay) for both the non-PEGylated and the PEGylated microreactor, demonstrating that the designed microreactor is able to scavenge the most dangerous ROS ($O_2^{\cdot -}$). What is more, such antioxidant activity was proved to be reusable for at least to five enzymatic rounds.

Finally, the CAT contained in the L^{CAT} remained highly active in both the non-PEGylated and the PEGylated microreactor and it was also demonstrated that it could be reused for at least five enzymatic rounds.

All in all, the results presented in this chapter represent a different approach towards ROS detoxification which has been proved to be successful in test tubes. Further *in vitro* experiments, in the presence of relevant cell populations (i.e., RAW 264.7 and HUVEC cells), are needed in order to confirm the promising results presented and discussed here.

Chapter VI Concluding remarks

The development of multicompartment carriers has attracted great attention in the biomedical field. To date, the research has been focused on their application as drug delivery carriers and as extra and intracellular microreactors. However, despite all the great efforts invested in their design most of the reported systems are in the micron range limiting their therapeutic potential. In an attempt to move the field a step forwards, a multicompartment carrier in the submicron range with potential as drug delivery carrier and extracellular microreactor has been assembled, characterised, described and discussed in this PhD thesis.

For this, four different building blocks (*i.e.*, P(NIPAM)-*co*-AAc MGs, liposomes, PDA and PLL-*g*-PEG), which have been proved to be highly useful in both the assembly of drug delivery and microreactors, were combined to create a new multicompartment carrier.

In particular, the combination of P(NIPAM)-*co*-AAc MGs and liposomes (creating the so-called hydrogel-liposome complex) offers the possibility to co-encapsulate different hydrophilic and/or hydrophobic cargos in the different compartments (*i.e.*, MG and liposome). This co-encapsulation guarantees their co-localization at their target site while being release in a tandem manner due to the different release profile from the P(NIPAM)-*co*-AAc MGs and liposomes. Next, the usage of PDA reduces the efforts in the building of the multicompartment carrier compared to other techniques such as LbL technique due to its self-assembly behaviour. Likewise, PDA not only offers structural protection to the system but it also provides an easy functionalisation strategy due to its reactivity towards amines and thiols. What is more, the *O*-quinones and catechol groups present in the PDA structure provides the multicompartment carrier with antioxidant properties. Finally, the PEGylation of the carrier´s surface is envisioned to protect the surface from protein adsorption and unwanted cellular uptake/association resulting in a prolonged circulation time in the body.

Two different diameter-sized MGs (*i.e.*, MG_{700} and MG_{350}) were evaluated as the best candidate for the carrier´s core in terms of facile production, colloidal stability and

PEGylation effect. The assembly of the multicompartment carrier was thoroughly investigated by different techniques (*i.e.*, flow cytometry, ξ-potential, DIC and fluorescence imaging, QCM-D) as well as the cellular interaction with three relevant cell lines: RAW 264.7 (macrophages, first line of defence in the body), HUVEC (endothelial cells lining the blood vessels) and HeLa (cancer cells, as an example of a therapeutic target). Both MGs exhibit a similar behaviour with small differences. The MG_{700} demonstrated an overall better colloidal stability along the assembly process while MG_{350} demonstrated a better PEGylation effect towards cellular uptake/association. Importantly, a promising finding is the preferential internalisation of the multicompartment carrier by the cancer cell line regardless of the PEGylation of the surface over RAW 264.7 and HUVEC cells. It is worth mentioning that although MG_{350} was not chosen as the carrier´s core (due to the difficulty in producing larger scales) its small size and high cellular uptake/association with all the three tested cell lines make it an interesting tool for intracellular delivery.

Once MG_{700} was selected as the carrier´s core the research was focused on the study of the multicompartment carrier as a drug delivery platform by co-encapsulating two model molecules leading to a faster release of the MB encapsulated in the MGs core than the Cal encapsulated in the liposome core. Next, the impact of shear stress was valuated in terms of protein adsorption. The results regarding this topic corroborated the importance of shear stress when evaluating a carrier designed for intravenous administration, as evidenced by the favoured protein adsorption upon shear stress exposure. Finally, a thorough study regarding the interaction of the non-PEGylated and the PEGylated carrier with relevant cell lines (*i.e.*, RAW 264.7, HUVEC and HeLa cells) in the absence and presence of shear stress (which is normally neglected in *in vitro* studies) was also presented. The results indicate an important impact of shear stress on the cell/carrier interaction in terms of cell internalisation/association, CUE and cellular pathway, emphasizing the importance of including this physiological parameter in *in vitro* set ups. It was also demonstrated that although the applied shear stress promoted cell association/internalisation by the three studied cell lines, the developed multicompartment carrier has always been internalised preferentially by the target cell line (HeLa cells).

Lastly, aiming to improve the PEGylation effect, PLL-*g*-PEG of different GRs was synthesised and evaluated by means of protection towards protein adsorption and cellular uptake/association. Next, preliminary results regarding the potential of the multicompartment carrier as a detoxifying microreactor towards ROS were presented and discussed. While the mechanisms underlying the reaction mechanism between $O_2^{\cdot -}$ are complex and not completely understood, it was demonstrated that both the PEGylated and non-PEGylated carriers were able to successfully scavenge $O_2^{\cdot -}$ for up to five independent reaction cycles. What is more, the combination of the antioxidant activity of PDA with the scavenging activity of CAT towards H_2O_2 resulted in a great tandem towards a successful ROS detoxification.

On a final note, the future *in vitro* confirmation of the cascade reaction presented in this PhD thesis by means of resorufin formation and improved cell viability will represent an interesting new approach for ROS detoxification at an extracellular level. Although this project is still at its infancy, this microreactor combines the appropriate size, efficient PEGylation coating and high antioxidant activity to potentially remove ROS from blood upon a more extensive optimisation.

References

[1] J. Gaitzsch, X. Huang, B. Voit, Engineering Functional Polymer Capsules toward Smart Nanoreactors, Chem. Rev. 116 (2016) 1053–1093. doi:10.1021/acs.chemrev.5b00241.

[2] M.J. York-Duran, M. Godoy-Gallardo, C. Labay, A.J. Urquhart, T.L. Andresen, L. Hosta-Rigau, Recent advances in compartmentalized synthetic architectures as drug carriers, cell mimics and artificial organelles, Colloids Surf., B. 152 (2017) 199–213. doi:10.1016/j.colsurfb.2017.01.014.

[3] J.W. Hindley, Y. Elani, C.M. McGilvery, S. Ali, C.L. Bevan, R. V. Law, O. Ces, Light-triggered enzymatic reactions in nested vesicle reactors, Nat. Commun. 9 (2018) 1–16. doi:10.1038/s41467-018-03491-7.

[4] N.-N. Deng, M. Yelleswarapu, L. Zheng, W.T.S. Huck, Microfluidic assembly of monodisperse vesosomes as artificial cell models, J. Am. Chem. Soc. 139 (2017) 587–590. doi:10.1021/jacs.6b10977.

[5] X. Liu, P. Formanek, B. Voit, D. Appelhans, Functional Cellular Mimics for the Spatiotemporal Control of Multiple Enzymatic Cascade Reactions, Angew. Chem., Int. Ed. 56 (2017) 16233–16238. doi:10.1002/anie.201708826.

[6] X. Huang, B. Voit, Progress on multi-compartment polymeric capsules, Polym. Chem. 4 (2013) 435–443. doi:10.1039/c2py20636f.

[7] A. Peyret, E. Ibarboure, N. Pippa, S. Lecommandoux, Liposomes in Polymersomes: Multicompartment System with Temperature-Triggered Release, Langmuir. 33 (2017) 7079–7085. doi:10.1021/acs.langmuir.7b00655.

[8] C.D. Driever, X. Mulet, L.J. Waddington, A. Postma, H. Thissen, F. Caruso, C.J. Drummond, Layer-by-layer polymer coating on discrete particles of cubic lyotropic liquid crystalline dispersions (cubosomes), Langmuir. 29 (2013) 12891–12900. doi:10.1021/la401660h.

[9] C.D. Driever, X. Mulet, A.P.R. Johnston, L.J. Waddington, H. Thissen, F. Caruso, C.J. Drummond, Converging layer-by-layer polyelectrolyte microcapsule and cubic lyotropic liquid crystalline nanoparticle approaches for molecular encapsulation, Soft Matter. 7 (2011) 4257–4266. doi:10.1039/c0sm01410a.

[10] L. Hosta-Rigau, R. Chandrawati, E. Saveriades, P.D. Odermatt, A. Postma, F. Ercole, K. Breheney, K.L. Wark, B. Städler, F. Caruso, Noncovalent Liposome Linkage and Miniaturization of Capsosomes for Drug Delivery, Biomacromolecules. 11 (2010) 3548–3555.

[11] M. Godoy-Gallardo, C.C. Labay, V.D. Trikalitis, P.J. Kempen, J.B. Larsen, T.L. Andresen, L. Hosta-Rigau, Multi-compartment Artificial Organelles Conducting Enzymatic Cascade Reactions inside Cells, ACS Appl. Mater. Interfaces. 9 (2017) 15907–15921. doi:10.1021/acsami.6b16275.

[12] M. Godoy-Gallardo, C. Labay, M.M.T. Jansman, P.K. Ek, L. Hosta-Rigau, Intracellular microreactors as artificial organelles to conduct multiple enzymatic reactions simultaneously, Adv. Healthcare Mater. 6 (2017) 1–14. doi:10.1002/adhm.201601190.

[13] L. Hosta-Rigau, B. Städler, Y. Yan, E.C. Nice, J.K. Heath, F. Albericio, F. Caruso, Capsosomes with multilayered subcompartments: Assembly and loading with hydrophobic Cargo, Adv. Funct. Mater. 20 (2010) 59–66. doi:10.1002/adfm.200901297.

[14] L. Hosta-Rigau, M.J. York-Duran, Y. Zhang, K.N. Goldie, B. Städler, Confined multiple enzymatic (cascade) reactions within poly(dopamine)-based capsosomes, ACS Appl. Mater. Interfaces. 6 (2014) 12771–12779. doi:10.1021/am502743z.

[15] M. Godoy-Gallardo, M.J. York-Duran, L. Hosta-Rigau, Recent Progress in Micro/Nanoreactors toward the Creation of Artificial Organelles, Adv. Healthcare Mater. 7 (2018) 1–35. doi:10.1002/adhm.201700917.

[16] A.D. Bangham, M.M. Standish, J.C. Watkins, Diffusion of univalent ions across the lamellae of swollen phospholipids, J. Mol. Biol. 13 (1965) 238–252. doi:10.1016/S0022-2836(65)80093-6.

[17] C. Zylberberg, S. Matosevic, Pharmaceutical liposomal drug delivery: a review of new delivery systems and a look at the regulatory landscape, Drug Delivey. 23 (2016) 3319–3329. doi:10.1080/10717544.2016.1177136.

[18] R.P. Brinkhuis, F.P.J.T. Rutjes, J.C.M. Van Hest, Polymeric vesicles in biomedical applications, Polym. Chem. 2 (2011) 1449–1462. doi:10.1039/c1py00061f.

[19] Z. Karami, M. Hamidi, Cubosomes: Remarkable drug delivery potential, Drug Discovery Today. 21 (2016) 789–801. doi:10.1016/j.drudis.2016.01.004.

[20] L. Hosta-Rigau, M.J. York-Duran, T.S. Kang, B. Städler, Extracellular Microreactor for the Depletion of Phenylalanine Toward Phenylketonuria Treatment, Adv. Funct. Mater. 25 (2015) 3860–3869. doi:10.1002/adfm.201404180.

[21] B. Thingholm, P. Schattling, Y. Zhang, B. Stadler, Subcompartmentalized Nanoreactors as Artificial Organelle with Intracellular Activity, Small. 12 (2016) 1806–1814. doi:10.1002/smll.201502109.

[22] J.H. Lee, A. Nan, Combination Drug Delivery Approaches in Metastatic Breast Cancer, J. Drug Delivery. 2012 (2012) 1–17. doi:10.1155/2012/915375.

[23] J.M. Stewart, B.G. Keselowsky, Combinatorial drug delivery approaches for

immunomodulation, Adv. Drug Delivery Rev. 114 (2017) 161–174. doi:10.1016/j.addr.2017.05.013.

[24] S.E. Inzucchi, Oral Antihyperglycemic Therapy for Type 2 Diabetes, JAMA. 287 (2002) 360–372.

[25] D.M. Lee, M.E. Weinblatt, Rheumatoid arthritis., Lancet. 358 (2001) 903–911. doi:10.1016/S0140-6736(01)06075-5.

[26] Q. Saleem, Z. Zhang, C.C. Gradinaru, P.M. Macdonald, Liposome-coated hydrogel spheres: delivery vehicles with tandem release from distinct compartments, Langmuir. 29 (2013) 14603–14612. doi:10.1021/la402796k.

[27] F. Itel, P.S. Schattling, Y. Zhang, B. Städler, Enzymes as key features in therapeutic cell mimicry, Adv. Drug Delivery Rev. 118 (2017) 94–108. doi:10.1016/j.addr.2017.09.006.

[28] M. Li, Enzyme Replacement Therapy: A Review and Its Role in Treating Lysosomal Storage Diseases, Pediatric Annals. 47 (2018) 191–197. doi:10.3928/19382359-20180424-01.

[29] J.M. Kelly, A. Bradbury, D.R. Martin, M.E. Byrne, Emerging therapies for neuropathic lysosomal storage disorders, Prog. Neurobiol. 152 (2017) 166–180. doi:10.1016/j.pneurobio.2016.10.002.

[30] P. Tanner, V. Balasubramanian, C.G. Palivan, Aiding nature's organelles: Artificial peroxisomes play their role, Nano Lett. 13 (2013) 2875–2883. doi:10.1021/nl401215n.

[31] T.J. Guzik, D.G. Harrison, Vascular NADPH oxidases as drug targets for novel antioxidant strategies, Drug Discovery Today. 11 (2006) 524–533. doi:10.1016/j.drudis.2006.04.003.

[32] T. Fukai, M. Ushio-Fukai, Superoxide Dismutases: Role in Redox Signaling, Vascular Function, and Diseases, Antioxid. Redox Signal. 15 (2011) 1583–1606. doi:10.1089/ars.2011.3999.

[33] P.Y. Bolinger, D. Stamou, H. Vogel, An integrated self-assembled nanofluidic system for controlled biological chemistries, Angew. Chem., Int. Ed. 47 (2008) 5544–5549. doi:10.1002/anie.200801606.

[34] Y. Elani, R. V. Law, O. Ces, Vesicle-based artificial cells as chemical microreactors with spatially segregated reaction pathways, Nat. Commun. 5 (2014) 1–5. doi:10.1038/ncomms6305.

[35] R.J.R.W. Peters, M.M. Marguet, S. Marais, M.W. Fraaije, J.C.M. Van Hest, S. Lecommandoux, Cascade reactions in multicompartmentalized polymersomes, Angew. Chem., Int. Ed. 53 (2014) 146–150. doi:10.1002/anie.201308141.

[36] W. Siti, H.-P.M. de Hoog, O. Fischer, W.Y. Shan, N. Tomczak, M. Nallani, B.

Liedberg, An intercompartmental enzymatic cascade reaction in channel-equipped polymersome-in-polymersome architectures, J. Mater. Chem. B. 2 (2014) 2733–2737. doi:10.1039/c3tb21849j.

[37] R. Chandrawati, L. Hosta-Rigau, D. Vanderstraaten, S.A. Lokuliyana, B. Städler, F. Albericio, F. Caruso, Engineering Advanced Capsosomes : Maximizing the Number of Temperature-Triggered Reaction, ACS Nano. 4 (2010) 1351–1361. doi:10.1021/nn901843j.

[38] L. Hosta-Rigau, S.F. Chung, A. Postma, R. Chandrawati, B. Städler, F. Caruso, Capsosomes with “free-Floating” Liposomal Subcompartments, Adv. Mater. 23 (2011) 4082–4087. doi:10.1002/adma.201100908.

[39] A. Armada-Moreira, B. Thingholm, K. Andreassen, A.M. Sebastião, S.H. Vaz, B. Städler, On the Assembly of Microreactors with Parallel Enzymatic Pathways, Adv. Biosyst. 2 (2018) 1–8. doi:10.1002/adbi.201700244.

[40] B. Städler, R. Chandrawati, A.D. Price, S.F. Chong, K. Breheney, A. Postma, L. a. Connal, A.N. Zelikin, F. Caruso, A microreactor with thousands of subcompartments: Enzyme-loaded liposomes within polymer capsules, Angew. Chem., Int. Ed. 48 (2009) 4359–4362. doi:10.1002/anie.200900386.

[41] R. Chandrawati, P.D. Odermatt, S.F. Chong, A.D. Price, B. Städler, F. Caruso, Triggered cargo release by encapsulated enzymatic catalysis in capsosomes, Nano Lett. 11 (2011) 4958–4963. doi:10.1021/nl202906j.

[42] M.E. Lynge, P. Schattling, B. Städler, Recent developments in poly(dopamine)-based coatings for biomedical applications, Nanomedicine (London, U.K.). 10 (2015) 2725–2742. doi:10.2217/nnm.15.89.

[43] F. Itel, J. Skovhus Thomsen, B. Städler, Matrix Vesicles-Containing Microreactors as Support for Bonelike Osteoblasts to Enhance Biomineralization, ACS Appl. Mater. Interfaces. 10 (2018) 30180–30190. doi:10.1021/acsami.8b10886.

[44] Y. Zhang, M. Baekgaard-Laursen, B. Städler, Small Subcompartmentalized Microreactors as Support for Hepatocytes, Adv. Healthcare Mater. 6 (2017) 1–8. doi:10.1002/adhm.201601141.

[45] Y. Zhang, P.S. Schattling, F. Itel, B. Städler, Planar and cell aggregate-like assemblies consisting of microreactors and HepG2 cells, ACS Omega. 2 (2017) 7085–7095. doi:10.1021/acsomega.7b01234.

[46] M. Valko, D. Leibfritz, J. Moncol, M.T.D. Cronin, M. Mazur, J. Telser, Free radicals and antioxidants in normal physiological functions and human disease, Int. J. Biochem. Cell Biol. 39 (2007) 44–84. doi:10.1016/j.biocel.2006.07.001.

[47] E. Hood, E. Simone, P. Wattamwar, T. Dziubla, V. Muzykantov, Nanocarriers for vascular delivery of antioxidants, Nanomedicine. 6 (2011) 1257–1272. doi:10.2217/nnm.11.92.

[48] I. Zelko, T. Mariani, R. Folz, Superoxide dismutase multigene family: A comparison of the CuZn-SOD (SOD1), Mn-SOD (SOD2), and EC-SOD (SOD3) gene structures, evolution and expression, Free Radical Biol. Med. 4 (2002) 18–22. doi:10.7897/2277-4343.04115.

[49] C. Glorieux, P.B. Calderon, Catalase, a remarkable enzyme: Targeting the oldest antioxidant enzyme to find a new cancer treatment approach, Biol. Chem. 398 (2017) 1095–1108. doi:10.1515/hsz-2017-0131.

[50] J.F. Turrens, J.D. Crapo, B.A. Freeman, Protection against oxygen toxicity by intravenous injection of liposome-entrapped catalase and superoxide dismutase, J. Clin. Invest. 73 (1984) 87–95. doi:10.1172/JCI111210.

[51] M. Nucci, J. Olejarczyk, A. Abuchowski, Immunogenicity of polyethylene glycol-modified superoxide dismutase and catalase, J. Free Radicals Biol. Med. 2 (1986) 321–325. doi:10.1016/S0748-5514(86)80031-9.

[52] F.P. Chang, Y.P. Chen, C.Y. Mou, Intracellular implantation of enzymes in hollow silica Nanospheres for protein therapy: Cascade System of Superoxide Dismutase and Catalase, Small. 10 (2014) 4785–4795. doi:10.1002/smll.201401559.

[53] G.J.M. Den Hartog, S. Qi, J.H.O. Van Tilburg, G.H. Koek, A. Bast, Superoxide anion radicals activate hepatic stellate cells after entry through chloride channels: A new target in liver fibrosis, Eur. J. Pharmacol. 724 (2014) 140–144. doi:10.1016/j.ejphar.2013.12.033.

[54] S.F. Assimakopoulos, K. Grintzalis, K.C. Thomopoulos, I. Papapostolou, C.D. Georgiou, C. Gogos, C.E. Vagianos, Plasma superoxide radical in jaundiced patients and role of xanthine oxidase, Am. J. Med. Sci. 336 (2008) 230–236. doi:10.1097/MAJ.0b013e3181601158.

[55] J. Quintero-Saumeth, D.A. Rincón, M. Doerr, M.C. Daza, Concerted double proton-transfer electron-transfer between catechol and superoxide radical anion, Phys. Chem. Chem. Phys. 19 (2017) 26179–26190. doi:10.1039/c7cp03930a.

[56] S. Xiong, Y. Wang, J. Yu, L. Chen, J. Zhu, Z. Hu, Polydopamine particles for next-generation multifunctional biocomposites, J. Mater. Chem. A. 2 (2014) 7578–7587. doi:10.1039/c4ta00235k.

[57] K.Y. Ju, Y. Lee, S. Lee, S.B. Park, J.K. Lee, Bioinspired polymerization of dopamine to generate melanin-like nanoparticles having an excellent free-radical-scavenging property, Biomacromolecules. 12 (2011) 625–632. doi:10.1021/bm101281b.

[58] Q. Wang, R. Zhang, M. Lu, G. You, Y. Wang, G. Chen, C. Zhao, Z. Wang, X. Song, Y. Wu, L. Zhao, H. Zhou, Bioinspired Polydopamine-Coated Hemoglobin as Potential Oxygen Carrier with Antioxidant Properties, Biomacromolecules. 18 (2017) 1333–1341. doi:10.1021/acs.biomac.7b00077.

[59] Y. Huang, Z. Liu, C. Liu, Y. Zhang, J. Ren, X. Qu, Selenium-Based Nanozyme as Biomimetic Antioxidant Machinery, Chem. - Eur. J. 24 (2018) 10224–10230. doi:10.1002/chem.201801725.

[60] M.J. York-Duran, P.K. Ek, M. Godoy-Gallardo, L. Hosta-Rigau, Shear stress regulated uptake of liposome-decorated microgels coated with a poly(dopamine) shell, Colloids Surf., B. 171 (2018) 427–436. doi:10.1016/j.colsurfb.2018.07.031.

[61] B. Sierra-Martin, J.R. Retama, M. Laurenti, A. Fernández Barbero, E. López Cabarcos, Structure and polymer dynamics within PNIPAM-based microgel particles, Adv. Colloid Interface Sci. 205 (2014) 113–123. doi:10.1016/j.cis.2013.11.001.

[62] J.-O. You, D. Almeda, G.J. Ye, D.T. Auguste, Bioresponsive matrices in drug delivery, J. Biol. Eng. 4 (2010) 1–12. doi:10.1186/1754-1611-4-15.

[63] M.R. Islam, Y. Gao, X. Li, M.J. Serpe, Responsive polymers for biosensing and protein delivery, J. Mater. Chem. B. 2 (2014) 2444–2451. doi:10.1039/C3TB21657H.

[64] M.S. Kim, S.J. Park, H.J. Chun, C.-H. Kim, Thermosensitive hydrogels for tissue engineering, Tissue Eng. Regener. Med. 8 (2011) 117–123.

[65] S. Xu, J. Zhang, C. Paquet, Y. Lin, E. Kumacheva, From hybrid microgels to photonic crystals, Adv. Funct. Mater. 13 (2003) 468–472. doi:10.1002/adfm.200304338.

[66] T. Hoare, R. Pelton, Impact of microgel morphology on functionalized microgel-drug interactions, Langmuir. 24 (2008) 1005–1012. doi:10.1021/la7024507.

[67] J. Gan, X. Guan, J. Zheng, H. Guo, K. Wu, L. Liang, M. Lu, Biodegradable, thermoresponsive PNIPAM-based hydrogel scaffolds for the sustained release of levofloxacin, RSC Adv. 6 (2016) 32967–32978. doi:10.1039/C6RA03045A.

[68] M.H. Kwok, Z. Li, T. Ngai, Controlling the synthesis and characterization of micrometer-sized PNIPAM microgels with tailored morphologies, Langmuir. 29 (2013) 9581–9591. doi:10.1021/la402062t.

[69] P.C. Periyasamy, J.C.H. Leijten, P.J. Dijkstra, M. Karperien, J.N. Post, Nanomaterials for the local and targeted delivery of osteoarthritis drugs, J. Nanomater. 2012 (2012) 1–13. doi:10.1155/2012/673968.

[70] T. Bhatia, P. Husen, J. Brewer, L.A. Bagatolli, P.L. Hansen, J.H. Ipsen, O.G. Mouritsen, Preparing giant unilamellar vesicles (GUVs) of complex lipid mixtures on demand : Mixing small unilamellar vesicles of compositionally heterogeneous mixtures, Biochim. Biophys. Acta. 1848 (2015) 3175–3180. doi:10.1016/j.bbamem.2015.09.020.

[71] J. Li, X. Wang, T. Zhang, C. Wang, Z. Huang, X. Luo, Y. Deng, A review on phospholipids and their main applications in drug delivery systems, Asian J. Pharm.

Sci. 10 (2014) 81–98. doi:10.1016/j.ajps.2014.09.004.

[72] A. Jesorka, O. Orwar, Liposomes: Technologies and Analytical Applications, Annu. Rev. Anal. Chem. 1 (2008) 801–832. doi:10.1146/annurev.anchem.1.031207.112747.

[73] M. Anderson, A. Omri, The Effect of Different Lipid Components on the In Vitro Stability and Release Kinetics of Liposome Formulations, Drug Delivey. 11 (2004) 33–39. doi:10.1080/10717540490265243.

[74] B. Kneidl, M. Peller, G. Winter, L.H. Lindner, M. Hossann, Thermosensitive liposomal drug delivery systems: state of the art review, Int. J. Nanomedicine. 9 (2014) 4387–4398. doi:10.2147/IJN.S49297.

[75] H. Karanth, R.S.R. Murthy, pH-Sensitive liposomes-principle and application in cancer therapy, J. Pharm. Pharmacol. 59 (2007) 469–483. doi:10.1211/jpp.59.4.0001.

[76] E. Heidarli, S. Dadashzadeh, A. Haeri, State of the art of stimuli-responsive liposomes for cancer therapy, Iran. J. Pharm. Res. 16 (2017) 1273–1304.

[77] Y. Lee, D.H. Thompson, Stimuli-responsive liposomes for drug delivery, Wiley Interdiscip. Rev.: Nanomed. Nanobiotechnol. 9 (2017). doi:10.1002/wnan.1450.

[78] U. Bulbake, S. Doppalapudi, N. Kommineni, W. Khan, Liposomal formulations in clinical use: An updated review, Pharmaceutics. 9 (2017) 1–33. doi:10.3390/pharmaceutics9020012.

[79] J.A. Zasadzinski, B. Wong, N. Forbes, G. Braun, G. Wu, Novel Methods of Enhanced Retention in and Rapid, Targeted Release from Liposomes, Curr. Opin. Colloid Interface Sci. 16 (2011) 203–214. doi:10.1016/j.cocis.2010.12.004.Novel.

[80] R. van der Westen, L. Hosta-Rigau, D.S. Sutherland, K.N. Goldie, F. Albericio, A. Postma, B. Städler, Myoblast cell interaction with polydopamine coated liposomes, Biointerphases. 7 (2012) 1–9. doi:10.1007/s13758-011-0008-4.

[81] S.M. Moghimi, J. Szebeni, Stealth liposomes and long circulating nanoparticles: Critical issues in pharmacokinetics, opsonization and protein-binding properties, Prog. Lipid Res. 42 (2003) 463–478. doi:10.1016/S0163-7827(03)00033-X.

[82] H. He, Y. Lu, J. Qi, Q. Zhu, Z. Chen, W. Wu, Adapting liposomes for oral drug delivery, Acta Pharm. Sin. B. (2018). doi:10.1016/j.apsb.2018.06.005.

[83] K. Fujimoto, T. Toyoda, Y. Fukui, Preparation of bionanocapsules by the layer-by-layer deposition of polypeptides onto a liposome, Macromolecules. 40 (2007) 5122–5128. doi:10.1021/ma070477w.

[84] H. Lee, S.M. Dellatore, W.M. Miller, P.B. Messersmith, Mussel-Inspired Surface Chemistry for Multifunctional Coatings, Science. 318 (2007) 426–430. doi:10.1126/science.1147241.

[85] J.H. Ryu, P.B. Messersmith, H. Lee, Polydopamine Surface Chemistry: A Decade of Discovery, ACS Appl. Mater. Interfaces. 10 (2018) 7523–7540. doi:10.1021/acsami.7b19865.

[86] S. Hong, Y.S. Na, S. Choi, I.T. Song, W.Y. Kim, H. Lee, Non-covalent self-assembly and covalent polymerization co-contribute to polydopamine formation, Adv. Funct. Mater. 22 (2012) 4711–4717. doi:10.1002/adfm.201201156.

[87] J. Liebscher, R. Mrówczyński, H.A. Scheidt, C. Filip, N.D. Haìdade, R. Turcu, A. Bende, S. Beck, Structure of polydopamine: A never-ending story?, Langmuir. 29 (2013) 10539–10548. doi:10.1021/la4020288.

[88] D.R. Dreyer, D.J. Miller, B.D. Freeman, D.R. Paul, C.W. Bielawski, Elucidating the structure of poly(dopamine), Langmuir. 28 (2012) 6428–6435. doi:10.1021/la204831b.

[89] Z. Zhang, J. Zhang, B. Zhang, J. Tang, Mussel-inspired functionalization of graphene for synthesizing Ag-polydopamine-graphene nanosheets as antibacterial materials, Nanoscale. 5 (2013) 118–123. doi:10.1039/c2nr32092d.

[90] Y. Li, W. Yang, X. Li, X. Zhang, C. Wang, X. Meng, Y. Pei, X. Fan, P. Lan, C. Wang, X. Li, Z. Guo, Improving Osteointegration and Osteogenesis of Three-Dimensional Porous Ti6Al4V Scaffolds by Polydopamine-Assisted Biomimetic Hydroxyapatite Coating, ACS Appl. Mater. Interfaces. 7 (2015) 5715–5724. doi:10.1021/acsami.5b00331.

[91] M. Nurunnabi, Z. Khatun, M. Nafiujjaman, D.G. Lee, Y.K. Lee, Surface coating of graphene quantum dots using mussel-inspired polydopamine for biomedical optical imaging, ACS Appl. Mater. Interfaces. 5 (2013) 8246–8253. doi:10.1021/am4023863.

[92] J. Cui, Y. Yan, G.K. Such, K. Liang, C.J. Ochs, A. Postma, F. Caruso, Immobilization and intracellular delivery of an anticancer drug using mussel-inspired polydopamine capsules, Biomacromolecules. 13 (2012) 2225–2228. doi:10.1021/bm300835r.

[93] H.P. Peng, R.P. Liang, L. Zhang, J.D. Qiu, Facile preparation of novel core-shell enzyme-Au-polydopamine-Fe3O4magnetic bionanoparticles for glucose sensor, Biosens. Bioelectron. 42 (2013) 293–299. doi:10.1016/j.bios.2012.10.074.

[94] Q. Zheng, T. Lin, H. Wu, L. Guo, P. Ye, Y. Hao, Q. Guo, J. Jiang, F. Fu, G. Chen, Mussel-inspired polydopamine coated mesoporous nanoparticles as pH sensitive nanocarriers for controlled release, Int. J. Pharm. 463 (2014) 22–26. doi:10.1016/j.ijpharm.2013.12.045.

[95] J. Park, T.F. Brust, H.J. Lee, S.C. Lee, V.J. Watts, Y. Yeo, Polydopamine-Based Simple and Versatile Surface Modification of Polymeric Nano Drug Carriers, ACS Nano. 8 (2014) 3347–3356. doi:10.1021/nn405809c.

[96] B.M. Teo, R. van der Westen, L. Hosta-Rigau, B. Städler, Cell response to PEGylated poly(dopamine) coated liposomes considering shear stress, Biochim. Biophys. Acta - Gen. Subj. 1830 (2013) 4838–4847. doi:10.1016/j.bbagen.2013.06.022.

[97] A. Abuchowski, J.R. McCoy, N.C. Palczuk, T. van Es, F.F. Davis, Effect of covalent attachment of polyethylene glycol on immunogenicity and circulating life of bovine liver catalase, J. Biol. Chem. 252 (1977) 3582–3586.

[98] J. Milton Harris, R.B. Chess, Effect of pegylation on pharmaceuticals, Nat. Rev. Drug Discovery. 2 (2003) 214–221. doi:10.1038/nrd1033.

[99] A.C. Anselmo, S. Mitragotri, Nanoparticles in the clinic, Bioeng. Transl. Med. 1 (2016) 10–29. doi:10.1002/btm2.10003.

[100] N. Bertrand, J.C. Leroux, The journey of a drug-carrier in the body: An anatomo-physiological perspective, J. Controlled Release. 161 (2012) 152–163. doi:10.1016/j.jconrel.2011.09.098.

[101] J.S. Suk, Q. Xu, N. Kim, J. Hanes, L.M. Ensign, PEGylation as a strategy for improving nanoparticle-based drug and gene delivery, Adv. Drug Delivery Rev. 99 (2016) 28–51. doi:10.1016/j.addr.2015.09.012.

[102] N. MacKinnon, G. Guérin, B. Liu, C.C. Gradinaru, P.M. Macdonald, Liposome-hydrogel bead complexes prepared via biotin-avidin conjugation, Langmuir. 25 (2009) 9413–9423. doi:10.1021/la900163r.

[103] N. MacKinnon, G. Guérin, B. Liu, C.C. Gradinaru, J.L. Rubinstein, P.M. Macdonald, Triggered instability of liposomes bound to hydrophobically modified core-shell PNIPAM hydrogel beads, Langmuir. 26 (2010) 1081–1089. doi:10.1021/la902423v.

[104] E.S. Jeong, H.A. Son, M.K. Kim, K.-H. Park, S. Kay, P.S. Chae, J.W. Kim, Fabrication of monodisperse liposomes-in-microgel hybrid microparticles in capillary-based microfluidic devices, Colloids Surf., B. 123 (2014) 339–344. doi:10.1016/j.colsurfb.2014.09.039.

[105] C.F. Buchanan, S.S. Verbridge, P.P. Vlachos, M.N. Rylander, Flow shear stress regulates endothelial barrier function and expression of angiogenic factors in a 3D microfluidic tumor vascular model, Cell Adhes. Migr. 8 (2014) 517–524. doi:10.4161/19336918.2014.970001.

[106] D.A. Chistiakov, A.N. Orekhov, Y. V. Bobryshev, Effects of shear stress on endothelial cells: go with the flow, Acta Physiol. 219 (2017) 382–408. doi:10.1111/apha.12725.

[107] W.J. Polacheck, J.L. Charest, R.D. Kamm, Interstitial flow influences direction of tumor cell migration through competing mechanisms, Proc. Natl. Acad. Sci. 108 (2011) 11115–11120. doi:10.1073/pnas.1103581108.

[108] T. Kang, Y. Cho, C. Park, S.D. Kim, E. Oh, J.H. Cui, Q.R. Cao, B.J. Lee, Effect of biomimetic shear stress on intracellular uptake and cell-killing efficiency of doxorubicin in a free and liposomal formulation, Int. J. Pharm. 510 (2016) 42–47. doi:10.1016/j.ijpharm.2016.06.017.

[109] M. Godoy-Gallardo, P.K. Ek, M.M.T. Jansman, B.M. Wohl, L. Hosta-Rigau, Interaction between drug delivery vehicles and cells under the effect of shear stress, Biomicrofluidics. 9 (2015) 1–20. doi:10.1063/1.4923324.

[110] A.J. Ditto, K.N. Shah, N.K. Robishaw, M.J. Panzer, W.J. Youngs, Y.H. Yun, The Interactions between L‐Tyrosine Based Nanoparticles Decorated with Folic Acid and Cervical Cancer Cells under Physiological Flow, Mol. Pharmaceutics. 9 (2012) 3089–3098. doi:10.1021/mp300221f.

[111] L. Li, C.M. Terry, Y.T.E. Shiu, A.K. Cheung, Neointimal hyperplasia associated with synthetic hemodialysis grafts, Kidney Int. 74 (2008) 1247–1261. doi:10.1038/ki.2008.318.

[112] T. Kang, C. Park, B.J. Lee, Investigation of biomimetic shear stress on cellular uptake and mechanism of polystyrene nanoparticles in various cancer cell lines, Arch. Pharm. Res. 39 (2016) 1663–1670. doi:10.1007/s12272-016-0847-0.

[113] J. Han, B.J. Zern, V. V Shuvaev, P.F. Davies, S. Muro, V. Muzykantov, Acute and Chronic Shear Stress Di ff erently Regulate Endothelial Internalization of Nanocarriers Targeted to Platelet- Endothelial Cell Adhesion Molecule - 1, ACS Nano. 6 (2012) 8824–8836. doi:10.1021/nn302687n.

[114] T. Kang, T.T.T. Tran, C. Park, B.J. Lee, Biomimetic shear stress and nanoparticulate drug delivery, J. Pharm. Invest. 47 (2017) 133–139. doi:10.1007/s40005-017-0313-0.

[115] E.T. Kisak, Nanocompartments enclosing vesicles, colloids, and macromolecules via interdigitated lipid bilayers, Langmuir. 18 (2002) 284–288. doi:10.1021/la0156053.

[116] H. Lomas, A.P.R. Johnston, G.K. Such, Z. Zhu, K. Liang, M.P. Van Koeverden, S. Alongkornchotikul, F. Caruso, Polymersome-loaded capsules for controlled release of DNA, Small. 7 (2011) 2109–2119. doi:10.1002/smll.201100744.

[117] C.C. Evans, J. Zasadzinski, Encapsulating vesicles and colloids from cochleate cylinders, Langmuir. 19 (2003) 3109–3113. doi:10.1021/la0265171.

[118] S. Ogue, Y. Takahashi, H. Onishi, Y. Machida, Preparation of double liposomes and their efficiency as an oral vaccine carrier, Biol. Pharm. Bull. 29 (2006) 1223–8. doi:10.1248/bpb.29.1223.

[119] Y. Elani, A. Gee, R. V. Law, O. Ces, Engineering multi-compartment vesicle networks, Chem. Sci. 4 (2013) 3332–3338. doi:10.1039/c3sc51164b.

[120] H.C. Chiu, Y.W. Lin, Y.F. Huang, C.K. Chuang, C.S. Chern, Polymer vesicles

containing small vesicles within interior aqueous compartments and pH-responsive transmembrane channels, Angew. Chem., Int. Ed. 47 (2008) 1875–1878. doi:10.1002/anie.200704078.

[121] M. Marguet, L. Edembe, S. Lecommandoux, Polymersomes in polymersomes: Multiple loading and permeability control, Angew. Chem., Int. Ed. 51 (2012) 1173–1176. doi:10.1002/anie.201106410.

[122] H.C. Shum, Y.J. Zhao, S.H. Kim, D.A. Weitz, Multicompartment polymersomes from double emulsions, Angew. Chem., Int. Ed. 50 (2011) 1648–1651. doi:10.1002/anie.201006023.

[123] O. Kulygin, A.D. Price, S.F. Chong, B. St??dler, A.N. Zelikin, F. Caruso, Subcompartmentalized polymer hydrogel capsules with selectively degradable carriers and subunits, Small. 6 (2010) 1558–1564. doi:10.1002/smll.201000453.

[124] D. McPhail, L. Tetley, C. Dufes, I.F. Uchegbu, Liposomes encapsulating polymeric chitosan based vesicles - A vesicle in vesicle system for drug delivery, Int. J. Pharm. 200 (2000) 73–86. doi:10.1016/S0378-5173(00)00348-3.

[125] L. Hosta-Rigau, P. Schattling, B.M. Teo, M.E. Lynge, B. Städler, Recent progress of liposomes in nanomedicine, J. Mater. Chem. B. 2 (2014) 6686–6691. doi:10.1039/c4tb00825a.

[126] A. Khanal, M.N. Bui, S.S. Seo, Breast Cancer Microgel-Encapsulated Methylene Blue for the Treatment of Breast Cancer Cells by Photodynamic Therapy, J. Breast Cancer. 17 (2014) 18–24. doi:10.4048/jbc.2014.17.1.18.

[127] M.C. Dixon, Quartz Crystal Microbalance with Dissipation Monitoring: Enabling Real-Time Characterization of Biological Materials and Their Interactions, J. Biomol. Tech. 19 (2008) 151–158. https://www.ncbi.nlm.nih.gov/pmc/articles/PMC2563918/pdf/jbt-19-151.pdf (accessed January 15, 2018).

[128] Q. Chen, S. Xu, Q. Liu, J. Masliyah, Z. Xu, QCM-D study of nanoparticle interactions, Adv. Colloid Interface Sci. 233 (2016) 94–114. doi:10.1016/j.cis.2015.10.004.

[129] M. D'Ischia, A. Napolitano, V. Ball, C.T. Chen, M.J. Buehler, Polydopamine and eumelanin: From structure-property relationships to a unified tailoring strategy, Acc. Chem. Res. 47 (2014) 3541–3550. doi:10.1021/ar500273y.

[130] R. Batul, T. Tamanna, A. Khaliq, A. Yu, Recent progress in the biomedical applications of polydopamine nanostructures, Biomater. Sci. 5 (2017) 1204–1229. doi:10.1039/c7bm00187h.

[131] D. Chang, Y. Gao, L. Wang, G. Liu, Y. Chen, T. Wang, W. Tao, L. Mei, L. Huang, X. Zeng, Polydopamine-based surface modification of mesoporous silica nanoparticles as pH-sensitive drug delivery vehicles for cancer therapy, J. Colloid

Interface Sci. 463 (2016) 279–287. doi:10.1016/j.jcis.2015.11.001.

[132] W. Cheng, J. Nie, L. Xu, C. Liang, Y. Peng, G. Liu, T. Wang, L. Mei, L. Huang, X. Zeng, pH-Sensitive Delivery Vehicle Based on Folic Acid-Conjugated Polydopamine-Modified Mesoporous Silica Nanoparticles for Targeted Cancer Therapy, ACS Appl. Mater. Interfaces. 9 (2017) 18462–18473. doi:10.1021/acsami.7b02457.

[133] J. Yang, M.A. Cohen Stuart, M. Kamperman, Jack of all trades: Versatile catechol crosslinking mechanisms, Chem. Soc. Rev. 43 (2014) 8271–8298. doi:10.1039/c4cs00185k.

[134] Y. Jing, H. Trefna, M. Persson, B. Kasemo, S. Svedhem, Formation of supported lipid bilayers on silica: relation to lipid phase transition temperature and liposome size., Soft Matter. 10 (2014) 187–195. doi:10.1039/c3sm50947h.

[135] F. Michor, J. Liphardt, M. Ferrari, J. Widom, What does physics have to do with cancer? Franziska, Nat. Rev. Cancer. 11 (2011) 657–670. doi:10.1016/j.immuni.2010.12.017.Two-stage.

[136] M.A. Swartz, A.W. Lund, Lymphatic and interstitial flow in the tumour microenvironment: Linking mechanobiology with immunity, Nat. Rev. Cancer. 12 (2012) 210–219. doi:10.1038/nrc3186.

[137] M. Björnmalm, Y. Yan, F. Caruso, Engineering and evaluating drug delivery particles in microfluidic devices, J. Controlled Release. 190 (2014) 139–149. doi:10.1016/j.jconrel.2014.04.030.

[138] A. Albanese, A.K. Lam, E.A. Sykes, J. V. Rocheleau, W.C.W. Chan, Tumour-on-a-chip provides an optical window into nanoparticle tissue transport, Nat. Commun. 4 (2013) 1–8. doi:10.1038/ncomms3718.

[139] L. Hosta-rigau, B. Städler, Shear Stress and Its E ff ect on the Interaction of Myoblast Cells with Nanosized Drug Delivery Vehicles, Mol. Pharmaceutics. 10 (2013) 2707–2712. doi:10.1021/mp4001298.

[140] N. Huang, R. Michel, J. Voros, M. Textor, R. Hofer, A. Rossi, D.L. Elbert, J. a Hubbell, N.D. Spencer, Poly (l-lysine) -g-poly (ethylene glycol) Layers on Metal Oxide Surfaces : Surface-Analytical Characterization and Resistance to Serum and Fibrinogen Adsorption Poly (L -lysine) -g-poly (ethylene glycol) Layers on Metal Oxide Surfaces : Surface-An, Langmuir. 17 (2001) 489–498. doi:10.1021/la000736+.

[141] A.N. Zelikin, K. Breheney, R. Robert, E. Tjipto, K. Wark, Cytotoxicity and internalization of polymer hydrogel capsules by mammalian cells, Biomacromolecules. 11 (2010) 2123–2129. doi:10.1021/bm100500v.

[142] S. Palchetti, V. Colapicchioni, L. Digiacomo, G. Caracciolo, D. Pozzi, A.L. Capriotti, G. La Barbera, A. Laganà, The protein corona of circulating PEGylated

liposomes, Biochim. Biophys. Acta - Biomembr. 1858 (2016) 189–196. doi:10.1016/j.bbamem.2015.11.012.

[143] J.-J. Chiu, S. Chien, Effects of Disturbed Flow on Vascular Endothelium: Pathophysiological Basis and Clinical Perspectives, Physiolo. 91 (2011) 1–106. doi:10.1152/physrev.00047.2009.Effects.

[144] P.F. Davies, Hemodynamic shear stress and the endothelium in cardiovascular pathophysiology Peter, Nat. Clin. Pract. Cardiovasc. Med. 6 (2009) 16–26. doi:10.1038/ncpcardio1397.Hemodynamic.

[145] M.J. Mitchell, M.R. King, Computational and Experimental Models of Cancer Cell Response to Fluid Shear Stress, Front. Oncol. 3 (2013) 1–11. doi:10.3389/fonc.2013.00044.

[146] K. Panneerselvam, S. Mena-Hernando, B.M. Teo, K.N. Goldie, B. Städler, Liposomes equipped with poly(N-isopropyl acryl amide)-containing coatings as potential drug carriers, RSC Adv. 4 (2014) 44769–44776. doi:10.1039/c4ra07720b.

[147] K. Panneerselvam, M.E. Lynge, C.F. Riber, S. Mena-Hernando, A.A.A. Smith, K.N. Goldie, A.N. Zelikin, B. Städler, Phospholipid-polymer amphiphile hybrid assemblies and their interaction with macrophages, Biomicrofluidics. 9 (2015). doi:10.1063/1.4929405.

[148] H.Y. Nam, S.M. Kwon, H. Chung, S.Y. Lee, S.H. Kwon, H. Jeon, Y. Kim, J.H. Park, J. Kim, S. Her, Y.K. Oh, I.C. Kwon, K. Kim, S.Y. Jeong, Cellular uptake mechanism and intracellular fate of hydrophobically modified glycol chitosan nanoparticles, J. Controlled Release. 135 (2009) 259–267. doi:10.1016/j.jconrel.2009.01.018.

[149] D. Dutta, J.G. Donaldson, Search for inhibitors of endocytosis, Cell. Logist. 2 (2012) 203–208. doi:10.4161/cl.23967.

[150] A.I. Ivanov, Exocytosis and Endocytosis. Chapter 2, 2008.

[151] A.D. Stuart, T.D.K. Brown, Entry of Feline Calicivirus Is Dependent on Clathrin-Mediated Endocytosis and Acidification in Endosomes, J. Virol. 80 (2006) 7500–7509. doi:10.1128/JVI.02452-05.

[152] J.P.X. Cheng, C. Mendoza-Topaz, G. Howard, J. Chadwick, E. Shvets, A.S. Cowburn, B.J. Dunmore, A. Crosby, N.W. Morrell, B.J. Nichols, Caveolae protect endothelial cells from membrane rupture during increased cardiac output, J. Cell Biol. 211 (2015) 53–61. doi:10.1083/jcb.201504042.

[153] J. Yu, S. Bergaya, T. Murata, I.F. Alp, M.P. Bauer, M.I. Lin, M. Drab, T. V. Kurzchalia, R. V. Stan, W.C. Sessa, Direct evidence for the role of caveolin-1 and caveolae in mechanotransduction and remodeling of blood vessels, J. Clin. Invest. 116 (2006) 1284–1291. doi:10.1172/JCI27100.

[154] M. Althaus, R. Bogdan, W.G. Clauss, M. Fronius, Mechano-sensitivity of epithelial

sodium channels (ENaCs): laminar shear stress increases ion channel open probability, FASEB J. 21 (2007) 2389–2399. doi:10.1096/fj.06-7694com.

[155] E. Tkachenko, E. Gutierrez, S.K. Saikin, P. Fogelstrand, C. Kim, A. Groisman, M.H. Ginsberg, The nucleus of endothelial cell as a sensor of blood flow direction, Biol. Open. 2 (2013) 1007–1012. doi:10.1242/bio.20134622.

[156] W.A. Shihata, D.L. Michell, K.L. Andrews, J.P.F. Chin-Dusting, Caveolae: A Role in Endothelial Inflammation and Mechanotransduction?, Front. Physiol. 7 (2016) 628. doi:10.3389/fphys.2016.00628.

[157] Z. Li, L. Sun, Y. Zhang, A.P. Dove, R.K. O'Reilly, G. Chen, Shape Effect of Glyco-Nanoparticles on Macrophage Cellular Uptake and Immune Response, ACS Macro Lett. 5 (2016) 1059–1064. doi:10.1021/acsmacrolett.6b00419.

[158] X. Banquy, F. Suarez, A. Argaw, J.-M. Rabanel, P. Grutter, J.-F. Bouchard, P. Hildgen, S. Giasson, Effect of mechanical properties of hydrogel nanoparticles on macrophage cell uptake, Soft Matter. 5 (2009) 3984–3991. doi:10.1039/b821583a.

[159] J. V. Georgieva, D. Kalicharan, P.O. Couraud, I.A. Romero, B. Weksler, D. Hoekstra, I.S. Zuhorn, Surface characteristics of nanoparticles determine their intracellular fate in and processing by human blood-brain barrier endothelial cells in vitro, Mol. Ther. 19 (2011) 318–325. doi:10.1038/mt.2010.236.

[160] N. Gunduz, H. Ceylan, M.O. Guler, A.B. Tekinay, Intracellular Accumulation of Gold Nanoparticles Leads to Inhibition of Macropinocytosis to Reduce the Endoplasmic Reticulum Stress, Sci. Rep. 7 (2017) 1–10. doi:10.1038/srep40493.

[161] K. Gulati, N. Rai, A. Ray, Effects of Stress on Reproductive and Developmental Biology, Academic Press, 2017. doi:10.1016/B978-0-12-804239-7.00056-1.

[162] H. Katsumi, M. Nishikawa, K. Nishiyama, R. Hirosaki, N. Nagamine, H. Okamoto, H. Mizuguchi, K. Kusamori, H. Yasui, F. Yamashita, M. Hashida, T. Sakane, A. Yamamoto, Development of PEGylated serum albumin with multiple reduced thiols as a long-circulating scavenger of reactive oxygen species for the treatment of fulminant hepatic failure in mice, Free Radic. Biol. Med. 69 (2014) 318–323. doi:10.1016/j.freeradbiomed.2014.01.036.

[163] D. Domanico, S. Fragiotta, A. Cutini, C. Carnevale, L. Zompatori, E.M. Vingolo, Circulating levels of reactive oxygen species in patients with nonproliferative diabetic retinopathy and the influence of antioxidant supplementation: 6-month follow-up, Indian J. Ophthalmol. 63 (2015) 9. doi:10.4103/0301-4738.151455.

[164] M. Marguet, C. Bonduelle, S. Lecommandoux, Multicompartmentalized polymeric systems: towards biomimetic cellular structure and function, Chem. Soc. Rev. 42 (2013) 512–529. doi:10.1039/C2CS35312A.

[165] A. Armada-Moreira, E. Taipaleenmäki, M. Baekgaard-Laursen, P.S. Schattling, A.M. Sebastião, S.H. Vaz, B. Städler, Platinum Nanoparticle-Based Microreactors

as Support for Neuroblastoma Cells, ACS Appl. Mater. Interfaces. 10 (2018) 7581–7592. doi:10.1021/acsami.7b10724.

[166] B. Lipinski, Hydroxyl radical and its scavengers in health and disease, Oxid. Med. Cell. Longev. 2011 (2011) 1–9. doi:10.1155/2011/809696.

[167] B.A. Lobo, S.A. Rogers, S. Choosakoonkriang, J.G. Smith, G. Koe, C.R. Middaugh, Differential scanning calorimetric studies of the thermal stability of plasmid DNA complexed with cationic lipids and polymers, J. Pharm. Sci. 91 (2002) 454–466. doi:10.1002/jps.10025.

[168] P. Gill, T.T. Moghadam, B. Ranjbar, Differential Scanning Calorimetry Techniques: Applications in Biology and Nanoscience, J. Biomol. Tech. 21 (2010) 167–193. doi:unavailable.

[169] U. Wattendorf, H. Merkle, PEGylation as a Tool for the Biomedical Engineering of Surface Modified Microparticles, J. Pharm. Sci. 97 (2008) 4655–4669. doi:10.1002/jps.

[170] S. Pasche, S.M. De Paul, J. Vörös, N.D. Spencer, M. Textor, Poly(l-lysine)-graft-poly(ethylene glycol) Assembled Monolayers on Niobium Oxide Surfaces: A Quantitative Study of the Influence of Polymer Interfacial Architecture on Resistance to Protein Adsorption by ToF-SIMS and in Situ OWLS, Langmuir. 19 (2003) 9216–9225. doi:10.1021/la034111y.

[171] U. Wattendorf, M.C. Koch, E. Walter, J. Vörös, M. Textor, H.P. Merkle, Phagocytosis of poly(L-lysine)-graft-poly(ethylene glycol) coated microspheres by antigen presenting cells: Impact of grafting ratio and poly(ethylene glycol) chain length on cellular recognition., Biointerphases. 1 (2006) 123–33. doi:10.1116/1.2409645.

[172] C. Zhu, F. Itel, R. Chandrawati, X. Han, B. Städler, Multi-compartmentalized microreactors containing nuclei and catalase-loaded liposomes, Biomacromolecules. (2018) acs.biomac.8b01260. doi:10.1021/acs.biomac.8b01260.

[173] Y. Liu, K. Ai, X. Ji, D. Askhatova, R. Du, L. Lu, J. Shi, Comprehensive insights into the multi-antioxidative mechanisms of melanin nanoparticles and their application to protect brain from injury in ischemic stroke, J. Am. Chem. Soc. 139 (2017) 856–862. doi:10.1021/Jacs.6b11013.

[174] M.I. Heller, P.L. Croot, Kinetics of superoxide reactions with dissolved organic matter in tropical Atlantic surface waters near Cape Verde (TENATSO), J. Geophys. Res. Ocean. 115 (2010) 1–13. doi:10.1029/2009JC006021.

[175] J. Cui, Y. Feng, S. Jia, Silica encapsulated catalase@metal-organic framework composite: A highly stable and recyclable biocatalyst, Chem. Eng. J. 351 (2018) 506–514. doi:10.1016/j.cej.2018.06.121.

Appendix A

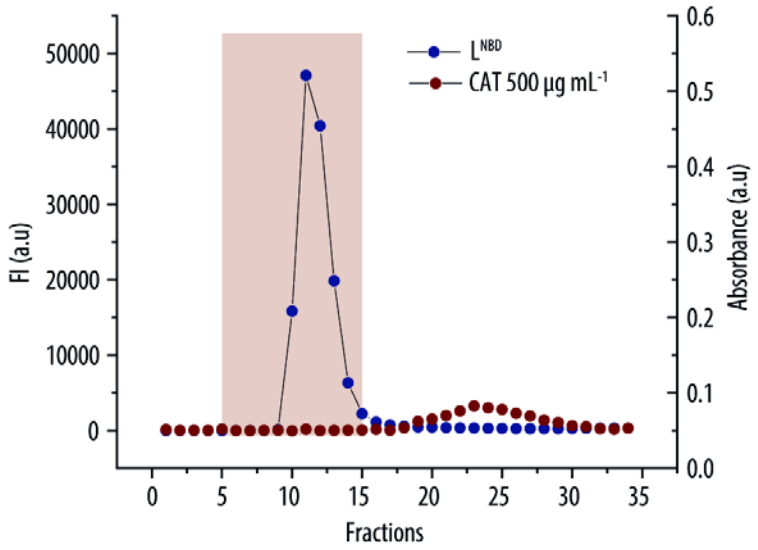

Figure A.1 Elution profile of liposomes and catalase in size exclusion chromatography. Fluorescence readings (FI) of the fractions containing fluorescent liposomes (L^{NBD}) and absorbance readings of fractions containing catalase (CAT). The fractions 5 to 15 are the ones collected for further experiments.

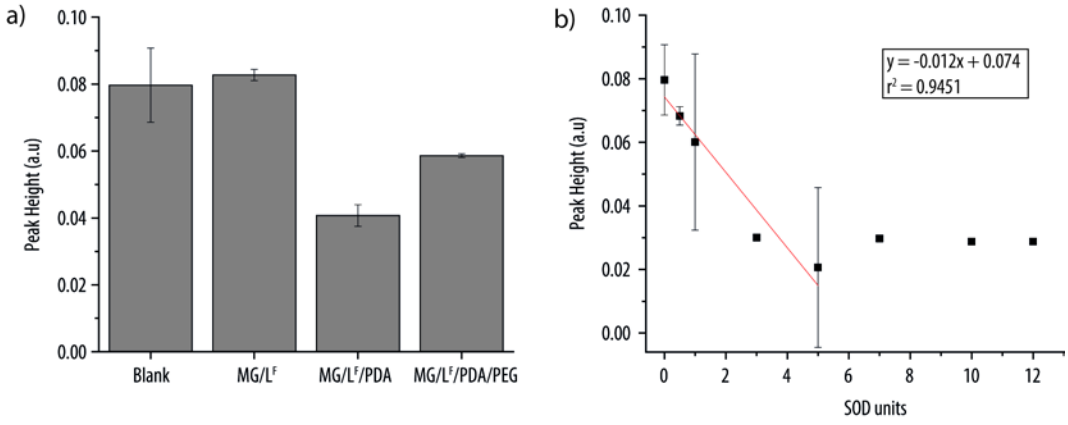

Figure A.2 Superoxide dismutase (SOD)-like activity of MG/L^F/PDA/PEG microreactors. a) Absorbance Peak Height of blank, MG/L^F and microreactors (MG/L^F/PDA and MG/L^F/PDA/PEG) upon incubation with xanthine, xanthine oxidase and cytochrome C for 0.5 h at 37°C. Measured at 550 nm. B) Calibration curve of SOD upon incubation with xanthine, xanthine oxidase and cytochrome C for 0.5 h at 37°C. Measured at 550 nm.

Appendix B

York-Duran, M. J.; Godoy-Gallardo, M.; Labay, C.; Urquhart, A. J.; Andresen, T. L.; Hosta-Rigau, L. Recent Advances in Compartmentalized Synthetic Architectures as Drug Carriers, Cell Mimics and Artificial Organelles. *Colloids Surf., B* **2017**, *152*, 199–213. https://www.sciencedirect.com/science/article/pii/S092777651730022X

Appendix C

Godoy-Gallardo, M.; **York-Duran, M. J.;** Hosta-Rigau, L. Recent Progress in Micro/Nanoreactors toward the Creation of Artificial Organelles. *Adv. Healthc. Mater.* **2018**, *7* (5), 1–35.

*First co-authorship

https://www.ncbi.nlm.nih.gov/pubmed/29205928